SEISMIC PERFORMANCE ASSESSMENT OF HISTORICAL BUILDINGS

by
Kültigin Demirlioğlu
B.S., Civil Engineering, Pamukkale University, 2011

Submitted to the Institute for Graduate Studies in
Science and Engineering in partial fulfillment of
the requirements for the degree of
Master of Science

Graduate Program in Civil Engineering
Boğaziçi University
2017

ACKNOWLEDGEMENTS

Firstly, I would like to express my deepest gratitude to my supervisor Associate Professor Serdar Soyöz who always trusted in me, supported my work and took the time to get my opinions. Thanks to his supervision and his continuous encouragement, I always believed in myself and kept motivated to finalize my study. Thank you.

I would also like to convey my gratefulness to Associate Professor Maria Giuseppina Limongelli who accepted to supervise my thesis study at Politecnico di Milano during my Erasmus experience. Her contributions to the direction and richness of this study are priceless for me.

I would like to present my sincere thankfulness to Prof. Gülay Altay. When she was the head of Civil Engineering Department, her endless support enabled me to be a student of Bogazici University.

I would like to extend my sincere thanks to the members of my thesis jury for participating.

I would like to especially thank Semih Gönen and Selahattin Akalp for their friendship, critical discussions and valuable helps. Thanks, my dear friends Massoud Pourmandi, Oğuz Şenkardeşler and Emre Aytulun for your helps and valuable comments.

Finally, I must express the profoundest gratitude from my deep heart to my beloved parents and my brother for their endless support and love. I never imagine this thesis would have been possible without them.

ABSTRACT

SEISMIC PERFORMANCE ASSESSMENT OF HISTORICAL BUILDINGS

Aged construction materials and insufficient knowledge regarding the existing properties of territorial materials and the structural features make performance assessment of historical masonry buildings a challenging task. In an attempt to reduce the connatural complexity of masonry and uncertainties, ambient vibration tests (AVT) were implemented, and the available material test results were used in the definition of material properties. A 3D Finite Element Model (FEM) of the entire building was generated with initial material properties. Afterwards, the FEM was updated based on the global dynamic characteristics of the building extracted from AVT so as to minimize the difference between theoretical and experimental modal behaviour. Following this, by conducting linear response spectrum analysis using FE analysis, the seismic demand was obtained in terms of drift ratio, which corresponds to limit states of masonry. Also, the distribution of stresses enabled verifying the possible shear hinge locations as described in the literature. In addition, the front facade of the building was modelled with 2D Equivalent Frame (EF). In-plane behaviour of the facade was considered and modelled as EFM in analyses. Series of simulations was performed using a set of Non-linear Time History analyses and incremental dynamic pushover curves (based on base shear vs top displacement) were generated. Consequently, the seismic fragility curve was derived to perform vulnerability assessment. The study aims at contributing to the seismic performance assessment of a historic brick masonry building constructed in Istanbul by means of FE and EF Modelling approaches.

ÖZET

TARİHİ BİNALARIN SİSMİK PERFORMANS DEĞERLENDİRMESİ

Zaman içinde yıpranmış yapı malzemeleri, yapısal ve mevcut yerel malzeme özellikleri hakkında yetersiz bilgiye sahip olma, tarihi yığma binaların performans değerlendirmesini her zaman zorlu bir görev yapmıştır. Yığma malzemelerin kendi doğasından kaynaklı karmaşıklık ve belirsizlikleri azaltmak amacıyla, Ortamsal Titreşim Testleri uygulanmış ve mevcut malzeme test sonuçları malzeme özelliklerini tanımlamada kullanılmıştır. Tüm yapının 3 boyutlu sonlu elemanlar modeli, ilk mevcut malzeme özellikleri ile kurulmuştur. Takiben, sonlu elemanlar modeli, teorik ve deneysel model davranışı arasındaki farkı minimize etmek için ortamsal titreşim testlerinden elde edilen yapının asıl dinamik karakterlerine göre güncellenmiştir. Güncellemeden sonra doğrusal tepki spektrumu analizi yapılarak yığma yapının sınır durumlarına karşılık gelen ötelenme oranları cinsinden sismik talep elde edilmiştir. Aynı zamanda, elde edilen gerilme dağılımı, literatürde tarif edildiği gibi olası kesme mafsallarının yerlerini doğrulama imkanı sağlamııştır. Ayrıca, yapının ön cephe duvarı 2 boyutlu eşdeğer çerçeve ile modellenmiştir. Analizlerde, eşdeğer çerçeve modeliyle modellenmiş olan dış cephe duvarının düzlem içi davranışı hesaba katılmıştır. Bir seri simülasyonlar, zaman tanım alanında doğrusal olmayan dinamik analizler sayesinde yapılmış ve artımsal dinamik itme eğrileri (taban kesme kuvveti - üst kat ötelenmesi cinsinden) oluşturulmuştur. Sonuç olarak, yapının hasar görebilirlik değerlendirilmesi için, sismik kırılganlık eğrisi türetilmiştir.

TABLE OF CONTENTS

LIST OF FIGURES

LIST OF TABLES

LIST OF SYMBOLS

A	Area of cross section
A_n	Net mortared area
c	Masonry bed-joint cohesion
cm	Centimeter
D	Width of the pier
E_m	Elasticity modulus of masonry
E_{me}	Expected elasticity modulus of masonry
E_x	Earthquake force in x direction
E_y	Earthquake force in y direction
f	Frequency
f_a	Axial compression stress
F_a	Short-period site factor
f_e	Lateral load demand of earthquake from elastic structures
f_{dt}	Masonry diagonal tension strength
f_m	Mean compressive strength of masonry
f_u	Compressive strength of masonry
F_v	Long-period site factor
f_{v0d}	Design shear strength
f_{vm0}	Mean shear strength
F_X	Base reacion in direction x
f_y	Lateral load capacity of the structure
F_Y	Base reacion in direction y
F_Z	Base reacion in direction z
g	Gravitational acceleration
G	Dead load
G_m	Shear modulus of masonry
G_{me}	Expected shear modulus of masonry
H	Height of the pier

h_{eff}	Effective height of the wall
Hz	Heartz
kN	Kilonewton
k_s	Coefficient of soil reaction
L	Length of the wall
m	Meter
MPa	Megapascal
p	Mean compressive stress
P	Dead and superimposed dead load
P_{CE}	Expected gravity compressive force.
R_y	Capacity reduction coefficient
Q	Live load
S_1	Horizontal response spectral acceleration coefficient at 1.0 second period on rock
S_{a}	Elastic spectral acceleration
S_{d}	Linear elastic spectral displacement
S_{S}	Horizontal response spectral acceleration coefficient at 0.2 second period on rock
t	Thickness of the pier
T	Natural period of the structure
T_0	Reference period used to define spectral shape
T_1	Fundamental model period of the structure
T_{L}	Initial period at which constant displacement region starts
t_{nom}	Nominal thickness of wall
T_{S}	Corner period at which spectrum changes from being independent of period to being inversely proportional to period
U	Displacement
V_{bjs}	Bed-joint shear strength
V_{dt}	Diagonal tensile capacity
V_f	Shear capacity
V_r	Rocking capacity
V_s	Sliding shear capacity

V_{tc}	Toe crushing capacity
V_u^f	Diagonal tensile capacity in Italian Code
α	Factor depending on clamping type of the walls
β	Non-linear stress distribution factor
γ	Material weight
γ_m	safety factor
δ	Displacement
δ_e	Elastic displacement
δ_u	Ultimate displacement
κ	Coefficient related to vertical stress distribution
μ_f	Friction coefficient
ξ	Coefficient of pier aspect ratio
σ_0	Mean vertical stress due to gravity loads
υ_{te}	Average bed-joint shear strength

LIST OF ACRONYMS/ABBREVIATIONS

2D	Two Dimensional
3D	Three Dimensional
AVT	Ambient Vibration Test
CP	Collapse Prevention
DLH	Technical Earthquake Regulation Concerning Construction of Coastal and Port Structures, Railroads, Airports by the Ministry of Transport, Maritime and Communication
EF	Equivalent Frame
EFM	Equivalent Frame Modellling
EQ	Earthquake
FDD	Frequency Domain Decomposition
FEA	Finite Element Analysis
FEM	Finite Element Modelling
FEMA	Federal Emergency Management Agency
IDA	Incremental Dynamic Analysis
IDAs	Incremental Dynamic Analyses
IO	Immediate Occupancy
LS	Life Safety
NLTH	Nonlinear Time History
NZSEE	New Zealand Society for Earthquake Engineering
OMA	Operational Modal Analysis
PEER	Pasific Earthquake Engineering Research
PGA	Peak Ground Acceleration
PO	Pushover
PSD	Power Spectral Density
RSA	Response Spectrum Analysis
SRSS	Square Root of Sum of Squares
URM	Unreinforced Masonry

1. INTRODUCTION

1.1. Overview

Heritage structures and historical monuments hold important cultural place in European society; old stone bridges, palaces, churches, cathedrals, monuments, etc., represent an enormous civilizing value, and most famous cities and places have also been identified with their historic structures (see Figure 1.1).

Nowadays, despite developing technology and increasing trend towards high-rise buildings, Unreinforced Masonry (URM) construction keeps its popularity and significance particularly in regions with low-seismic intensity. Ease of construction, low cost and suitability with nature for sustainable environment make URM structure still preferable and common.

Most of the building stock and cultural heritage world-wide consist of URM. Particularly, existing or historical ones were built by traditional methods, which lack engineering and design criteria. Territorial materials used in their construction bear inherent uncertainties. Aged construction materials, insufficient knowledge regarding the existing properties of territorial materials and the structural features, as well as the lack of performance criteria make structural assessment of historical masonry buildings a challenging task.

These structures are also vulnerable to natural hazards such as earthquakes and landslides, and they are susceptible to aggressive environments which cause aging and degradation of materials throughout their lifespan. Not only due to their high potential vulnerability to hazard events but also their high importance being cultural heritage, it is crucial to improve the knowledge of their seismic behaviour, design concepts and assessment techniques.

Strenght and deformation capacities of URM structures, which are main parameters influencing their non-linear behaviour have not been fully understood yet. Moreover, there are no reliable and practical analytical models for the force-deformation relationship of structural masonry [1]. Therefore, there is more research needed on this topic.

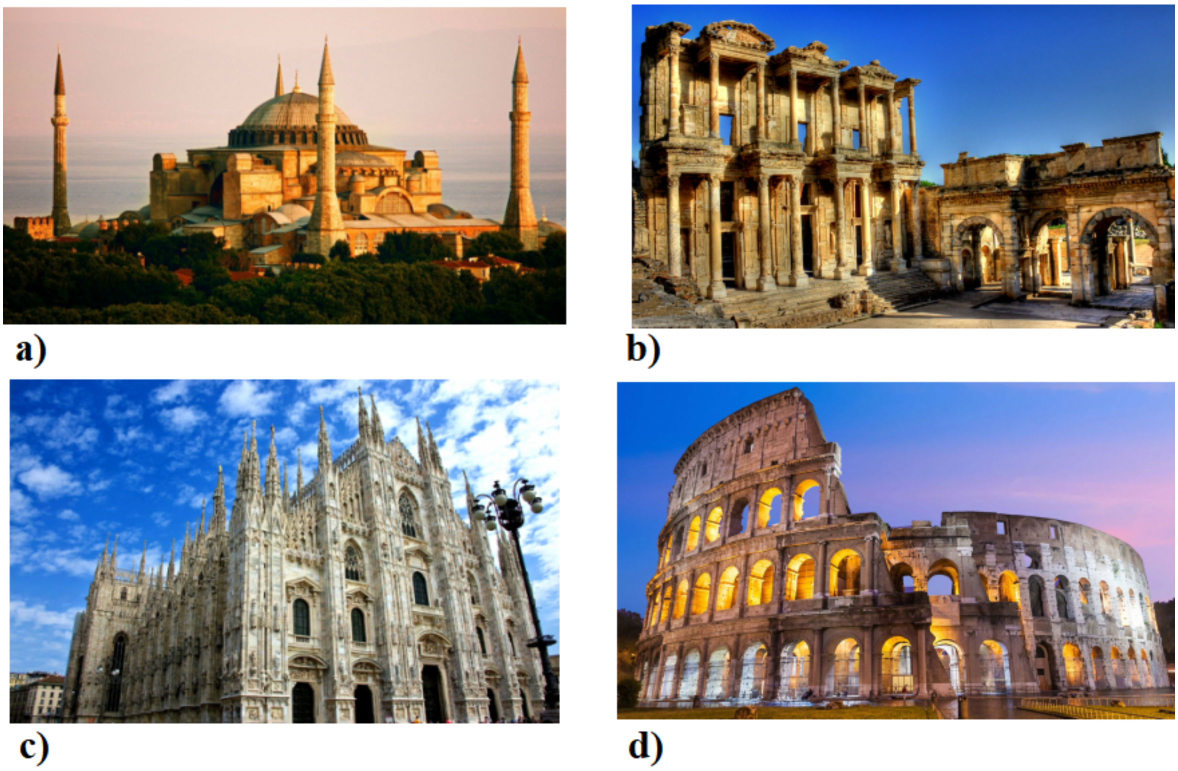

Figure 1.1. Historic URM Structures a) Hagia Sophia, Istanbul b) Celsus Library, Ephesus c) Duomo, Milan d) Colosseum, Rome

Furthermore, the physical and mechanical condition of URM structures which are vulnerable to dynamic and environmental effects must be monitored, and strengthened. Unfortunately, improper restoration and retrofitting techniques have frequently caused the deterioration and even the loss of historic structures. Therefore, appropriate rehabilitation works must be chosen carefully and carried out by depicting the original form, features and character of the structures. Afterwards, continuous health monitoring should be applied so as to detect the effectiveness of rehabilitation done.

1.2. Objectives

Seismic performance and vulnerability assessment of URM structures has always been a challenging task due to connatural complexity and uncertainty based on mechanical material properties of masonry composites. Since uncertainty in parameters are directly associated with the accuracy of dynamic response of the structures, these parameters are required to be identified by utilizing the experimental and numerical techniques proposed in the literature. In order to overcome this drawback, non-destructive testing is recommended from experimental studies, and Equivalent Frame Method (EFM) in 2-D modelling is claimed to be a numerical approach which is least affected by uncertainties. In addition, ambient vibration testing is one of the most preferred non-destructive methods. The reliability of use of this method on masonry structures has been verified by means of Finite Element Analysis (FEA) [2].

In this study, in order to make a contribution to the seismic performance and vulnerability assessment of historical structures, a historical building in Istanbul was investigated using FEM technique by linear dynamic analysis, and EFM technique by both incremental dynamic Non-Linear Time History Analyses (NLTH) and Pushover analyses (PO). In an attempt to reduce material based uncertainties, Ambient Vibration Tests (AVT) were implemented. Uncertain dynamic characteristics of the model were extracted from AVT by using Frequency Domain Decomposition (FDD). A 3-D FEM model of the building was generated based on the geometric survey and then was updated based on identified modal frequencies. Model updating procedure allowed to minimize the difference between experimental and theoretical modal behaviours and investigate the influence of the elasticity modulus and the coefficient of soil interaction on the modal behaviour. Since the outcomes of FEA demonstrate variations depending on the selected mesh size from coarse to fine, they were examined using different mesh sizes and eventually the FEM model was meshed by the most appropriate size, taking elapsed time in modal analysis and convergence based on dynamic parameters of the model into account. Following this, by conducting linear response spectrum analysis, the seismic demand was obtained in terms of drift ratio, which corresponds to limit states of masonry. Besides, it was examined whether principal and shear stresses occurring under the dynamic excitation exceeded the threshold values in order to predict the possible in-plane failure modes.

In order to simulate the in-plane behaviour of the URM wall, a 2D Equivalent Frame (EF) model of the front facade was established. 15 earthquake records, obtained from PEER NGA West2 Data Base in accordance with the Design Spectrum, were used for a set of NLTH analyses. Meantime, the pushover analyses with two different lateral load cases (mass proportional and mode proportional) were performed, and the results obtained from both analyses were compared. With the generation of incremental dynamic pushover curves as a result of NLTH analyses, a comprehensive study was carried out by plotting all dynamic curves and PO curves on the same figure. In addition to this, by obtaining a seismic fragility curve from NLTH analyses, it was provided to determine which PGA values lead the structure to attain corresponding limit states, and predict the collapse probability of the structure for each PGA. This study highlights following important points:

- Which load case assumption in PO is more appropriate to present similar behaviour with incremental dynamic pushover curves.
- The results of Capacity Reduction Coefficient and Ductility Demand Coefficient by comparing base shear and top displacement values of linear and non-linear analyses.
- Collapse probability of the structure for each PGA.
- Determination of the weak storey.
- Verification of possible hinge locations described in the literature.
- Model updating procedure.
- The interaction between Elasticity modulus and the coefficient of soil interaction on modal parameters.
- Seismic performance assessment in terms of drift ratio.

1.3. Scope

In Chapter 1, overview of historical masonry structures, the objectives of the study and the organization of the thesis were presented.

In Chapter 2, recent studies were discussed in detail. The seismic response of masonry walls, in-plane capacity of URM walls and their failure modes, definition of mechanical material properties, and modelling techniques used for URM walls were described.

In Chapter 3, general information about the building under consideration was given. Existing material test results and investigations were demonstrated. Implementation of ambient vibration tests and the extraction of dynamic parameters from AVT by Operational Modal Analysis were explained.

In Chapter 4, a 3D FEM of the entire structure was established. Each phase of the modelling and its effect on the dynamic characteristics were investigated. The model updating procedure based on Elasticity Modulus and soil interaction coefficient was mentioned. After completing the procedure of model updating, the final results of the modal analysis were showed.

In Chapter 5, the seismic performance assessment of the building was carried out by means of linear dynamic Response Spectrum Analysis (RSA). This assessment is a quantitative procedure, which determines whether an existing structure is capable of withstanding the design seismic combination safely. This chapter included the evaluation of relative storey displacements, drift ratios corresponding the limit states described in the literature, and the comparison of shear and principal stresses with their threshold values.

In Chapter 6, EFM was introduced in detail. For validation of EFM, some researches carried out were explained.

Using the criterion proposed by Dolce (1991), a 2D EFM of the front facade was established, and the assumptions made in modelling were presented.

In Chapter 7, the seismic performance assessment of the front facade which was modelled by using EFM technique was described. The non-linear behaviour of masonry was defined by means of lumped plastic hinges governed by in-plane failure mechanisms, and two nonlinear analysis methods were utilized for seismic evaluation. Pushover analysis was adopted as an incremental static nonlinear method where both mass proportional and mode proportional load cases were applied in analyses. As a non-linear dynamic method, a set of Non-Linear Time History (NLTH) analyses was used to perform series of simulations and incremental dynamic pushover curves were generated. Consequently, the seismic fragility curve was derived to achieve vulnerability assessment.

In Chapter 8, the conclusions obtained from all analyses were summarized. The recommendation for the future work was provided.

2. LITERATURE REVIEW

2.1. Recent studies

Dolce (1989) first developed Equivalent Frame Modelling (EFM) that principally involves the discretization of masonry facades into spandrels, piers and node panels, taking inspiration from the damages observed after seismic events. Dolce (1989) observed that wall deformation concentrates in piers and spandrels under dynamic excitations. Therefore, these portions were modelled as deformable elements, whereas node panels were characterized by rigid offsets. Thanks to the empirical rule proposed by Dolce (1989), the effective heights of piers were described for even irregular alignment of openings. Nowadays, EFM method has been widely used to carry out the seismic performance assessment of URM structures, since it is capable of giving accurate results in achieving global response of structural masonry [3].

Even though, the utilization of Equivalent Frame Modelling enable engineers in professional and scientific fields to obtain quick and reliable outcomes in the analysis and assessment of URM structures, some uncertainties arise in the application of EFM to existing masonry structures, which particularly hold irregular aligned openings.

In an attempt to encounter this gap, Siano *et al.* (2017) investigated the classification and measure of irregularity based on horizontal, vertical, offset, and irregularity in number of openings, and carried out a comparative study between EFM and FEM (reference model). The objective of study was to provide accurate recommendations as a function of the wall geometry in establishing EFM. Hence, a great number of walls bearing different geometrical arrangements in increasing complexity were tested. For these arrangements, the concept of frame-like was proposed to evaluate the effectiveness of EFM and differentiate the walls complying with an ideal frame configuration or not. Explicit constraints for the practicality and competence of EFM in both regular and irregular walls have been presented by Siano *et al.* (2017). In this study, it is observed that as geometrical complexity and the volume of irregularity in the alignment of walls increase, this change also gives rise to an increase in differences between EFM and FEM [4].

A general outline in modelling was developed for uncertainties influencing URM walls. In order to evolve the accuracy of EFM method by maintaining its ease of application, a reference was provided for calibration of updated EFM for walls with complex geometric irregularities. The significance of a geometrical calibration was drawn by comparative results obtained.

Magenes *et al.* (1995) made a highly remarkable contribution to the complete masonry building assessment process, performing the seismic testing of a full-scale two-storey masonry structure at the University of Pavia to simulate dynamic load/displacement patterns. The detailed test results, the assessment of the structural response to seismic excitation, and the advance of cracking were presented in terms of displacements and forces, thus many research groups have found a great opportunity to validate and compare their results obtained by applying different numerical modelling approaches, with the outcomes presented by Magenes *et al.* (1995). Furthermore, this research study aimed at providing a basis for the assessment of URM structures, such as survey and observation, interpretation of non-destructive testing in comparison to the outcomes of the destructive laboratory testing, analytical modelling of masonry components and entire building, design of strengthening methods, and analytical modelling of reinforced structures. Hereby, the experimental data illustrated that the collapse mechanisms of URM structures may be quite complex, due to the interaction of lateral and horizontal bearing elements and the effect of both constant and varying axial loads. In addition, it was acknowledged that spandrels, vertical components without axial loads, are prone to early shear cracking but still the ultimate resistance is controlled by pier failure, and pier heights other than clear opening heights are linked to rocking mechanisms [5].

Lourenco (1997) carried out a comprehensive research to provide a number of tools for the analysis of URM structures in plane stress conditions. Since a detailed modelling of masonry components such as interface, units and mortar, causes computational burden and impractical application in analysing large structures, this study encompassed simplified approaches under the assumption of a homogenous material and investigated the accuracy of homogenization technique, which may enable expecting the behaviour of the different composites, taking the properties of the components into account [6].

Magenes *et al.* (1997) aimed at developing a procedure for the assessment of strength, deformability and energy dissipation capacity of URM walls. Brick masonry having nearly constant mechanical characteristics was adopted as only one type of masonry in an attempt to decrease the scatter of experimental results. The influence of aspect ratio and shear ratio on shear strength of masonry walls were investigated by using finite element simulations, and the simplified existing formulations for prediction of shear strength was compared with shear strength obtained from shear tests of walls. The most significant parameters influencing deformation capacity of brick masonry walls subject to cyclic loading were handled. In order to accurately simulate hysteretic behaviour of masonry panels under dynamic loading, energy dissipation was measured. Findings from this study showed how ultimate drifts can be a procedure that is directly related to the shear failure occurring in walls [7].

D'Ayala *et al.* (2003) developed a tool which is able to withstand a great number of buildings and carry out statistical analysis, utilizing basic and realistic mechanical modelling built on limit analysis and macro elements. By means of the mechanical model established for dry block masonries, in- plane overturning and sliding of isolated walls were analysed in both absence and presence of live loads imposed. Besides, this study encompassed the derivation of the ultimate load factors by applying limit-state approach, and the implementation of parametric analysis. It was observed that robustness condition and clamping type of connections between masonry walls have a significant impact on out-of-plane behaviour. Based on damage type occurred after analysing and structure size, the failure mechanisms of wall assemblies were graded. Eventually, vulnerability functions reproduced and case studies done demonstrated how the technique can be operated for proper definition of strengthening interventions [8].

Pasticier *et al.* (2008) explored the possibilities for seismic performance analyses of masonry buildings using SAP 2000, which is a user-friendly software program for practising engineers. In order to validate the consistency of SAP 2000 in analysing URM, Catania Research Project, a nationwide project already investigated by many research groups in Italia, was initially considered for seismic assessment and comparison, and Equivalent Frame modelling method was applied by conducting the static pushover analysis. After obtaining a significant correlation in the results matching with those represented by other research groups, a case study building with two storeys located in the north-east of Italy was then investigated to determine the seismic performance and vulnerability of the masonry structure by means of static pushover and nonlinear time history analyses. In order to define the nonlinear behaviour of the structure during the pushover analysis, rocking hinges and shear hinges were employed in piers, but only shear hinges employed at mid-span in spandrels. The occurrence of structural collapse was assumed once the in-plane deformation capacity of piers was firstly reached due to the ultimate shear displacement controlled by shear hinges or the ultimate rotation controlled by rocking hinges. For this case study building, shear failure with diagonal cracking in terms of displacement demand was found as more brittle compared to failure mechanisms based on rocking and sliding after examining the results of pushover analysis. Therefore, only nonlinear shear link was assigned to the mid-heights of piers in an attempt to diminish time consuming and computational burden in nonlinear time history analyses. Finally, the seismic fragility curve was generated by applying incremental dynamic analyses in which several earthquake inputs were used, and scaling each PGA value of them was performed [9].

Salonikios *et al.* (2003) studied on URM plane frames for seismic capacity evaluation of existing masonry structures according to FEMA 273 guideline. The numerical models were established by using SAP 2000 where linear elements with proper plastic hinges were employed and by using CAST3M program where two different types of models were investigated, considering either homogenous components or discrete unit and joint elements. Pushover analysis was adopted as a non-linear method in which three different lateral load distributions were induced. Load case ACC (uniform distribution) was proportional to the mass tributary to that node, Load case LOAD (inverse triangular) proportional to the product of mass times the height of the node and Load case MODE proportional to the product of mass times mode shapes in the first mode. Depending on the modelling strategies, analysis results exhibited big differences in terms of shear strength, corresponding displacements and type of collapse mechanism. This study drawn a conclusion that simplified model established by SAP 2000 yields more conservative outcomes in terms of maximum shear strength values. With regards to load cases, ACC load case resulted in higher strength but different failure mechanism, whereas same failure mechanisms occurred when LOAD and MODE load cases were imposed [10].

Since masonry structures have been usually constructed by using traditional methods and territorial construction materials with connatural uncertainties, their assessment procedures have always been a challenging task. In order to overcome these uncertainties, vibration-based tests may be recently performed to catch accurate modal parameters of URM structures in analyses.

Gentile *et al.* (2007) assessed the structural health condition and damage scenario of the historic masonry bell-tower located in Monza, Italy, applying full-scale ambient vibration testing. Operational Modal Analysis was used to extract the modal parameters from output- only experimental data and 3-D FE model was established based on the geometric survey. For structural identification, the Inverse Eigen-Sensitivity (IE) and the Douglas – Reid (DR) methods were employed. As a result of model updating, a good agreement between theoretical and experimental modal parameters was attained by means of the distribution of Young's modulus in the masonry. This study demonstrated the dynamic-based assessment of masonry towers can be an effective method to assess damage in such structures in case of damage scenario principally involving the lower regions of the building [2].

In order to perform structural implementations such as retrofitting and performance assessment of existing structures, and design of new ones, it is required to utilize an effective tool that can constitute reliable non-linear models. Lagomarsino *et al.* (2013) developed TREMURI software specifically oriented to seismic assessment of masonry structures, which provides the possibility of inserting different formulations for masonry panels, alternate algorithms for pushover analysis and explicit modelling of horizontal flexible diaphragm. In this study, the discretization of masonry walls in EFM, 3D modelling of whole masonry buildings and seismic analysis procedures were explained. Finally, solutions acknowledged for the application of equivalent frame in TREMURI program were presented, and results obtained from this developed software were illustrated for comparison and validation with some experimental studies previously done [11].

Betti *et al.* (2015) investigated the seismic behaviour of URM buildings with flexible diaphragms by means of a comparison between finite element (FE) technique and macro element (ME) approach [12]. A two-storey prototype was set up at the CNR-ENEA research center, and tested on a shaking table until the extensive damage and collapse occurred. The tests in summary were performed by implementing the ground accelerations with a steady increase of 0.05 g, starting from 0.05 g up to collapse represented by PGA of 0.50 g. At each increment, the condition of the prototype was interpreted by examining crack patterns, thicknesses and detachments of the bearing walls. The dynamic responses of two numerical models were initially compared by conducting six shaking tables test in the range of 0.05 g and 0.3 g in linear field. In order to simulate non-linear behaviour of the prototype structure, two additional tests were applied with PGA of 0.35 g and 0.4 g. Emerging damages corresponding the change in PGA due to gradual increment were illustrated on the figures. When compared to ME model, it was observed that FE model significantly matched the experimental collapse mode. Meantime, the comparison was achieved in terms of the absolute accelerations, displacements, shear forces and stiffness degradation. Consequently, this study pointed out that FE model is very reliable tool to provide good agreements with experimental damages, however, ME model does not present a satisfactory development of failure mechanisms. In all outcomes obtained from two models, the ME underestimates the shear forces, since more stiffness degradation is considered, compared to FE model.

Simoes *et al.* (2012) aimed to contribute to the seismic vulnerability assessment of URM by means of nonlinear equivalent frame modelling analysis. Using SAP

2000 (CSI) software program, the in-plane behaviour of ‘Gaioleiro Building’ facade was investigated. Nonlinear behaviour was defined by lumped plastic hinges, and Incremental Pushover analysis was applied to identify the capacity curve of the facade. Consequently, the shear capacity of piers controls the occurrence of global collapse [13].

Sonekar *et al.* (2015) simulated the non-linear behaviour of two structural masonry facades established in EFM, applying different lateral load patterns in Pushover analyses. Uniform load pattern is only proportional to mass. Mode load pattern is proportional to first mode shapes multiplied by storey masses. The last one is called Parabolic load pattern, which was determined according to IS 1893 (part1). In order to carry out the performance assessment of the considered building, the fragility curves in both x and y direction were generated in terms of spectral acceleration vs spectral displacement curves [14]. According to four damage states defined in FEMA 2003 corresponding to spectral displacement limits proposed by Kappos *et al.*, the fragility curves obtained were examined. It was concluded that the structural collapse was dictated by shear failure. The higher lateral force- displacement capacity for the investigated building was attained under uniform load pattern compared to mode and parabolic load patterns. Finally, it was observed that the damage probability made up around 65 % in moderate damage level represented by Gr 2 in FEMA 2003.

Petry (2015) contributed the improvement of the design and assessment methods for URM walls made from modern hollow core clay bricks. Quasi-static cyclic tests were performed to test two series of URM walls at both full-scale and half-scale in increasing drift demands by governing boundary conditions. By examining test results obtained and wall tests from literature, an empirical equation was established to predict the ultimate drift capacity of URM walls, taking boundary conditions, size effect and aspect ratio into account. Limit states corresponding to typical points on global force-displacement curve and deformation parameters to be utilized for mechanical and numerical models of masonry walls were identified. Consequently, based on these outcomes, a new mechanical model was set up to accurately simulate non-linear response of flexural dominated URM walls up to the limit state of Near Collapse [15].

2.2. Seismic responses of masonry walls

According to post-earthquake damage surveys, it has been observed that seismic responses of masonry walls based on both in-plane and out-of-plane occur simultaneously and local damage mechanisms are mainly dominated by out-of-plane response of masonry walls due to overturning of portions of walls in large scale as shown in Figure 2.1.

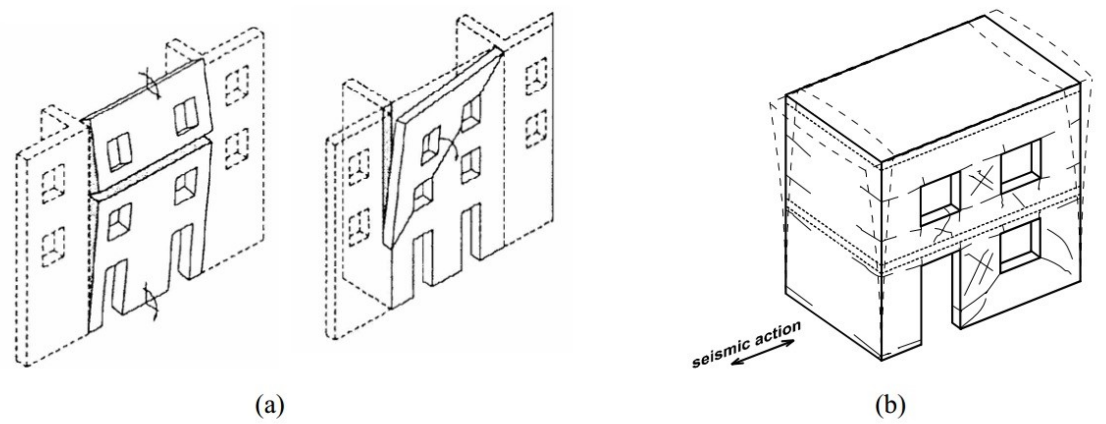

Figure 2.1. (a) local damage mechanisms [8] , (b) global response mechanism [16].

In masonry structures, poor connections between orthogonal walls and vulnerable clamping between bearing walls and floors give rise to the local damage mechanism characterized by out-of-plane response [16]. An accurate seismic performance of masonry structures can only be carried out by preventing out-of-plane responses. As a result, the global response of the structure occurs [12]. For existing unreinforced masonry buildings, the global behaviour can be performed by means of proper elements (ties, rods etc) strengthening connections. In presence of these required conditions that links to the global behaviour, in-plane walls satisfy adequate resistance to structural collapse [7].

2.3. Walls subjected to face loads

One of the main reasons lying behind the demolition of unreinforced masonry buildings is the collapse of out-of-plane walls subjected to face loads, when a timber floor and roof are supported by these walls. Robustness of connections (between bearing walls) and the interlock (between bearing walls and diaphragms), and the type of diaphragm have a significant effect on the seismic performance of the face-loaded URM walls. Under face loads, the responses of walls that have different type of diaphragm and connections between them are illustrated in Figure 2.2.

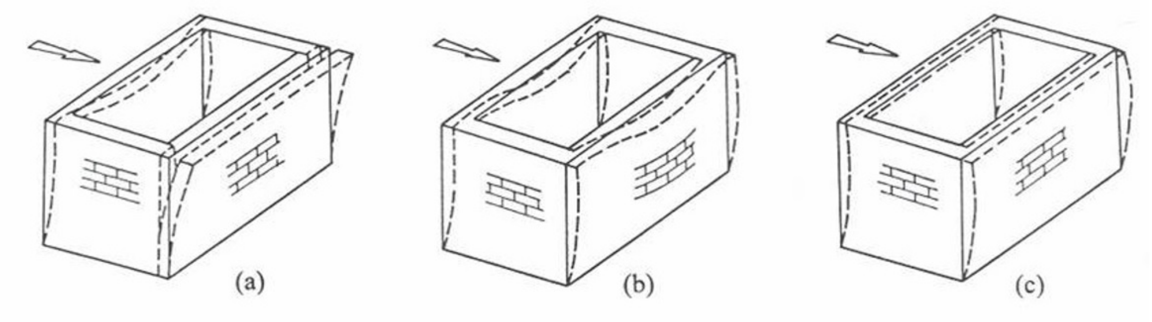

Figure 2.2. a) inferior wall-to-wall connection and no diaphragm, b) good wall-to-wall connection and ring beam with flexible diaphragm, c) good wall-to-wall connection and rigid diaphragm [17].

In presence of poor connection between Gamble end wall sitting at the end of buildings with pitched roofs and the roof or ceiling, the wall will act as a free cantilever. Therefore, this behaviour makes it vulnerable to collapse and causes one of the common sorts of out-of-plane failure of gable walls [17]. In addition, out-of-plane demands are largest at the upper level of walls, but its capacity is lowest in these areas as vertical loads acting on them decreases. Hence, the overturning of walls begins from the top if these are not properly connected to the diaphragm.

Figure 2.3. Out-of-plane instability of the wall subjected to face load due to a lack of ties between the face-loaded wall and rest of the structure [17].

Tomazevic (1999) demonstrated that out-of-plane vibration of URM walls is more apparent at the top floor level. That is stemmed from the lack of overburden load on the walls and amplification of earthquake shaking at that level [18].

2.4. Walls subjected to in-plane loads

In-plane walls may be described as structural members resisting lateral forces acting parallel to their wall lengths and categorized into two main groups namely unpenetrated and penetrated walls. With regards to unpenetrated walls, if the wall height is larger than length, it is called solid wall but if not so, it is termed squat wall. Main difference between them as well as their aspect ratio is the behaviour under lateral forces. Solid walls behave as cantilevered vertical flexural elements and principally withstand lateral forces with flexural mechanisms, whereas the latter withstands lateral forces with shear mechanisms. Penetrated walls can be defined as a system consisting of piers, vertical structural elements, and spandrels, horizontal structural elements, connecting piers to each other. If spandrels have adequate stiffness in bending, piers can be assumed to be fully restrained against rotation at their both ends. If the wall has relatively large openings, it demonstrates the behaviour of a cantilevered shear element from the foundation. Pier deformations give rise to storey drifts with little rotations of the storey level [19].

Damage occurring in URM walls under in-plane seismic effects is less significant than damage because of out-of-plane seismic effects. The major failure modes that govern the global seismic response of in-plane walls to the seismic excitation can be classified into 4 groups namely rocking, diagonal shear cracking, sliding shear and toe crushing. Under in-plane earthquake shaking, one or the combination of these failure modes have been observed in piers, in parallel to this, spandrels also have some of them including diagonal shear cracking, joint sliding and unit cracking failure modes. The potential in-plane failure modes occurring in penetrated and unpenetrated walls are illustrated in Figure 2.4.

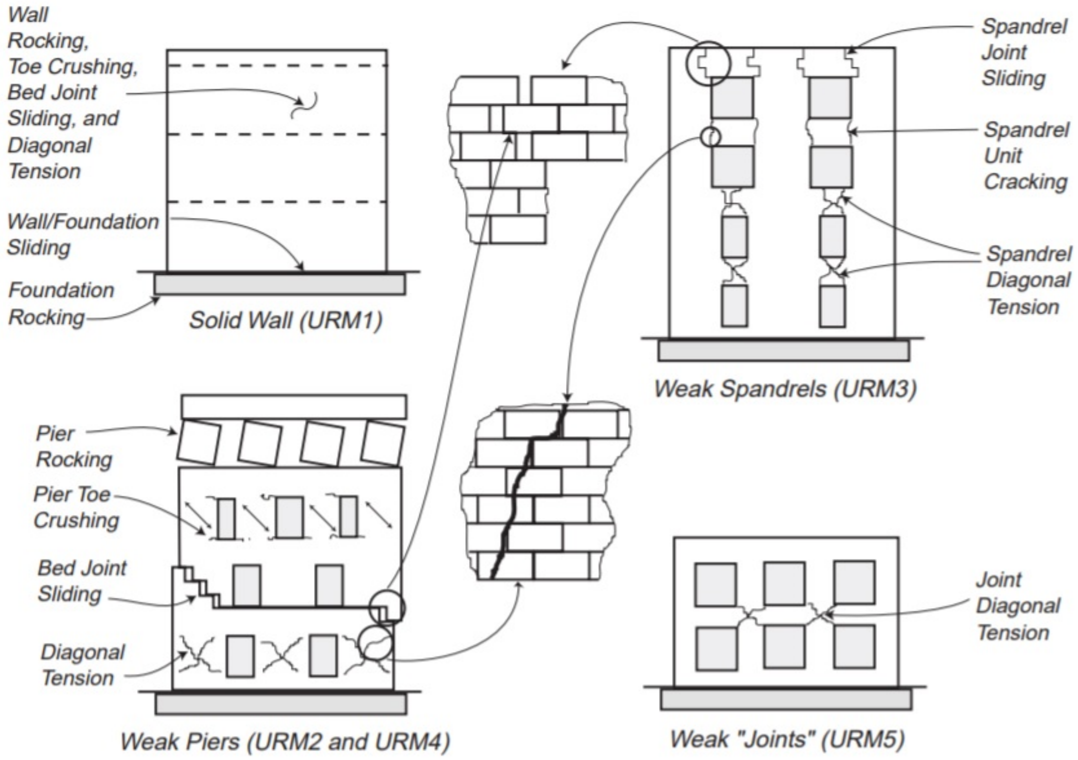

Figure 2.4. In-plane failure mechanisms of URM walls [20].

2.5. In-plane capacity of URM walls

Mechanism of lateral resistance is primarily affected by the pier geometry, boundary conditions, the volume of lateral loads and the properties of masonry components (mortar, unit and mortar-unit interface). Flexural response is prone to be characterized by rocking of piers and failure is mostly dominated by shear either diagonal tensile mode or sliding [7].

In an attempt to enable masonry structures to demonstrate non-linear behaviour and reach limit states accurately, the definition of the in-plane capacity of structural masonry is a crucial phase. Therefore, equations proposed by codes or experimental studies giving the strength capacity of URM walls for diagonal tension, rocking, bed-joint sliding and toe crushing should be carefully evaluated and the lower value of strength capacity should be taken into account in calculations.

2.5.1. Diagonal tensile capacity

If principal stresses emerging due to dynamic excitation exceed the tensile strength of walls or piers, diagonal cracks develop and diagonal tension failure mode occurs. Since this type of failure brings about a sudden reduction in stiffness and strength after the cracks develops, it is seen as one of the unwelcome failure modes. Inclined diagonal cracks may advance in either a stair- step pattern along the bed and head joints depending on the relative strength of masonry components or a straight diagonal path along masonry units. The first action is observed in case of weak mortar in terms of tensile strength relative to unit, otherwise the latter is observed. If the wall has an aspect ratio (L/h) larger than 1.5, less tensile strength and high axial stresses, diagonal tension failure is more likely to occur [19].

According to NZSEE (2015), the maximum diagonal tensile strength of URM walls is calculated, as shown below.

$$V_{dt} = f_{dt} A_n \beta \sqrt{1 + \frac{f_a}{f_{dt}}} \tag{2.1}$$

where f_{dt} is the masonry diagonal tension strength, A_n is the area of net mortared/ grouted section of the wall web, f_a is the axial compression stress due to gravity loads at the base of the wall, and β is a factor to correct nonlinear stress distribution. Take $\beta = 0.67$ when h_{eff}/L >1.5, $\beta = 1$ when h_{eff}/L <0.5, and linear interpolation is used for intermediate values.

According to Italian code (2003), the equation below was originally developed by Turnsek and Sheppard (1980) [21].

$$V_u^f = \frac{1.5 f_{v0d} D t}{\xi} \sqrt{1 + \frac{\sigma_0}{1.5 f_{v0d}}} \tag{2.2}$$

where f_{v0d} is the design shear strength with no axial force, σ_0 the mean vertical stress due to gravity loads, D is the pier width, t is the pier thickness, and ξ is the coefficient dependent on pier aspect ratio (1.5 if h_{eff}/D >1.5; h_{eff}/D if 1≤ h_{eff}/D ≤1.5; 1 if h_{eff}/D <1).

According to FEMA 356,

$$V_{dt} = f'_{dt} A \frac{L}{h_{eff}} \sqrt{1 + \frac{p}{f'_{dt}}} \tag{2.3}$$

where f'_{dt} is the lower bound masonry diagonal tension strength, A is the area of cross section, h_{eff} is the effective wall height, L is the wall length, and p is the mean compressive stress on the wall.

2.5.2. Rocking capacity

Under sustained cyclic loading, rocking of URM piers may end up with the crushing of pier end zones, and the delamination of units (brick) is observed in case of weak mortar. The rotation of entire piers causes the damage to the building [17]. Experimental investigations carried out have demonstrated that URM elements, whose failure mode is rocking, have significant displacement capacity, low levels of hysteretic energy dissipation and limited strength reduction. If the wall has an aspect ratio (L/h) less than 1, adequate mortar strength and light amount of axial stresses, rocking failure is more likely to occur. When the lateral force attains a value of $PL/2h$, rocking will develop about the pier toe [19].

According to NZSEE 2015, the rocking capacity of URM walls is calculated, as shown below.

$$V_r = 0.9(\alpha P + 0.5P_w)\frac{L_w}{h_{eff}} \tag{2.4}$$

where α is a factor equal to 0.5 for fixed-free cantilever wall or equal to 1 for fixed-fixed wall pier, P is the dead and superimposed dead load at top of the wall, P_w is the self-weight of the wall, L_w is the wall length, and h_{eff} is the wall effective height.

According to Magenes *et al.* (1997),

$$V_r = \frac{D^2 t}{H_0}\frac{p}{2}(1 - \frac{p}{\kappa f_u}) \tag{2.5}$$

where D is the pier length, t is the pier thickness, p is the mean vertical stress on the pier due to axial load P, H_0 is the effective pier height, κ is the coefficient related to vertical stress distribution (=0.85 due to the assumption of equivalent rectangular stress block), and f_u is the compressive strength of masonry.

According to Eurocode 6, the strength is described in terms of ultimate moment Mu that may be approached to a proper stress distribution for the masonry in compression, neglecting tensile strength [22]. This equation was derived from Equation 2.4.

$$M_u = \frac{\sigma_0 D^2 t}{2}(1 - \frac{\sigma_0}{\kappa f_d}) \tag{2.6}$$

where σ_0 is the mean vertical stress, D is the pier length, t is the pier thickness, κ is the coefficient related to vertical stress distribution (=0.85 due to the assumption of equivalent rectangular stress block), and f_d is the design compressive strength of masonry.

According to FEMA 356,

$$V_r = 0.9\alpha P_E \frac{L}{h_{eff}} \tag{2.7}$$

where P_E is the expected axial compressive force due to gravity loads, L is the wall or pier length, h_{eff} is the effective wall or pier height, and α is a factor equal to 0.5 for cantilever wall, equal to 1 for fixed-fixed wall.

2.5.3. Sliding (bed-joint and slip plane) shear capacity

Experimental investigations carried out have demonstrated that URM elements with an aspect ratio (L/h) larger than 1.5, whose failure mode is bed-joint sliding, have significant displacement capacity, high levels of hysteretic energy dissipation due to frictional resistance emerging between masonry components and limited strength reduction. This type of failure mode may demonstrate either a concentrated deformation at a few bed joints or a distributed deformation throughout several bed joints. The type of deformation observed is characterized by cohesion ratio and frictional coefficient. The equations for sliding shear strength are given below.

According to NZSEE 2015, bed-joint sliding is defined, as shown in Equation 2.8.

$$V_s = 0.7(t_{nom} L_w c + \mu_f (P + P_w)) \tag{2.8}$$

where t_{nom} is the nominal thickness of wall, L_w is the wall length, c is the masonry bed-joint cohesion, μ_f is the friction coefficient, P is the superimposed and dead load at top of wall/pier, and P_w is the self-weight of wall and pier. Slip plane sliding strength can be derived from Equation 2.7 where c is adopted as zero.

According to Italian code (2003), the equation for sliding shear was originally proposed by Magenes *et al.* (1997).

$$V_u^s = \frac{\frac{3}{2} f_{v0d} + \mu \frac{\sigma_0}{\gamma_m}}{1 + \frac{3H_0}{D\sigma_0} f_{v0d}} Dt \tag{2.9}$$

where f_{v0d} is the design shear strength with no axial force, σ_0 is the mean vertical stress due to gravity loads, μ is the coefficient of friction, γ_m is the safety factor (equal to 2), D is the pier length, t is the pier thickness, and H_0 is the effective pier height [23].

According to FEMA 356, bed-joint shear strength is proposed below.

$$V_{bjs} = 0.5(0.75 \upsilon_{te} A_n + P_{CE}) \tag{2.10}$$

where υ_{te} is the average bed-joint shear strength, A_n is the area of net mortared/grouted section of a wall/pier, and P_{CE} is the expected gravity compressive force.

According to Eurocode 8.3, for masonry elements under shear force, shear capacity can be calculated using the equation defined below [24].

$$V_f = f_{vd} D' t \tag{2.11}$$

where, D' is the depth of the compressed area of the wall, t is the wall thickness,and f_{vd} is the masonry shear strength in presence of vertical load and equal to $f_{vm0} + 0.4N/D't \leq 0.065f_m$, where f_{vm0} is the mean shear strength in the absence of vertical load, and f_m is the mean compressive strength.

2.5.4. Toe crushing capacity

For the walls with an aspect ratio (1<L/h<1.5), a significant increase in strength has been observed after the formation of flexural cracks at the heel of wall as a result of vertical compressive force moving towards the toe. As cracks develop, a nonlinear force-deformation relation starts with softening of URM walls, and a rapid degradation in stiffness and strength occur. If the shear capacity is not attained, the ultimate limit state is governed by toe crushing which is a force based failure mode [25]. The equations defined for toe crushing strength are given below.

According to NZSEE 2015,

$$V_{tc} = (\alpha P + 0.5P_W)(\frac{L_w}{h_{eff}})(1 - \frac{f_a}{0.7f'_m}) \tag{2.12}$$

where α is a factor equal to 0.5 for fixed-free cantilever wall or equal to 1 for fixed-fixed wall pier, P is the superimposed and dead load at top of wall/pier, P_W is the self-weight of wall and pier, L_w is the wall length, h_{eff} is the effective height of pier/wall, f_a is the axial compression stress due to gravity load at mid-span, and f'_m is the masonry compressive strength.

According to FEMA 356,

$$V_{tc} = \alpha P_L(\frac{L}{h_{eff}})(1 - \frac{f_a}{0.7f'_m}) \tag{2.13}$$

where P_L is the lower bound axial compressive force due to gravity loads.The variables of Equation 2.13 are also represented in Equation 2.12. Both are similarly generated.

2.6. Mechanical material properties of masonry

As it has been described in Section 2.1, the seismic response of URM buildings is substantially influenced by boundary conditions, aspect ratio of masonry elements and the behaviour of connections between bearing elements. In order to improve the reliability of seismic assessment and numerical models established for simulating seismic behaviour of URM buildings, on-site testing of material properties is to be performed. Primarily, two methods are utilized, namely field sampling and field testing of URM components. Field sampling applies to the extraction of prisms from an existing building for following testing offsite, whereas the latter method includes in-situ material testing where flat jack, bond wrench and hydraulic jack devices are used to determine compressive strengths and elastic modulus in compression, flexural tensile strength, and shear strength of URM components, respectively.

Furthermore, it is known that masonry structures are vulnerable to natural hazards such as earthquakes and landslides, and they are susceptible to aggressive environments which cause aging and degradation of materials throughout their lifespan. Therefore, the physical condition of existing masonry components and their connections should be evaluated to detect the damage and deterioration level of masonry units, mortars and grouts. The specific objectives of a condition assessment are to:

- Investigate the condition of components and the presence of any degradation.
- Verify the arrangement of components and the continuity of load transfer between components, elements and systems.
- Survey adjacent party walls and structures, existence of non-structural components and restrictions for rehabilitation.

Condition assessment of URM structures can be carried out by means of visual examination, non-destructive tests and supplemental tests. Visual examination is the quickest applicable one between them in order to obtain a general information regarding apparent condition states of masonry materials and quality of construction. This technique also determines if other test methods are required for further investigations.

In case of a need for more advanced assessment, non-destructive tests are highly suggested since they offer several advantages in implementation such as their minimum physical intervention and respect of the original construction. Non-destructive testing can be categorized into four major groups namely ultrasonic pulse velocity, mechanical pulse velocity, impact echo and radiography. Ultrasonic pulse velocity enables detecting changes in the density and modulus of masonry materials. However, ultrasonic methods cannot be performed if masonry structures under investigation hold poor quality and a great number of cracks. In addition to this, ultrasonic pulse has a high frequency but low energy content, thus it cannot reach long travel distances. Due this drawback, the mechanical pulse methods should be performed instead of ultrasonic methods to determine overall mean properties of masonry with huge portions. Another technique named impact echo is useful for detecting the void areas taking part in grouted reinforced walls while radiography technique can be utilized to determine the location of reinforcing steels in masonry walls. Apart from visual examination and non-destructive testing techniques described above, supplemental tests, classified as destructive methods, can be used for condition assessment of masonry structures as well. They are significant tools to identify material properties and, the seismic response of both in-plane and out-of-plane masonry walls. However, they give rise to high cost and significant local damage where they set up [19].

Based on visual observations and findings obtained from experimental studies, probable masonry material properties have been compiled and presented in the relevant tables of some codes such as Italian code (NTC 2008), NZSEE 2015 and FEMA274. In the absence of a comprehensive testing programme, these values proposed in the codes can be used for the assessment of URM structures.

2.6.1. Material properties of masonry defined in NZSEE 2015

Probable material strength parameters for clay bricks and lime/cement mortars are presented in Figure 2.5 and Figure 2.6, respectively, based on a simple scratch test against hardness of components. It is important to make sure that segregated material surface is removed before assessing hardness characteristics of components.

Brick hardness	Brick description	Probable brick compressive strength, f'_b (MPa)	Probable brick tensile strength, f_{bt} (MPa)
Soft	Scratches with aluminium pick	14	1.7
Medium	Scratches with 10 cent copper coin	26	3.1
Hard	Does not scratch with above tools	35	4.2

Figure 2.5. Probable strength parameters for clay bricks [17].

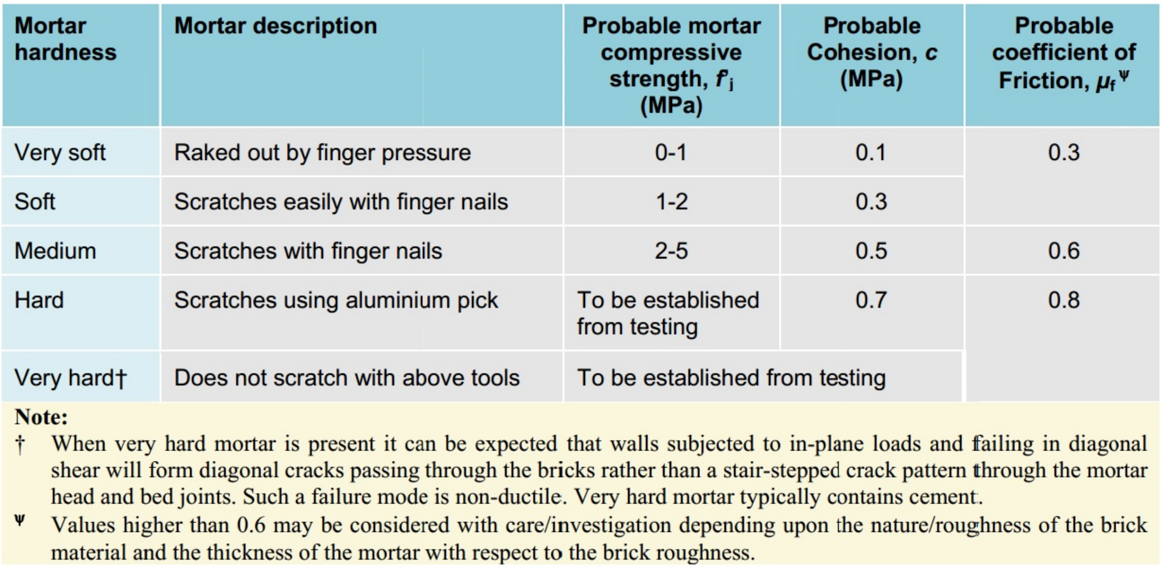

Mortar hardness	Mortar description	Probable mortar compressive strength, f'_j (MPa)	Probable Cohesion, c (MPa)	Probable coefficient of Friction, $\mu_f{}^{\Psi}$
Very soft	Raked out by finger pressure	0-1	0.1	0.3
Soft	Scratches easily with finger nails	1-2	0.3	
Medium	Scratches with finger nails	2-5	0.5	0.6
Hard	Scratches using aluminium pick	To be established from testing	0.7	0.8
Very hard†	Does not scratch with above tools	To be established from testing		

Note:

† When very hard mortar is present it can be expected that walls subjected to in-plane loads and failing in diagonal shear will form diagonal cracks passing through the bricks rather than a stair-stepped crack pattern through the mortar head and bed joints. Such a failure mode is non-ductile. Very hard mortar typically contains cement.

Ψ Values higher than 0.6 may be considered with care/investigation depending upon the nature/roughness of the brick material and the thickness of the mortar with respect to the brick roughness.

Figure 2.6. Probable strength parameters of mortar [17].

The probable modulus of rapture of clay bricks can be calculated using the equation given below.

$$f'_r = 0.12 f'_b \tag{2.14}$$

The probable compressive strength of masonry can be calculated using Equation 2.15 given below. using the equation given below.

$$f'_m = \begin{cases} 0.75 f'^{0.75}_b f'^{0.3}_j & \text{for } f'_j \geq 1MPa \\ 0.75 f'^{0.75}_b & \text{for } f'_j < 1MPa \end{cases} \tag{2.15}$$

Brick and mortar compressive strength values used in Equation 2.15 are presented in Figure 2.7.

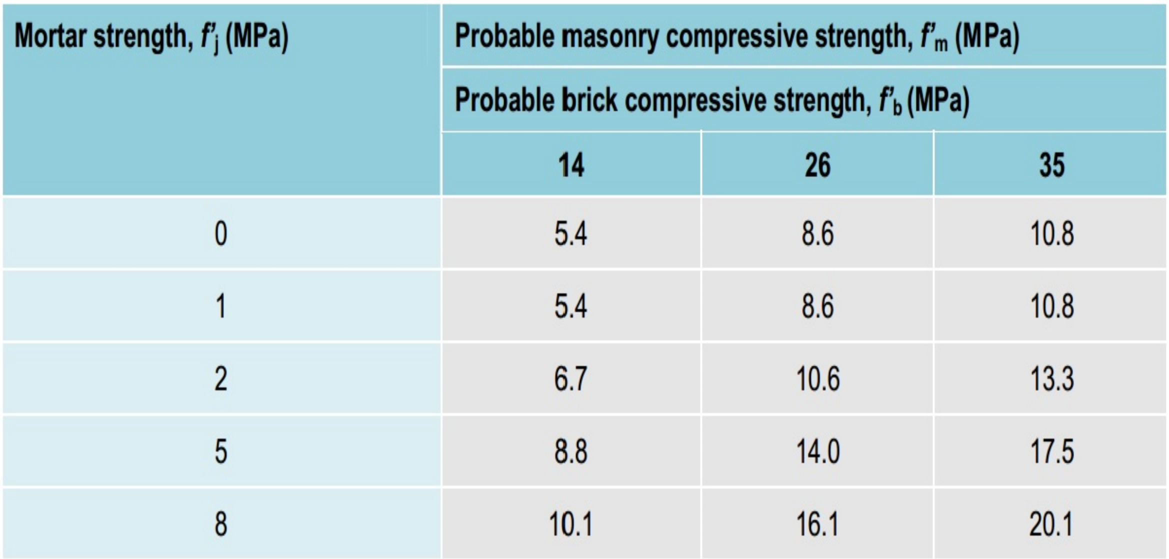

Mortar strength, f'_j (MPa)	Probable masonry compressive strength, f'_m (MPa)		
	Probable brick compressive strength, f'_b (MPa)		
	14	26	35
0	5.4	8.6	10.8
1	5.4	8.6	10.8
2	6.7	10.6	13.3
5	8.8	14.0	17.5
8	10.1	16.1	20.1

Figure 2.7. Probable compressive strength of brick masonry [17].

The probable diagonal tensile strength of masonry can be calculated using Equation 2.16 given below.

$$f_{dt} = 0.5c + f_a \mu_f \tag{2.16}$$

where c is the masonry bed-joint cohesion, f_a is the axial compression stress due to gravity loads, and μ_f is the masonry co-efficient of friction. Using Equation 2.17 and 2.18, Elasticity modulus and Shear modulus of clay brick masonry can be calculated, respectively.

$$E_m(MPa) = 300 f'_m \tag{2.17}$$

$$G_m(MPa) = 0.4 E_m \tag{2.18}$$

2.6.2. Material properties of masonry defined in FEMA 356

Initially, default lower bound values of material properties are presented in Figure 2.8, based on three types of masonry condition namely good, fair and poor. Figure 2.9 demonstrates factors that will be used to convert lower bound masonry properties into probable strength masonry properties.

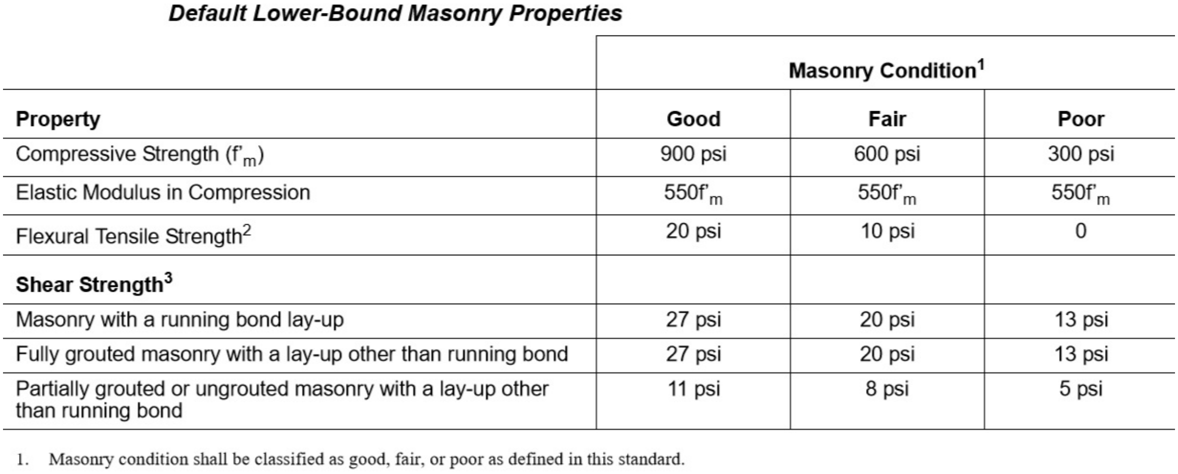

Default Lower-Bound Masonry Properties

	Masonry Condition[1]		
Property	**Good**	**Fair**	**Poor**
Compressive Strength (f'_m)	900 psi	600 psi	300 psi
Elastic Modulus in Compression	$550f'_m$	$550f'_m$	$550f'_m$
Flexural Tensile Strength[2]	20 psi	10 psi	0
Shear Strength[3]			
Masonry with a running bond lay-up	27 psi	20 psi	13 psi
Fully grouted masonry with a lay-up other than running bond	27 psi	20 psi	13 psi
Partially grouted or ungrouted masonry with a lay-up other than running bond	11 psi	8 psi	5 psi

1. Masonry condition shall be classified as good, fair, or poor as defined in this standard.

Figure 2.8. Default lower-bound masonry properties [25].

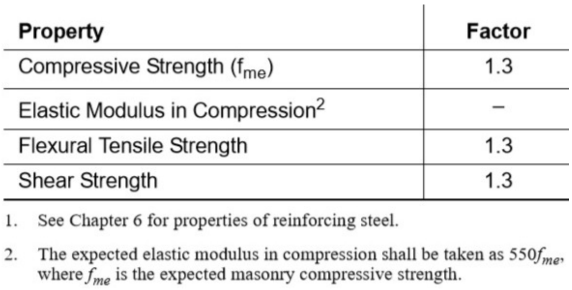

Property	Factor
Compressive Strength (f_{me})	1.3
Elastic Modulus in Compression[2]	–
Flexural Tensile Strength	1.3
Shear Strength	1.3

1. See Chapter 6 for properties of reinforcing steel.
2. The expected elastic modulus in compression shall be taken as $550f_{me}$, where f_{me} is the expected masonry compressive strength.

Figure 2.9. Factors to convert lower bound masonry properties into expected strength masonry properties [25].

Using Equation 2.19 and 2.20, expected Elasticity modulus and Shear modulus of masonry can be calculated, respectively.

$$E_{me}(MPa) = 300f'_{me} \tag{2.19}$$

$$G_{me}(MPa) = 0.4E_{me} \tag{2.20}$$

where f_{me} is the expected masonry compressive strength.

2.6.3. Material properties of masonry defined in Italian Code (NTC 2008)

According to the most common masonry typologies, reference values of mechanical material properties and average specific densities of masonry are presented in Figure 2.10.

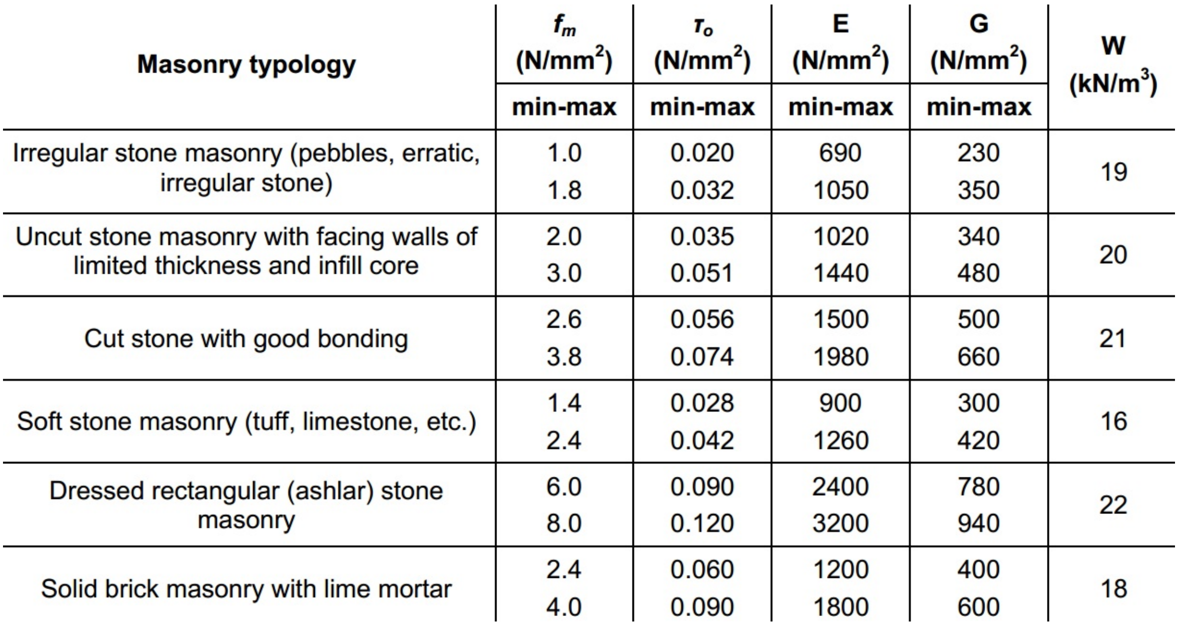

Masonry typology	**f_m (N/mm^2)**	**τ_o (N/mm^2)**	**E (N/mm^2)**	**G (N/mm^2)**	**W (kN/m^3)**
	min-max	**min-max**	**min-max**	**min-max**	
Irregular stone masonry (pebbles, erratic, irregular stone)	1.0 1.8	0.020 0.032	690 1050	230 350	19
Uncut stone masonry with facing walls of limited thickness and infill core	2.0 3.0	0.035 0.051	1020 1440	340 480	20
Cut stone with good bonding	2.6 3.8	0.056 0.074	1500 1980	500 660	21
Soft stone masonry (tuff, limestone, etc.)	1.4 2.4	0.028 0.042	900 1260	300 420	16
Dressed rectangular (ashlar) stone masonry	6.0 8.0	0.090 0.120	2400 3200	780 940	22
Solid brick masonry with lime mortar	2.4 4.0	0.060 0.090	1200 1800	400 600	18

Figure 2.10. Reference values of material properties for several masonry typologies [16].

2.7. Modelling Techniques for URM walls

The structural assessment of masonry has always been a challenging task due to its connatural complexity and uncertainty. These drawbacks have led engineers to develop effective modelling approaches. Finite Element Modelling (FEM) technique in all proposed approaches has been a more reliable and preferred tool for the analysis of URM structures. This is because FEM technique provides an opportunity to simply define all geometric configurations of masonry structures in modelling, and offers a considerable versatility in adopting various constitutive laws [26].

Lourenco (1996) made a significant contribution to the FEM technique, proposing three approaches namely detailed micro-modelling, simplified micro-modelling and macro-modelling. As seen in Figure 2.11, the three modelling approaches differ from each other with their level of refinements.

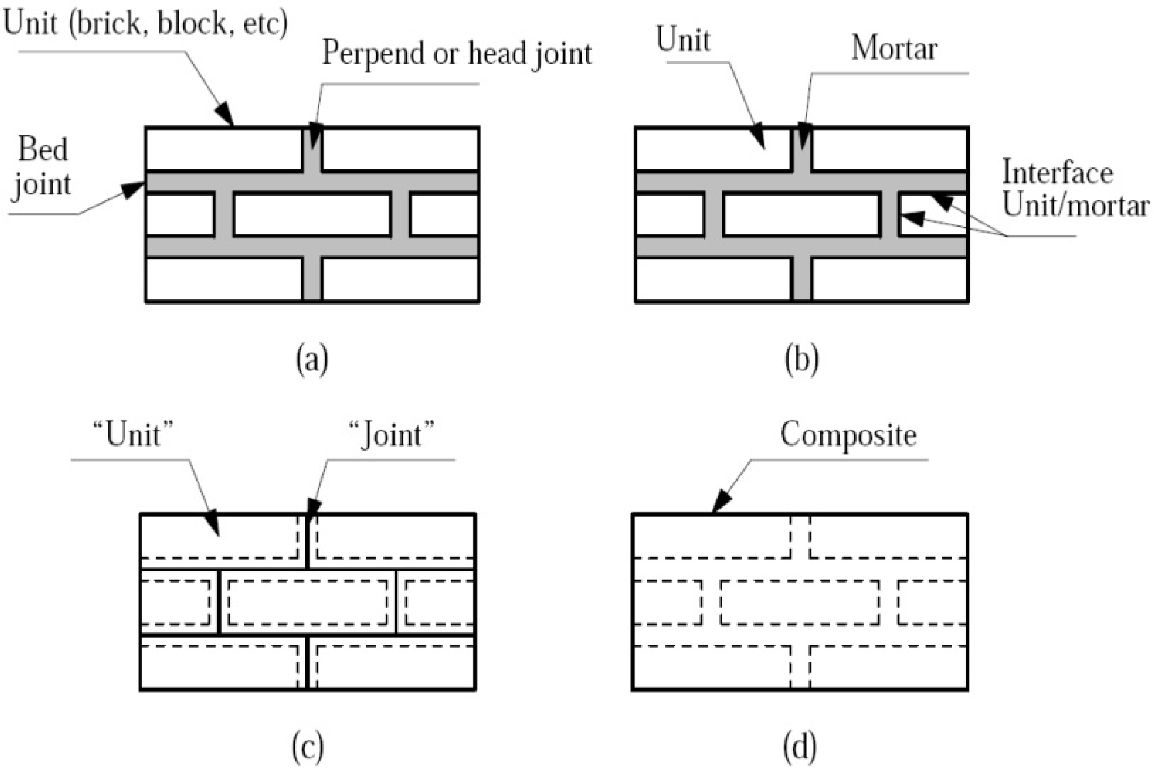

Figure 2.11. Modelling approaches for masonry structures (a) masonry sample, (b) detailed micro-modelling, (c) simplified micro-modelling, (d) macro-modelling [6].

Detailed micro-modelling includes discrete units and mortars characterized by continuum elements but unit-mortar interface characterised by discontinues elements. In simplified micro-modelling, expanded units are characterized by continuum elements whereas the behaviour of the mortar joints and unit-mortar interface is lumped in discontinuous elements. In Macro-modelling, all components of masonry are smeared out in the continuum [6].

2.7.1. Micro-modelling technique

Masonry components (units, mortar, and unit-mortar interfaces) are modelled on an individual basis. This discretisation of masonry composites constitutes a number of finite elements, which have accordingly different mechanical properties. Therefore, their complex behaviours are involved in analyses.

In order to accurately determine mechanical properties of masonry materials, there is a highly need for a great amount of data and comprehensive test programme. That is because every constituent has its distinct material property such as Elasticity Modulus, Poisson's ratio, etc. Besides, the dimension of units, arrangement of bed and head joints, craftsmanship quality and environmental conditions are major factors, which influence the accuracy of assessment of masonry structures. Hence, in-situ examination is required before applying detailed micro-modelling technique.

Regarding simplified micro-modelling technique, the size of units is enlarged to keep the geometry unaffected. Instead of modelling masonry components separately, each joint is lumped into an average interface and thus Poisson's effect of mortar is neglected. Therefore, the crack patterns of panels are governed by interfaces, and cracks are observed throughout these interfaces when the cracking capacities have been attained [6].

Particularly, micro-modelling studies are necessary so as to have a better understanding of the local behaviour of masonry structures. In addition, this technique is more applicable for masonry with small portions, rather than large scale structures.

2.7.2. Macro-modelling technique

Instead of the discretization of masonry composites, a single composite material, consisting of units and mortar joints, and acting as a homogeneous anisotropic continuum, is considered in macro-modelling technique. It is more practical to model a whole structure using this approach due to reduced time, less computational effort and user-friendly mesh generation. Since the homogenization of masonry components is utilized to generate a macro-model of masonry, less material properties are needed. Thus, simple test methods or reference values (see Section 2.6) can be adequate to define masonry material properties for macro-model generation, instead of applying experimental work that requires high budget and extensive effort.

However, macro modelling approach may not be able to properly simulate the crack patterns governed by local failure modes. For example, stair-step pattern along the bed and head joints is observed, in case of weak mortar and strong unit. Due to masonry composites acting as homogeneous anisotropic continuum, this kind of pattern cannot be illustrated by macro-modelling technique. Despite this drawback, when an agreement between accuracy and efficiency is required, macro-modelling approach is the most valuable [6].

3. BUILDING INFORMATION

In this study, Kadikoy Health Care Center that will be under investigation is a registered historical masonry building in Istanbul, which was constructed in 1925. It consists of basement, ground and first floors with a base area of 569,44 m^2. Views of building are shown below.

a) Front view

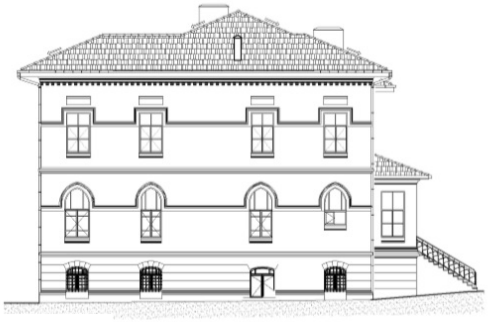

b) Rear view

Figure 3.1. Front view and rear view of the building, respectively.

When in-situ examination was carried out, it was observed that the building keeps its original form as seen in Figure 3.1. However, some interventions made were detected in the left facade where three window openings were converted into a large window by removal of the bearing walls between openings, as indicated in Figure 3.2. Besides, connection of intersecting walls and clamping between bearing walls and floor systems were detected in good condition. Therefore, proper conditions that may prevent the out-of-plane failure mechanism were observed during in-situ survey.

a) Right view

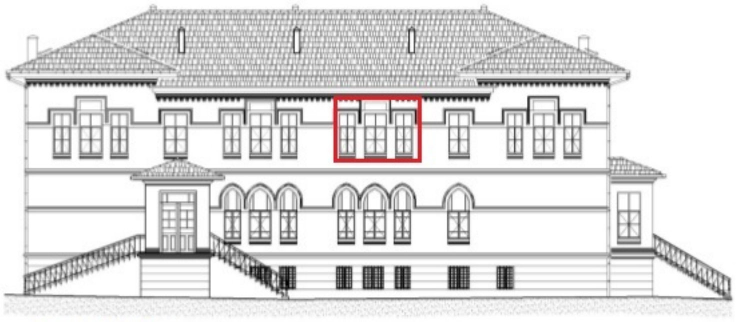

b) Left view

Figure 3.2. Right view and left view of the building, respectively.

Bearing walls are composed of solid bricks and Horosan type local mortar which is widely used in the construction of masonry structures in Turkey. Dimensional characteristics of the building are listed below.

- Plan measurements are 33.09 m in the longitudinal direction and 18.84 m in transversal direction.
- Storey heights of basement, ground and first floors are 3.45 m, 4.84 m and 4.45 m, respectively.
- The wall thicknesses vary between 68-88 cm in the basement, 45-76 cm in the ground floor and 32-65 cm in the first floor.
- The slabs of ground floor and 1st floor consists of brick arch floor systems, where the steel beams of INP180 are settled with an interval of 60 cm. The roof slab is made of oak timber elements.

As a summary of the structural features explained above, the plan of ground floor and load-bearing system details are demonstrated in Figure 3.3 and Figure 3.4, respectively.

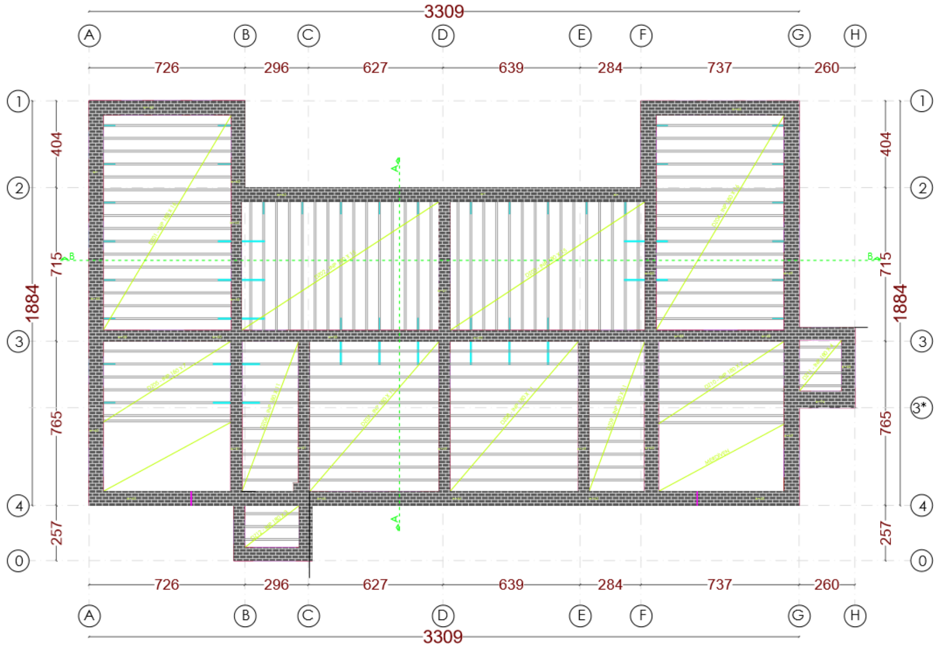

Figure 3.3. Plan of ground floor (dimensions are in centimetres).

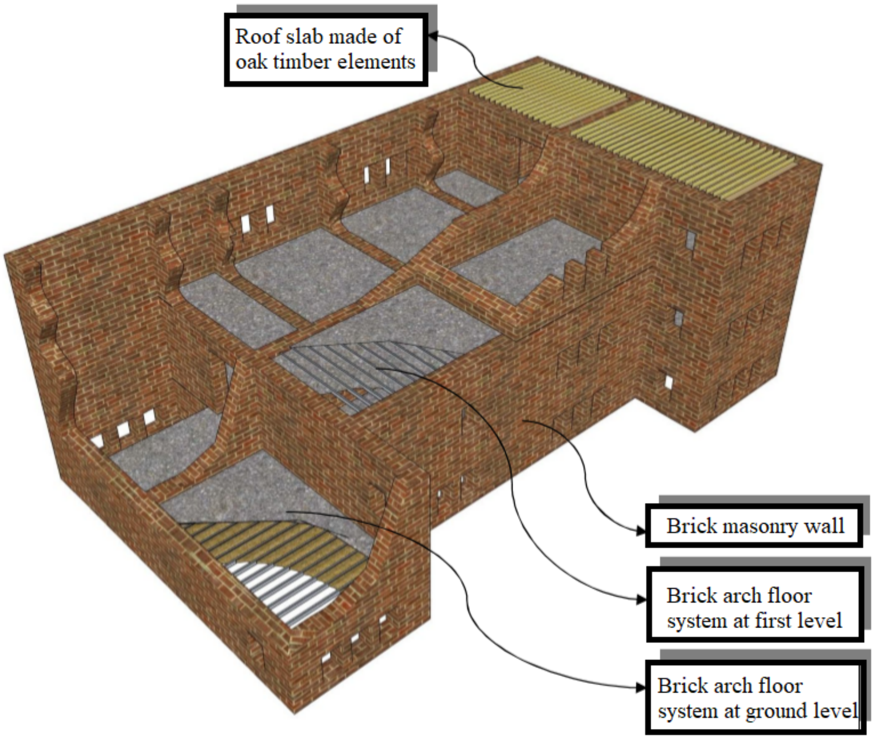

Figure 3.4. Illustration of load-bearing system of the URM building.

3.1. Material tests

In order to determine strength parameters of the URM walls, shear and compression tests were implemented by the owner both in-situ and in laboratory, and a detailed test report was presented. Three prisms at ground floor and two prisms at 1st floor were extracted from different locations of the masonry building, and afterwards these samples were loaded by hydraulic jacks for in-situ shear tests. In addition to in-situ tests, two another core samples were extracted from the masonry walls at ground floor and tested in laboratory conditions. Shear test results are presented in Table 3.1.

Table 3.1. Shear strength of masonry walls.

Sample No	**Location**	**Test Type**	**Shear Strength (MPa)**
Z-1	Ground Floor	In-situ	0.49
Z-2	Ground Floor	In-situ	0.68
Z-3	Ground Floor	In laboratory	0.32
Z-4	Ground Floor	In laboratory	0.58
Z-5	Ground Floor	In-situ	0.27
I-6	1^{st} Floor	In-situ	0.21
I-9	1^{st} Floor	In-situ	0.24

Average shear strengths of masonry walls for ground and 1^{st} floors can be calculated as 0.47 MPa and 0.23 MPa from the table, respectively. Due to the fact that strength values may vary from a sample to another one throughout the wall, strength values that are multiplied by reduction factors for safety should be considered in analyses. According to the test report, reduced shear strength values 0.2 MPa and 0.15 MPa were recommended by the owner for ground and 1^{st} floors, respectively.Finally, compression test was performed on brick-mortar samples, which were randomly extracted from different places of the floors to define the compressive strength of URM walls. The results obtained from the compression test are shown in Table 3.2. The compressive strength of the masonry wall is adopted as 5.65 MPa in calculations.

Table 3.2. Compressive strength of masonry walls.

Sample No	**Location**	**Test Type**	**Compressive Strength (MPa)**
1	Ground Floor	In laboratory	6.8
2	Ground Floor	In laboratory	4.5
3	1^{st} Floor	In laboratory	7.2

3.2. Site Investigation

Generally, site investigation aims at establishing parameters for foundation and substructure design, and evaluating the possible geotechnical, geologic and hydrological hazards to the environment and human life. The extent of the investigation must be sufficient to determine the physical and mechanical properties of soil in detail, since these properties will have a significant influence on the soil-structure interaction. The dynamic behaviour of structures is also dependent on the response of soil.

Therefore, a comprehensive site investigation was carried out by the owner to identify the mechanical and physical properties of soil and the foundation system of the structure. Basically, five boreholes, seismic refraction with four profiles, one resistivity and two microtremor measurements were performed so as to investigate the soil stratum. Based on findings obtained from the experimental study, a soil investigation report is presented in Table 3.3.

Table 3.3. The soil investigation report.

Soil Group			B
Local Site Class			Z2
Shear Wave Velocity		m/sec	705
Site Dominant Vibration Period	: T_0	sec	0,29
Spectrum Characteristics Periods		sec	T_A=0,15 T_B=0,40
Seismic Zone			1

In order to gather information about the foundation system of the building, an excavation work was performed. Stone strip foundation system was observed beneath the bearing walls, having 150 cm depth and a 20 cm-extension from both side of the wall, as indicated in Figure 3.5 below. Undisturbed stiff soil is in direct contact with the stone foundation.

Figure 3.5. Excavation work to determine the foundation system.

3.3. Ambient-Vibration based investigation

It is apparent that the assessment process of URM structures has been suffered from uncertainties and complexity based on the behaviour of structural masonry. Non-destructive tests can be more practical than other test methods in implementation, since they do not require excitation equipment and considerable physical intervention, and do not deteriorate structural integrity. Hence, full-scale Ambient Vibration Test (AVT) was implemented for the system identification of the building, using five Kinemetrics Episensors type accelerometers. Two sensors were placed on ground level and three sensors were placed on 1^{st} floor [27].

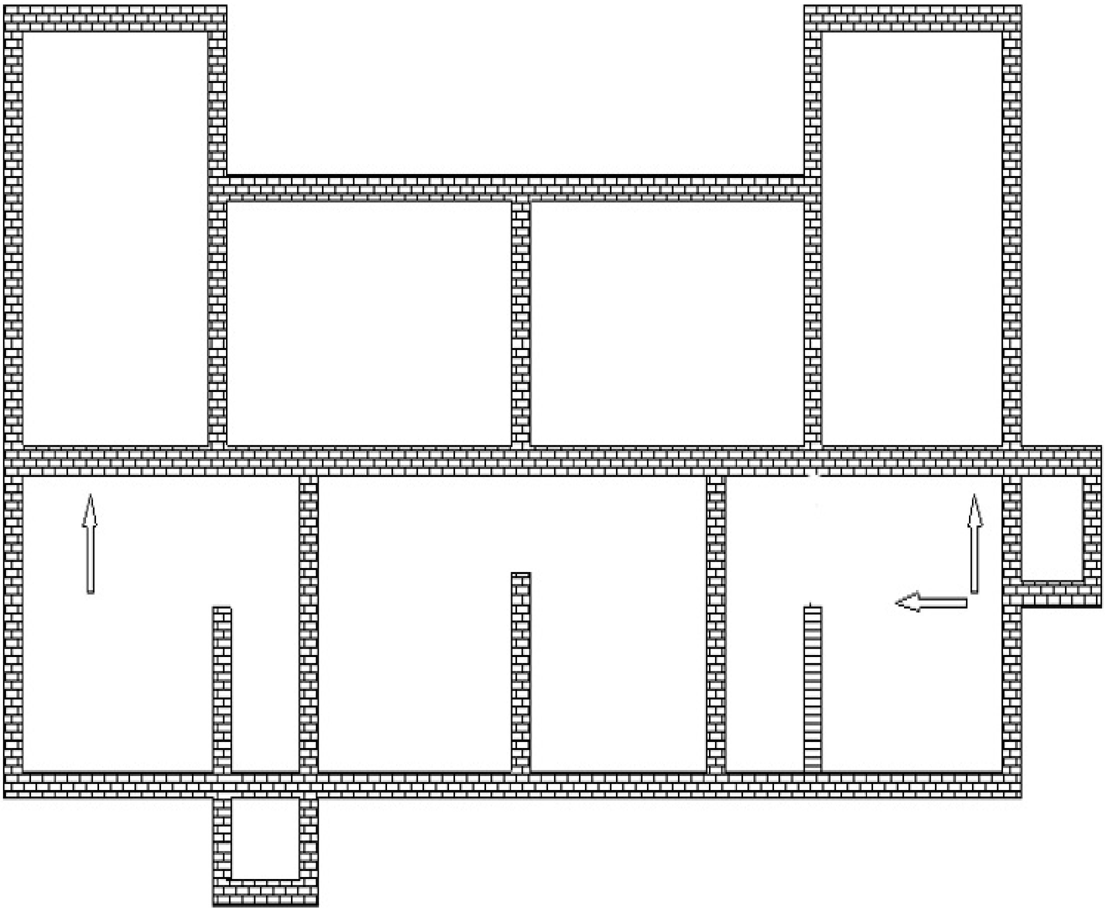

Figure 3.6. The directions and positions of sensors.

Following this, the global dynamic characteristics of the building was extracted from AVT by utilizing Frequency Domain Decomposition (FDD) which is an output-only technique in frequency domain. This procedure including the extraction of modal parameters from AVT is termed Operational Modal Analysis (OMA) in the literature. Figure 3.7 demonstrates Power Spectral Density (PSD) and modal frequency values obtained by means of FDD.

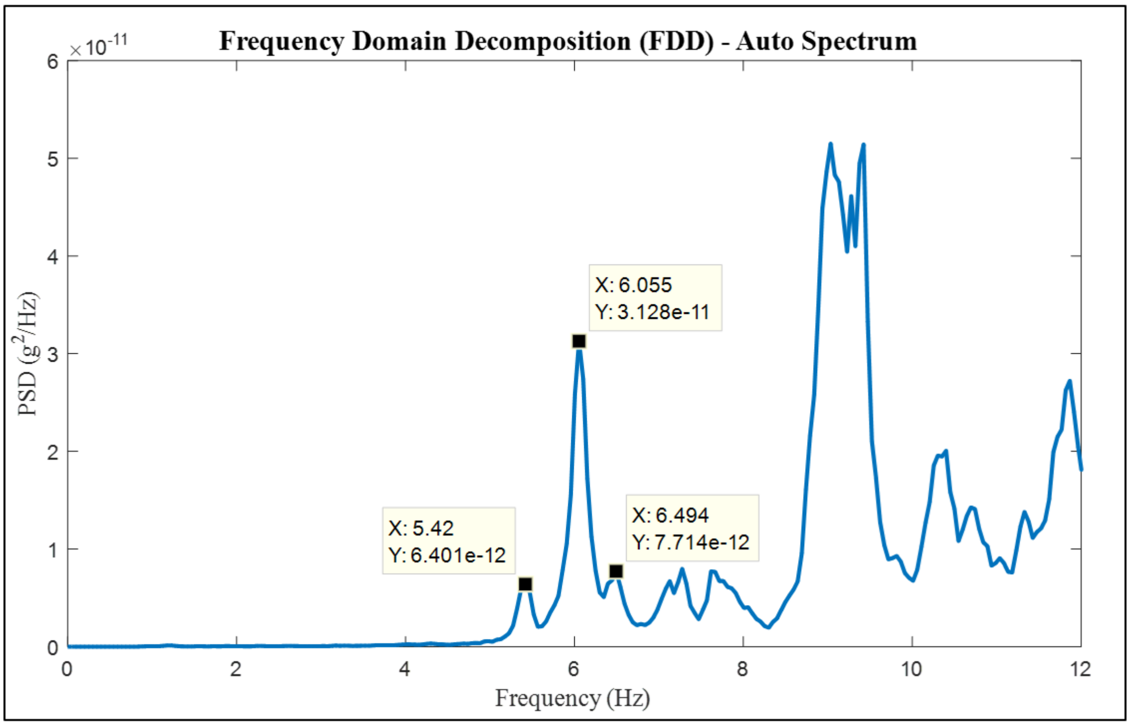

Figure 3.7. PSD of the acceleration data.

As a result of Operational Modal Analysis, modal frequencies obtained are as follows:

- Mode 1 (X) = 5.4 Hz
- Mode 1 (Y) = 6.0 Hz
- Mode 1 (T) = 6.45 Hz

For seismic performance assessment, identified dynamic parameters will be a reference to ensure whether the dynamic response of the structure is accurately simulated by conducting modal analysis, and will provide a basis for determining uncertain structural parameters of the model such as the Modulus of Elasticity.

4. FINITE ELEMENT MODELLING TECHNIQUE

Finite element models based on proper constitutive laws for the masonry components provide an accurate determination of the critical locations where the failure mechanisms occur, and a reliable simulation of force redistribution and coupling effect between orthogonal walls. Therefore, in this study, FEM technique was utilized in order to carry out the seismic performance assessment of the building by means of linear dynamic analysis.

4.1. Finite Element Model

A 3D Finite Element model of the entire building was generated with a total number of 12050 nodes, 11877 areas and 3994 frames, as shown in Figure 4.1. Two-dimensional shell with four nodes was used for building up the bearing walls and slabs. The beams settled with an interval of 60 cm in the slabs were modelled with frame elements. The bearing walls and slabs were divided into areas with a size of 60 x 60 cm to make space for door and window openings.

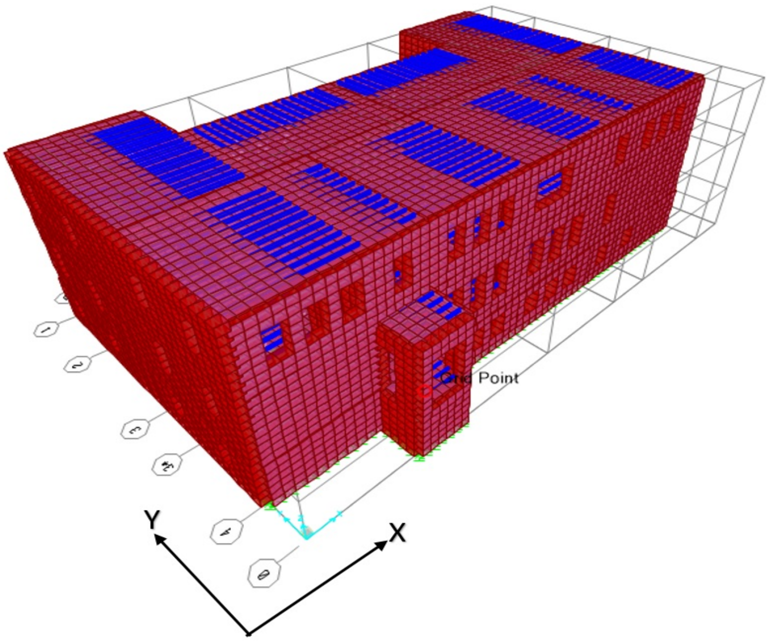

Figure 4.1. 3D Finite Element model of the entire building.

- The specific weights of materials γ_{wall}, γ_{slab}, $\gamma_{roof(oak)}$ and were adopted as 20 kN/m^3, 15 kN/m^3 and 8 kN/m^3 in the calculation of dead loads (G), respectively.
- Live loads (Q) acting on ground floor, 1st floor and roof floor were adopted as 3.5 kN/m^2, 3.5 kN/m^2 and 2.25 kN/m^2 according to EN 1991-1-1 for category C3 and category A [28].
- Mass source was defined as a combination of self-weight due to dead loads and specified load pattern (Live Load) multiplied by a coefficient of 0.3 according to EN1998-1 [29].

The summary of load patterns and material weights used in the model are listed above. At the first stage of modelling, the initial material properties presented in Chapter 3 were used, afterwards the determination procedure of uncertain structural parameters based on model updating is highlighted.

In the assessment of URM structures, it has always been a difficult task to anticipate the condition of clamping between bearing walls and floors, and the influence of floor systems on rigid diaphragm. Therefore, it is required to gradually investigate the change in each phase while modelling. The changes in modal frequency, period and modal participating mass ratio of the structure were examined under six different cases in an attempt to set up an accurate finite element model. For each case, all joints on the interaction surface between the foundation and soil were assumed to be fully restrained. The assignment of soil springs in vertical direction will be investigated afterwards.

Table 4.1. The completion level of the finite element model for each case. The columns corresponding to completed assignments are marked and others left blank.

CASE	WALLS	BEAMS	SLABS	DIAPHRAGM	OPENINGS	W/O OPENINGS
Case 1	✓			✓		✓
Case 2	✓	✓		✓		✓
Case 3	✓	✓				✓
Case 4	✓	✓	✓			✓
Case 5	✓	✓	✓		✓	
Case 6	✓	✓	✓	✓	✓	

Table 4.2. Modal parameters for each case.

Modal Parameters		**Case 1**	**Case 2**	**Case 3**	**Case 4**	**Case 5**	**Case 6**
Mode 1 (Bending)	T (sec)	0.117	0.118	0.155	0.133	0.183	0.177
	f (Hz)	8.529	8.466	6.47	7.495	5.456	5.664
	Modal Mass Participating %	67.1	67.43	18.9	67.26	63.75	62.89
	Direction	Y	Y	X	Y	X	X
Mode 2 (Bending)	T (sec)	0.115	0.116	0.152	0.13	0.165	0.158
	f (Hz)	8.693	8.645	6.569	7.72	6.073	6.321
	Modal Mass Participating %	65.25	65.55	0.58	67.46	65.38	66.58
	Direction	X	X	Y	X	Y	Y
Mode 3 (Torsional)	T (sec)	0.102	0.103	0.151	0.114	0.147	0.141
	f (Hz)	9.808	9.756	6.626	8.785	6.807	7.11
	Modal Mass Participating %	68.08	68.09	0.072	66.46	62.81	62.40
	Direction	RZ	RZ	RZ	RZ	RZ	RZ

The values of period, frequency, modal participating mass ratio and the directions of mode shapes for each case are shown in Table 4.2. When comparing Case 2 with Case 1, there is no significant change in terms of modal parameter values, since the cross-sectional areas of floor beams are not adequate to make a considerable contribution to the stiffness and mass. In Case 3, modal mass participating ratio significantly reduces to 18 % in x direction, to almost 0 % in y direction, since the load transfer in horizontal direction cannot be carried out effectively in the absence of rigid diaphragm assignment or slabs. However, Case 4, which is obtained by assigning the slabs to Case 3 holds approximately 67 % modal mass participating, which signifies that the slabs provide a sufficient diaphragm effect on the dynamic response of the structure. When taking Case 5 into consideration, a striking point is the change observed from 0.133 sec to about 0.18 sec in period, despite the same completion level of the finite element model except the presence of openings compared to Case 4. In the meantime, it is observed that the reduction in mass due to removal of some areas for openings has a less influence than the reduction in stiffness on the modal period. After analysing the results obtained from cases and comparing them to each other, Case 5 was taken as a reference model where rigid diaphragm constraint was not assigned to slabs in comparison with Case 6. Therefore, actual in-plane stiffness properties and behaviour are simulated, and this produces a more realistic distribution of the forces to the lateral resisting elements.

Table 4.3. Base reactions in z direction.

CASE	**BASE REACTIONS (z direction)**	
	DEAD (ton)	G +n*Q (ton)
Case 1	3314.79	-
Case 2	3357.28	-
Case 3	3357.28	-
Case 4	3737.3	3879.14
Case 5	3169.33	3311.17
Case 6	3169.33	3311.17

Base reactions acting in z direction are presented for each case in Table 4.3. A base reaction of 3314.79 ton in Case 1 corresponds to self-weight of complete bearing walls. Once all bearing elements are built without openings, as same as Case 4, the base reaction value is equal to 3737.30 ton. After applying live loads acting on the floors, the total weight of structure obtained from a load combination of $g + 0.3q$ corresponds to 3879.14 ton. When the 3D finite element model is completed as Case 5, it is seen that the total weight of openings which is 568 ton accounts for 18 percent of self-weight of the entire structure.

4.2. Soil flexibility

During in-situ examination, it was observed that the basement walls do not act as retaining walls since their lateral surface is not directly in contact with soil. Therefore, it was aimed to involve soil flexibility in analyses by assigning soil springs to the reference model “Case 5” only in the vertical direction. Required data was provided by the soil investigation report in Table 3.3. According to Turkish Seismic Code, the soil consists of dense sand and gravel for soil group B with a shear wave of 705 m/sec, as seen in Figure 4.2.

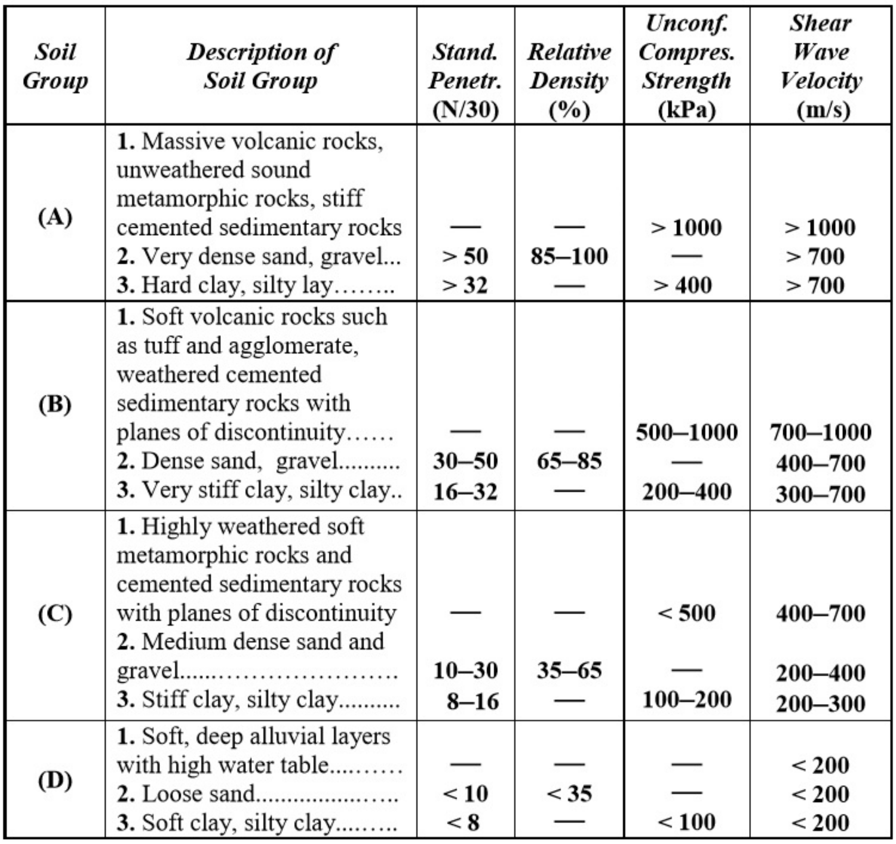

Soil Group	*Description of Soil Group*	*Stand. Penetr.* (N/30)	*Relative Density* (%)	*Unconf. Compres. Strength* (kPa)	*Shear Wave Velocity* (m/s)
(A)	**1.** Massive volcanic rocks, unweathered sound metamorphic rocks, stiff cemented sedimentary rocks	—	—	> 1000	> 1000
	2. Very dense sand, gravel...	> 50	85–100	—	> 700
	3. Hard clay, silty lay……..	> 32	—	> 400	> 700
(B)	**1.** Soft volcanic rocks such as tuff and agglomerate, weathered cemented sedimentary rocks with planes of discontinuity……	—	—	500–1000	700–1000
	2. Dense sand, gravel..........	30–50	65–85	—	400–700
	3. Very stiff clay, silty clay..	16–32	—	200–400	300–700
(C)	**1.** Highly weathered soft metamorphic rocks and cemented sedimentary rocks with planes of discontinuity	—	—	< 500	400–700
	2. Medium dense sand and gravel......…………………	10–30	35–65	—	200–400
	3. Stiff clay, silty clay..........	8–16	—	100–200	200–300
(D)	**1.** Soft, deep alluvial layers with high water table....……	—	—	—	< 200
	2. Loose sand..................…..	< 10	< 35	—	< 200
	3. Soft clay, silty clay....…..	< 8	—	< 100	< 200

Figure 4.2. Soil groups and their descriptions [31].

The coefficient of soil reaction k_s was identified for the soil Z2 belonging to Group B, referring to Bowles (1996) where k_s values for the soil types are suggested in Figure 4.3. According to this figure, k_s can be defined as a value between 64000- 128000 kN/m^3.

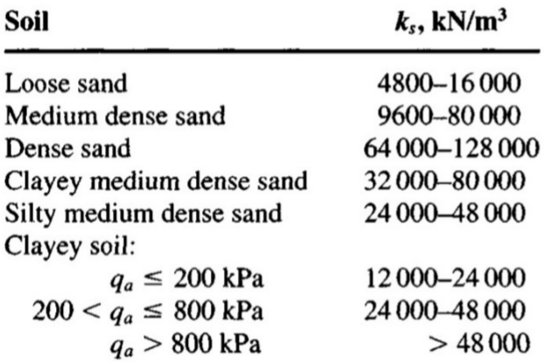

Soil	k_s, kN/m^3
Loose sand	4800–16 000
Medium dense sand	9600–80 000
Dense sand	64 000–128 000
Clayey medium dense sand	32 000–80 000
Silty medium dense sand	24 000–48 000
Clayey soil:	
$q_a \leq 200$ kPa	12 000–24 000
$200 < q_a \leq 800$ kPa	24 000–48 000
$q_a > 800$ kPa	> 48 000

Figure 4.3. Soil reaction coefficients corresponding to soil types [30].

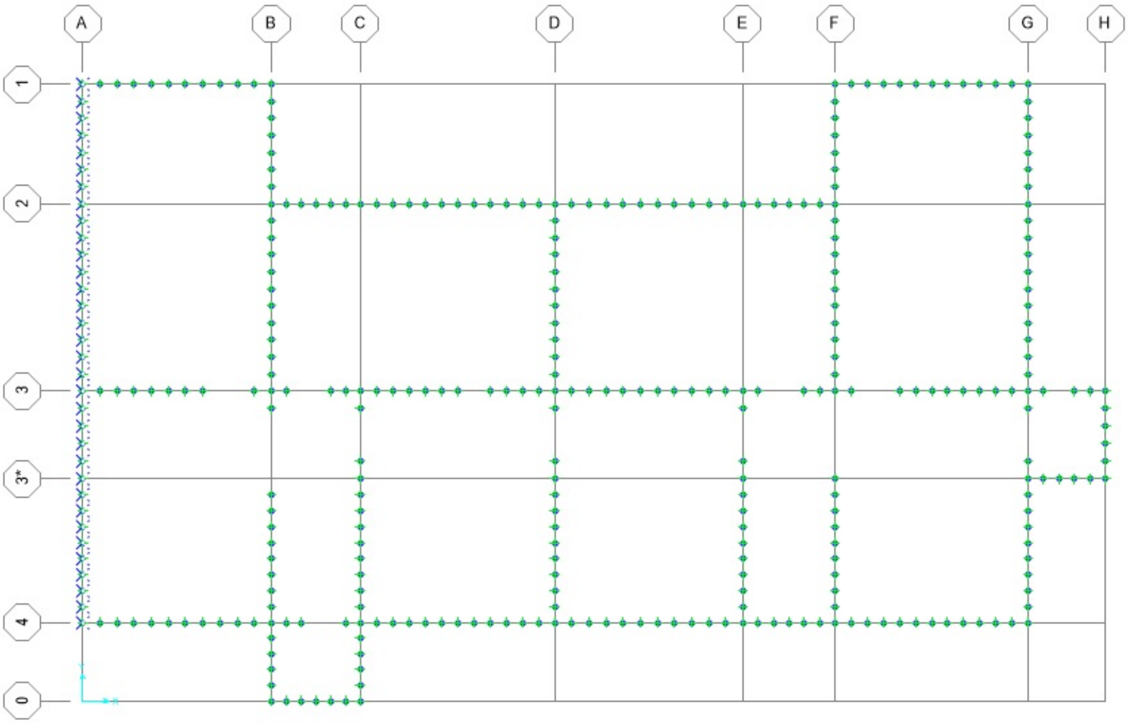

Figure 4.4. The joints of shell elements on the foundation-soil interaction surface.

Effective tributary area of each finite (shell) element contacting with the soil was calculated and multiplied by a soil reaction coefficient. As a result, soil spring constants obtained were individually assigned to 347 joints in translation z.

Table 4.4. The calculation of k spring coefficients of 347 joints for k_s=128000 kN/m^3.

Axis	**Interval**	**Length (m)**	**Wall tickness (m)**	**Footing (m)**	**Total Area (m^2)**	**# of Joints**	**k_{joint} kN/m**
A	1-4	19.03	0.8	1.2	22.84	33	88570
B	1-3	10.8	0.8	1.2	12.96	19	87303
	3-4	5.28	0.76	1.16	6.13	10	78422
	0-4	2.97	0.6	1	2.97	5	76027
C	3-4	6.43	0.75	1.15	7.39	13	72802
	0-4	2.97	0.6	1	2.97	5	76027
D	2-3	6.71	0.7	1.1	7.38	12	78725
	3-4	6.43	0.77	1.17	7.52	12	80241
E	3-4	6.73	0.75	1.15	7.74	13	76199
F	1-2	4.39	0.84	1.24	5.44	8	87092
	2-3	6.71	0.7	1.1	7.38	11	85882
	3-4	5.23	0.8	1.2	6.28	10	80327
G	1-3	10.8	0.7	1.1	11.88	19	80028
	3-3*	1.8	0.84	1.24	2.23	3	95225
	3*-4	5.23	0.88	1.28	6.69	9	95203
H	3-3*	3.6	0.6	1	3.6	6	76795
1	A-B	6.46	0.77	1.17	7.56	10	96738
	F-G	6.61	0.84	1.24	8.2	11	95370
2	B-D	9.7	0.86	1.26	12.22	17	92018
	D-F	9.58	0.84	1.24	11.88	16	95027
3	A-G	24.73	0.8	1.2	29.68	43	88335
	G-H	1.59	0.6	1	1.59	3	67835
3*	G-H	2.65	0.6	1	2.65	4	84794
4	A-D	16.16	0.8	1.2	19.39	24	103417
	D-E	6.43	0.84	1.24	7.97	10	102050
	E-G	9.76	0.8	1.2	11.71	16	93689
0	B-C	3.04	0.6	1	3.04	5	77819

For instance, 33 joints between axis 1 and axis 4 were selected on axis A, as indicated in Figure 4.4. Footing width is equal to 1.20 m obtained from the summation of the bearing wall width (0.80 m) and the total extension on both side (0.40 m). The mesh size of each shell element in longitudinal direction is 0.577 m. Each joint represents an area of 1.20 x 0.577. Therefore,

$$\begin{aligned} kspring &= 128000 \times 1.20 \times 0.577 \\ &= 88569.82 \quad kN/m \end{aligned}$$

In the same way, each soil spring constant was calculated, as indicated in Table 4.4.

4.3. Model updating

It is acknowledged that material properties and soil flexibility may demonstrate significant variations for the URM structures. This will influence the dynamic behaviour of the structures and eventually their seismic performance. Therefore, uncertain parameters affecting the model behaviour such as Elasticity Modulus (E) and the coefficient of soil reaction (k_s) are identified by model updating approach in order to minimize the difference between theoretical and experimental modal behaviour. It has been noticed that Bowles (1996) proposes a range of 64000 and 128000 for ks instead of a specified k_s value, and there are several assumptions made in the literature (see Section 2.6) to determine the value of Elasticity Modulus. So as to reduce the complexity in defining possible E and k_s values, both parameters of the model were iteratively modified until an agreement between the results of Finite Element Analysis (FEA) and Operational Modal Analysis (OMA) was provided. Hence, the interaction between E and k_s parameters on the modal period and frequency was investigated by a set of FEA.

4.3.1. First phase of model updating

In first phase of model updating, it is aimed at obtaining a range which provides upper and lower bounds for the values of E and k$_s$ parameters. When k$_s$ value is fixed and adopted as a maximum of 128000 kN/m^3, corresponding E will be the lowest value, which leads the dynamic characteristics obtained from FEA to reach those obtained from OMA. Contrary to this, when k$_s$ value is fixed and adopted as a minimum of 64000 kN/m^3, corresponding E will be the highest value, which leads the dynamic characteristics obtained from FEA to reach those obtained from OMA.

The FEA was initially performed by taking k$_s$ as 128000 kN/m^3 and E as 1130 MPa proposed by TSC 2007. As a result, frequency values corresponding to Mode 1 (bending), Mode 2 (bending) and Mode 3 (torsional) were obtained as 4.06, 4.35 and 5.09. Since the results of OMA could not be attained, the model updating was continued until a negligible difference between OMA and FEA was obtained.

Table 4.5. Modal parameters from system identification.

MODE	**PERIOD (sec)**	**FREQUENCY (Hz)**
Mode 1 (X)	0.185	5.4
Mode 2 (Y)	0.167	6
Mode 3 (T)	0.155	6.45

The modal parameters from system identification acknowledged as the reference in this study are presented in Table 4.5 and the change of modal parameters corresponding to increasing E is shown in Table 4.6.

Table 4.6. Modal parameters corresponding to increasing for fixed k_s = 128000 kN/m^3.

k_s (kN/m^3)	**E (MPa)**	**Mode 1 in X**		**Mode 2 in Y**		**Mode 3 in RZ**	
		T (sec)	f (Hz)	T (sec)	f (Hz)	T (sec)	f (Hz)
128000	1130	0.246	4.06	0.23	4.35	0.197	5.09
	1400	0.224	4.47	0.21	4.76	0.179	5.59
	1600	0.211	4.74	0.199	5.03	0.169	5.93
	1800	0.2	4.99	0.19	5.25	0.16	6.23
	1900	0.196	5.11	0.186	5.36	0.157	6.38
	2000	0.191	5.23	0.183	5.47	0.153	6.52
	2100	0.187	5.34	0.179	5.57	0.15	6.65
	2150	0.185	5.4	0.178	5.62	0.149	6.72

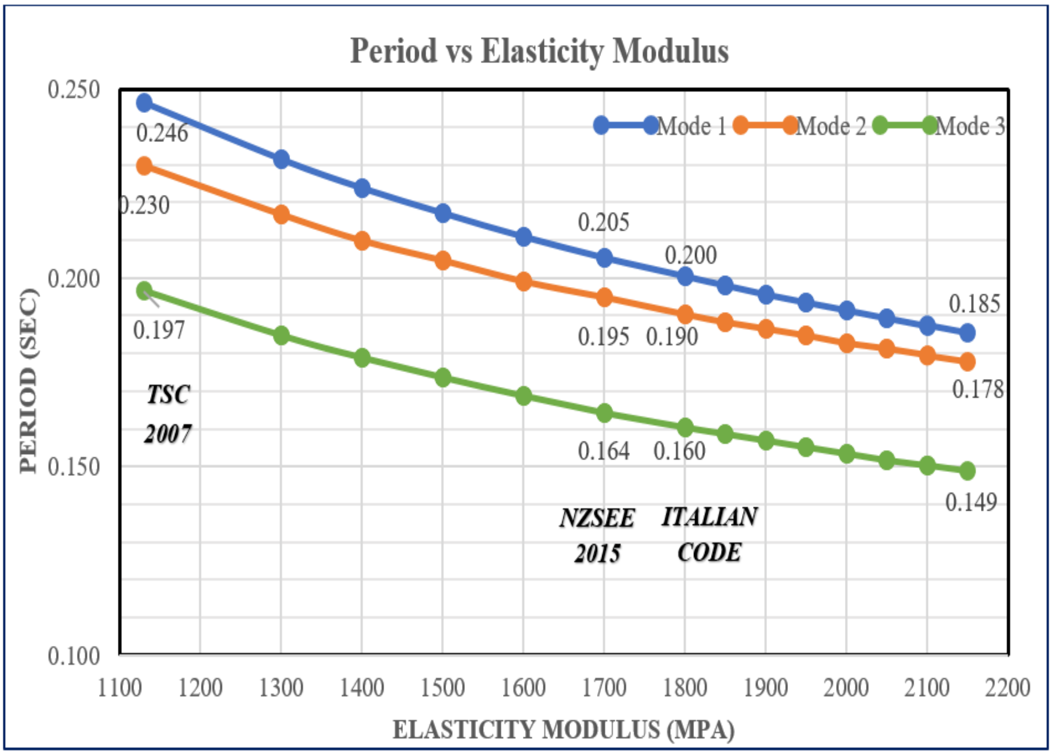

Figure 4.5. The change of modal parameters corresponding to increasing E for fixed k_s = 128000 kN/m^3. Period values corresponding to E values proposed in the codes are indicated.

The difference between FEA and OMA was minimized, when E reached a value of 2150 MPa that represents the lower bond for possible E values.

Secondly, model updating was performed, starting from the lower bond where E is equal to 2150 MPa. Since the lowest k_s with a value of 64000 kN/m^3 was fixed, the upper bond was obtained for possible E values. The results of this updating procedure are summarized in Table 4.7.

Table 4.7. Modal parameters corresponding to increasing E for fixed k_s= 64000 kN/m^3.

k_s (kN/m^3)	**E (MPa)**	**Mode 1 in X**		**Mode 2 in Y**		**Mode 3 in RZ**	
		T (sec)	f (Hz)	T (sec)	f (Hz)	T (sec)	f (Hz)
64000	2150	0.199	5.03	0.195	5.14	0.159	6.29
	2200	0.197	5.07	0.193	5.19	0.158	6.34
	2250	0.196	5.1	0.191	5.23	0.156	6.4
	2300	0.195	5.14	0.189	5.28	0.155	6.45
	2350	0.193	5.17	0.188	5.32	0.154	6.5
	2400	0.192	5.2	0.186	5.37	0.153	6.55
	2450	0.191	5.23	0.185	5.41	0.152	6.6
	2500	0.19	5.27	0.183	5.45	0.15	6.65
	2550	0.189	5.3	0.182	5.49	0.149	6.7
	2600	0.188	5.33	0.181	5.53	0.148	6.74
	2650	0.187	5.36	0.179	5.57	0.147	6.79
	2700	0.186	5.38	0.178	5.61	0.146	6.83
	2750	0.185	5.41	0.177	5.65	0.145	6.88

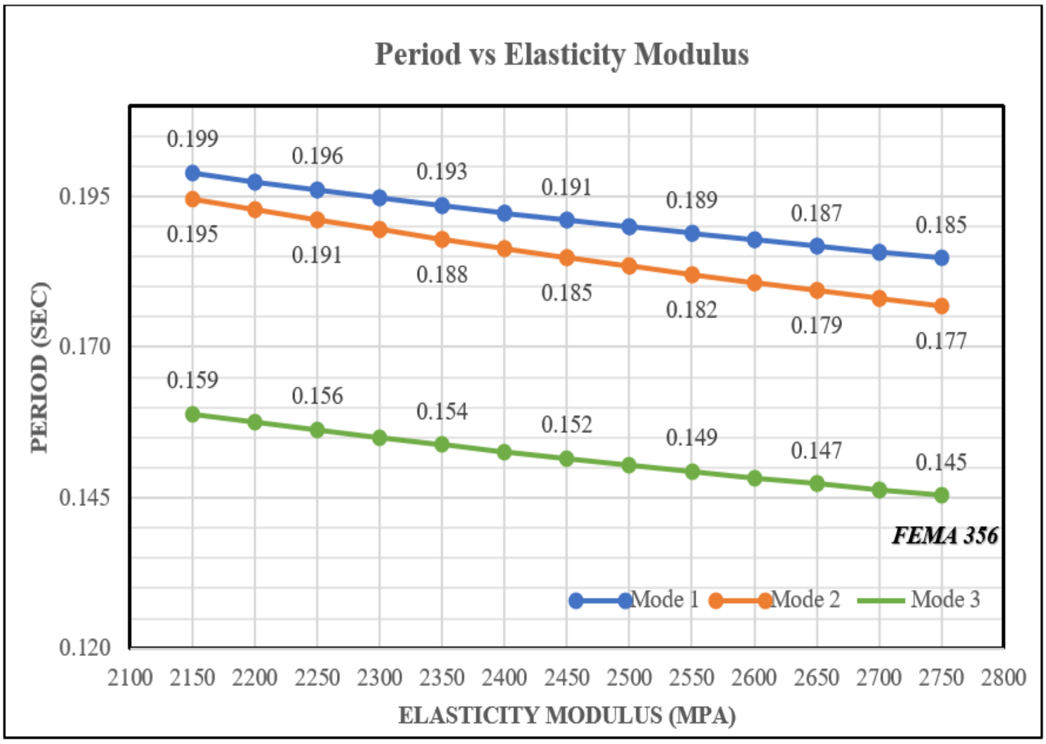

Figure 4.6. The change of modal parameters corresponding to increasing E for fixed $k_s = 64000$ kN/m^3. Period values corresponding to E values proposed in the codes are indicated.

The difference between FEA and OMA was minimized, when E reached a value of 2750 MPa that represents the upper bond for possible E values. Finally, a range was calculated to provide upper and lower bonds for a pair of E and k_s .

Table 4.8. Upper and lower bounds for both E and k_s.

Elasticity Modulus	**MPa**	**kN/m^3**	**Soil Interaction Coefficient**
E (max)	2750	64000	k_s(min)
E (min)	2150	128000	k_s(max)

4.3.2. Second phase of model updating

In the second phase, the FEM updating is carried out with respect to simultaneous alteration of both E and k_s parameters in contrast to first phase. Here, it is aimed at generating a curve that will show the decrease in the values of E corresponding to the increase in the values of k_s. Each pair of E and k_s on the curve will lead the dynamic parameters obtained from the FEA to coincide with those obtained from system identification.

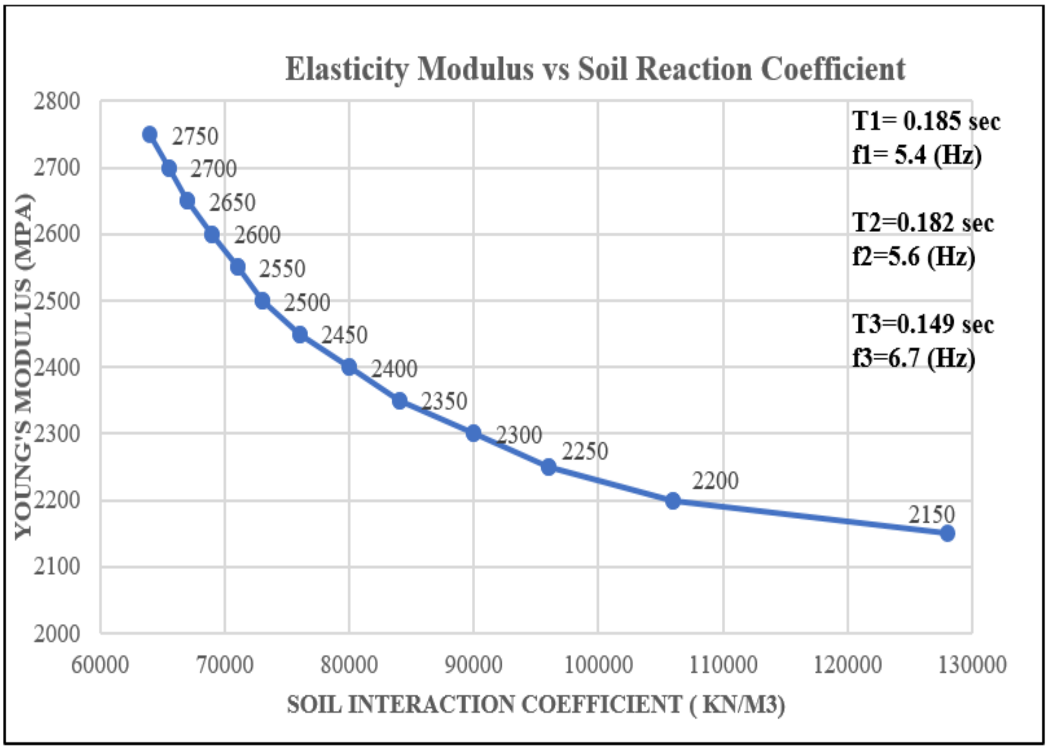

Figure 4.7. The interaction curve of E and k_s.

In consequence of the final model updating, the interaction curve of E and k_s was generated, as shown in Figure 4.7. Each intersection point on the curve can be adopted for correlation with identification based results. The striking point is that for a decrease of 50 MPa in E, the declination of the curve is steep between k_s values 64000 kN/m^3 and 84000 kN/m^3 , but it begins to flatten at the breakpoint where k_s and E are equal to 84000 kN/m^3 and 2350 MPa, respectively. Following this, the curve is approaching to be linearized. Thus, it can be concluded that the breakpoint represents average behaviour of the interaction curve. Consequently, the value of E was adopted as 2350 MPa corresponding to k_s with a value of 84000 kN/m^3 in order to be in more conservative side, instead of taking the values of upper and lower bounds.

4.4. Mesh size comparison

Mesh size selection is a significant parameter that influences the accuracy of the FEM and the duration of obtaining results from analysis. Refining the FEM from coarse to fine mesh size increases the number of frame, shell and solid elements used, and thus more nodes occur to be analysed. This accordingly may result in a time-consuming application if the mesh size is selected, being finer than what it is required to be. For the case study building, by considering the dimensions of openings and 60 cm intervals between floor beams, the bearing walls and slabs were firstly meshed into areas of 60 x 60 cm.

Table 4.9. The effect of mesh size on the modal parameters.

Mesh Size (cm x cm)	**Mode 1 (Bending) in Direction X**		**Mode 2 (Bending) in Direction Y**		**Mode 3 (Torsional) in Direction RZ**	
	T (sec)	f (Hz)	T (sec)	f (Hz)	T (sec)	f (Hz)
60 x 60	0.18	5.55	0.175	5.7	0.145	6.89
30 x 30	0.185	5.4	0.179	5.59	0.149	6.71
20 x 20	0.185	5.39	0.18	5.55	0.15	6.66
15 x 15	0.186	5.38	0.181	5.53	0.151	6.64

As a mesh size of 60 x 60 is getting finer, the distribution of masses improves and thus period values also increase, as seen in Table 4.9. The modal period starts to firstly converge at 0.185 (sec) for the selected mesh size of 30 x 30. When a mesh size of 20 x 20 compared to a mesh size of 30 x 30, the major difference is that elapsed time for modal analysis becomes four times longer.

Therefore, the 3D FEM was modified with a mesh size of 30 x 30 and eventually a relatively large number of finite elements were used in the model. The distribution of masses and stresses was developed.

4.5. Modal analysis

When the initial 3D FEM was modified, based on identified parameters and the selected mesh size of 30 x 30, the mode shapes were obtained from the modal analysis, as shown in Figure 4.8, Figure 4.9 and Figure 4.10.

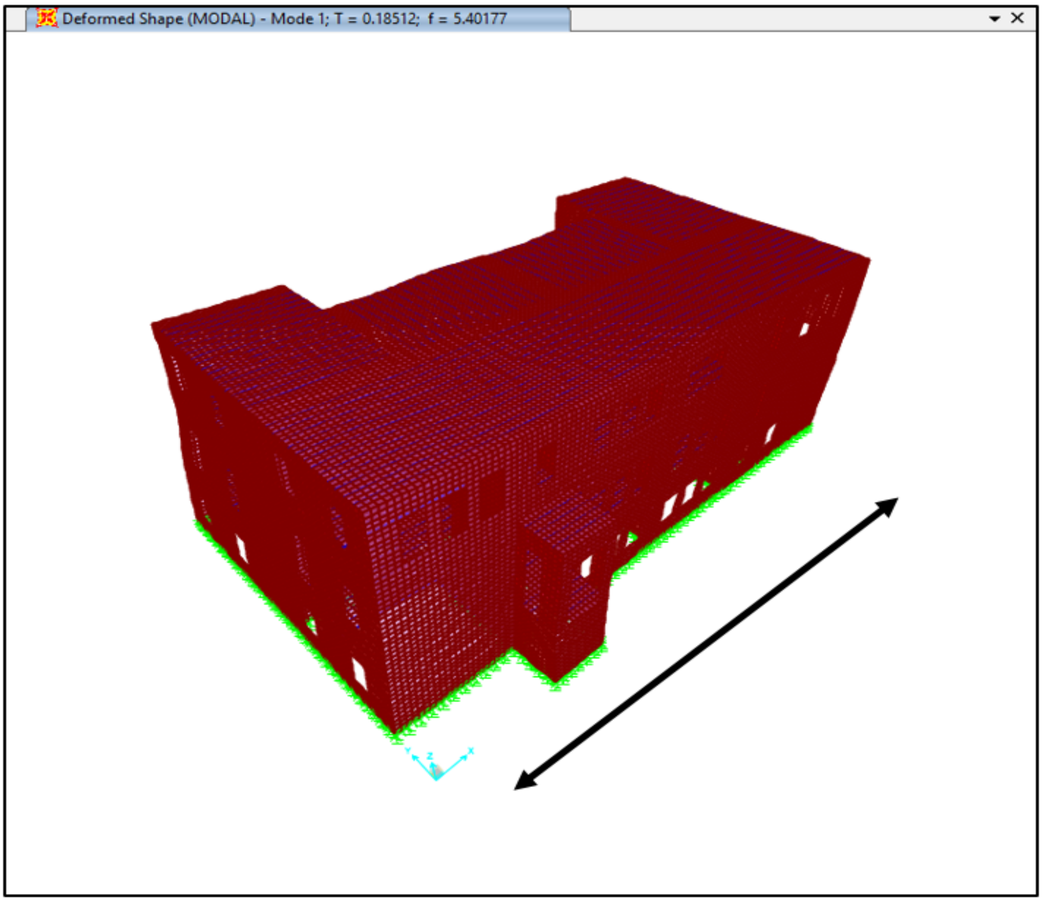

Figure 4.8. The illustration of Mode 1 (bending): T=0.185 sec; f=5.40 (Hz).

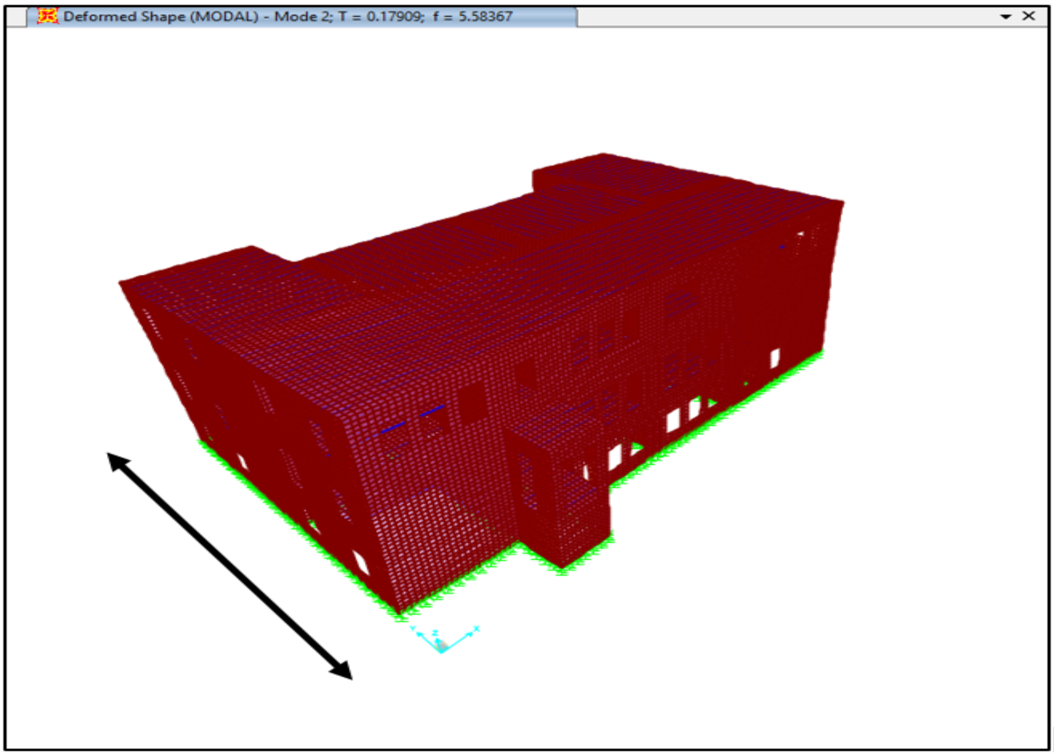

Figure 4.9. The illustration of Mode 2 (bending): T=0.179 sec; f=5.58 (Hz).

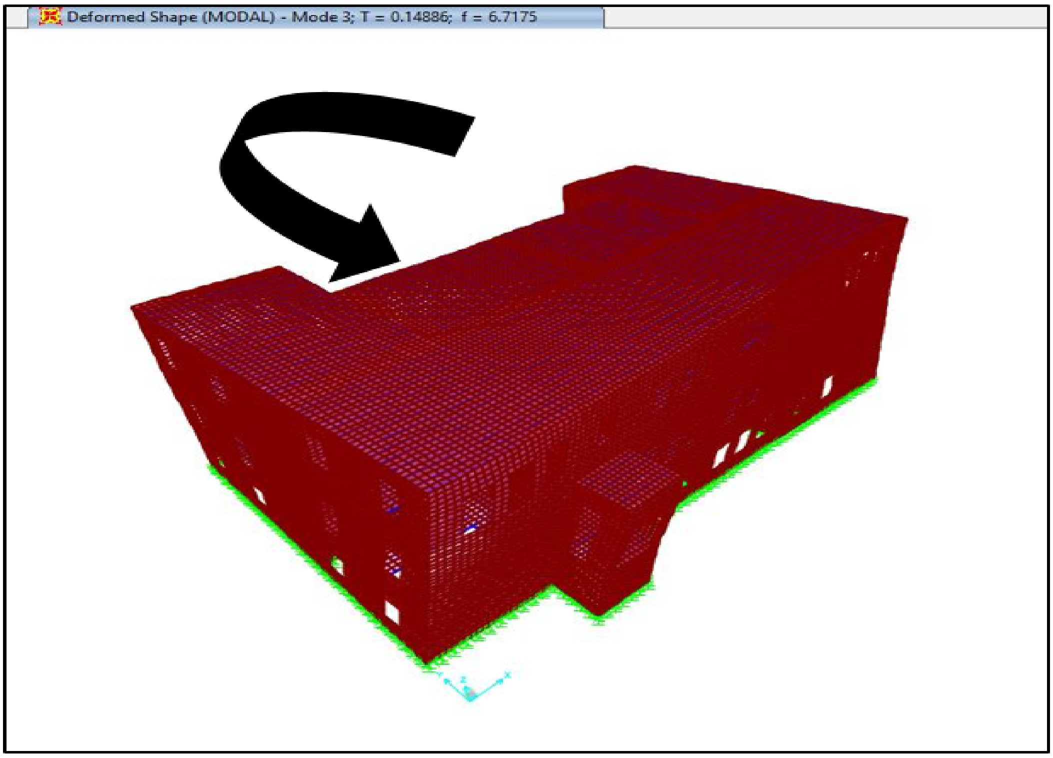

Figure 4.10. The illustration of Mode 3 (torsional): T=0.148 sec; f=6.7 (Hz).

5. PERFORMANCE ASSESSMENT BY LINEAR ANALYSIS

In this section, the seismic performance assessment of the building will be carried out by means of linear dynamic Response Spectrum Analysis (RSA). This assessment is a quantitative procedure, which determines whether an existing structure is capable of withstanding the design seismic combination safely. This section will include the evaluation of relative storey displacements, drift ratios corresponding the limit states described in the literature, and the comparison of shear and principal stresses with their threshold values.

5.1. Response spectrum analysis

The response spectrum was generated according to DLH 2008, which is seismic regulations for coastal and harbor constructions, railways, and airport constructions in Turkey. In order to obtain the design response spectrum, it is required to determine appropriate parameters for soil class, earthquake level and location of the building.

Initially, D2 earthquake level was taken into consideration, which represents earthquakes with strong ground motions having infrequent occurrence probability during the lifetime of structures. Besides, this earthquake level holds 10 % exceedance probability in 50 years with a return period of 475 years. According to Annex B.2 indicating soil classes in DLH 2008, soil class C is identified for soil group consisting of very stiff sand and soft rocks with 360 (m/ sec) $\leq V_s \leq$ 760 (m/sec).

Spectral acceleration values S_S and S_1 corresponding natural vibration periods 0.2 and 1.0 seconds, respectively, are given in the Annex A for soil class B as a reference. For other soil classes, spectral acceleration values S_{MS} and S_{M1} corresponding the same natural vibration periods are calculated by using Equation 5.1 and 5.2 given below. F_a

and F$_V$ parameters can be selected from Table 5.2 and Table 5.3, respectively.

$$S_{MS} = F_a \times S_S \tag{5.1}$$

$$S_{M1} = F_V \times S_1 \tag{5.2}$$

The coordinates of the historical building under consideration are required to determine spectral acceleration values. By means of Google maps, the coordinates were obtained as 41^0 N and 29^0 E. Figure 5.1 gives an information about the location and coordinated of the building.

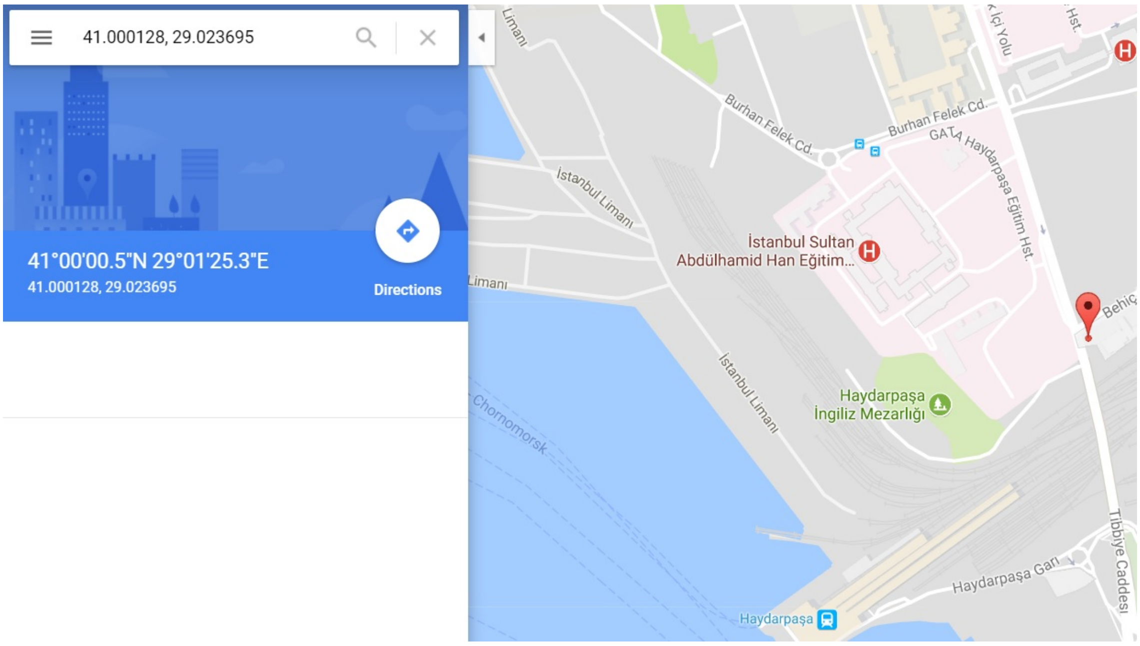
41.000128, 29.023695

41°00'00.5"N 29°01'25.3"E

41.000128, 29.023695

Figure 5.1. The location and coordinates of building on Google map.

Table 5.1. Spectral acceleration values for each exceedance probability from Annex A [31].

Coordinate		**S$_S$** **(T = 0.2)**			**S$_1$** **(T = 1)**		
Longitude	**Latitude**	**Exceedance probability**			**Exceedance probability**		
		50%	***10%***	***2%***	***50%***	***10%***	***2%***
29^0 E	41^0 N	0.62	1.19	1.8	0.23	0.58	1.02

For exceedance probability 10 %, spectral acceleration values S_S and S_1 were taken as 1.19 and 0.58, respectively, which belong to Soil class B.

Table 5.2. F_a values for soil classes.

Soil Class	**Soil coefficient “F_a”**				
	$S_S \leq 0.25$	**$S_S = 0.50$**	**$S_S = 0.75$**	**$S_S = 1.0$**	**$S_S \geq 1.25$**
A	0.8	*0.8*	*0.8*	*0.8*	*0.8*
B	1	1	1	1	1
C	1.2	1.2	1.1	1	1
D	1.6	1.4	1.2	1.1	1
E	2.5	1.7	1.2	0.9	0.9
F	$-^b$	$-^b$	$-^b$	$-^b$	$-^b$
*Linear interpolation will be applied for interval values. ** Specific geotechnical analysis to the site will be carried out.					

Table 5.3. F_V values for soil classes.

Soil Class	**Soil coefficient “F_V”**				
	$S_1 \leq 0.10$	**$S_1 = 0.20$**	**$S_1 = 0.30$**	**$S_1 = 0.40$**	**$S_1 \geq 0.50$**
A	0.8	*0.8*	*0.8*	*0.8*	*0.8*
B	1	1	1	1	1
C	1.7	1.6	1.5	1.4	1.3
D	2.4	2	1.8	1.6	1.5
E	3.5	3.2	2.8	2.4	2.4
F	$-^b$	$-^b$	$-^b$	$-^b$	$-^b$
*Linear interpolation will be applied for interval values. ** Specific geotechnical analysis to the site will be carried out.					

Spectral acceleration values taken from Annex A were converted to S_{MS} and S_{M1} by using soil coefficient parameters F_a and F_V. Design spectrum of the building were generated using the equations presented below.

$$S_{ae}(T) = 0.4S_{MS} + 0.6\frac{S_{MS}}{T_0}T \qquad (T_0 \leq T) \tag{5.3}$$

$$S_{ae}(T) = S_{MS} \qquad (T_0 \leq T \leq T_S) \tag{5.4}$$

$$S_{ae}(T) = \frac{S_{M1}}{T} \qquad (T_S \leq T_L) \tag{5.5}$$

$$S_{ae}(T) = \frac{S_{M1}T_L}{T^2} \qquad (T_L \leq T) \tag{5.6}$$

Period values T_0 and T_S forming the corner points of response spectrum are defined as follows:

$$T_S = \frac{S_{M1}}{S_{MS}} \tag{5.7}$$

$$T_0 = 0.2T_S \tag{5.8}$$

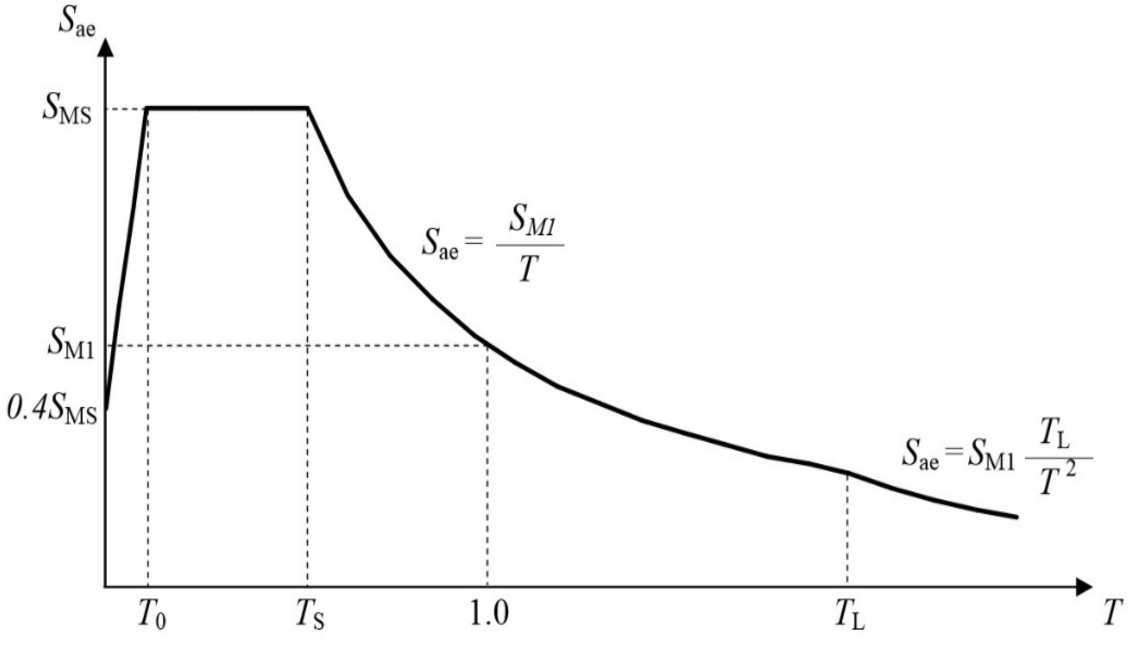

Figure 5.2. The schema of Design spectrum [31].

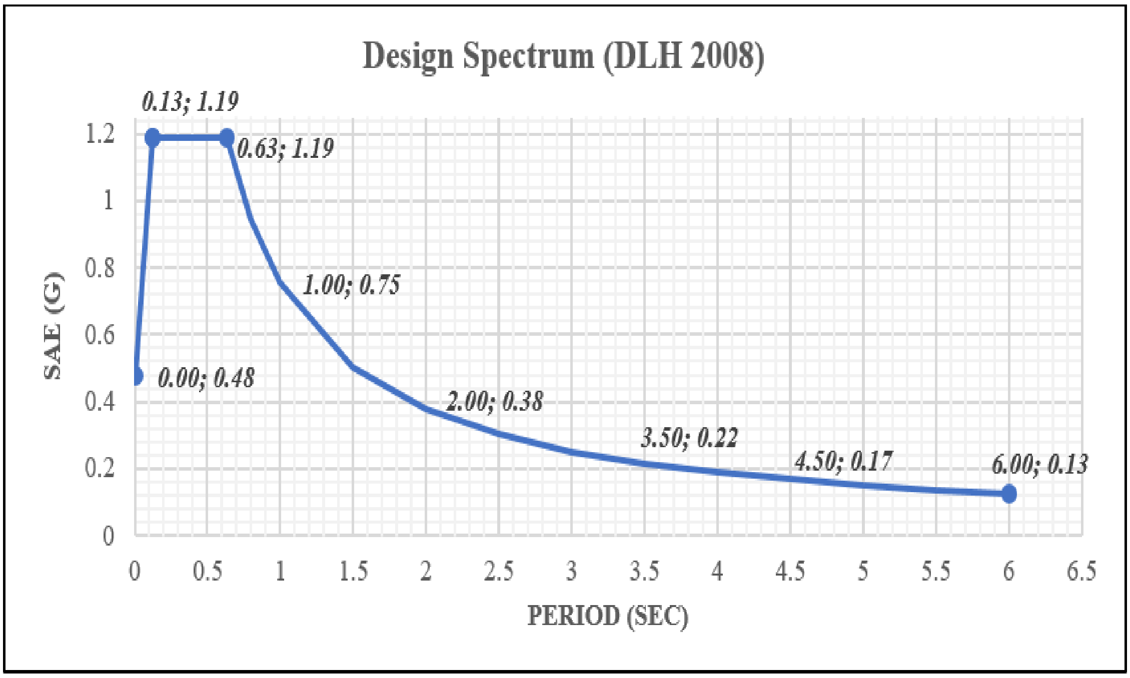

Figure 5.3. Design spectrum of the building according to DLH 2008.

Linear response spectrum analysis was conducted by SAP 2000 software program. Square Root of Sum of Squares (SRSS) was adopted as a modal combination method, which allows the multiple modes of response of a building to be considered. Therefore, an approximation of the total response of the structure is provided by combining responses obtained from the design spectrum for each mode. Earthquake forces were induced in x and y directions, as explained in Eurocode 8.1 below.

$$E_x = E_x + 0.3E_y \tag{5.9}$$

$$E_y = E_y + 0.3E_x \tag{5.10}$$

As well as earthquake forces, various load cases were defined in SAP 2000, which are W representing the total weight due to self-weight and live load acting on the slabs, and DEAD representing only self- weight of the structure. As a result, dead and live loads were combined with earthquake forces to determine base reactions in x, y and z directions. Finally base reaction results obtained from SAP 2000 were presented in Table 5.4.

Table 5.4. Base reaction values for different load cases.

BASE REACTIONS				
Load Case	**Type**	**Global FX (kN)**	**Global FY (kN)**	**Global FZ (kN)**
DEAD	Lin. Static	0	0	31080.5
W=G+0.3Q	Lin. Static	0	0	32471.5
R. Spectrum in X	Lin. Resp. Spec.	23088.7	10140.2	1026.08
R. Spectrum in Y	Lin. Resp. Spec.	10059.8	23475.8	1216.62
G+0.3Q+Ex	Combination	23088.7	10140.2	33497.6
G+0.3Q+Ey	Combination	10059.8	23475.8	33688.1

5.2. Drift ratios and displacements of the facades

For the evaluation of the damage states of the structure under a given earthquake demand, it is aimed at obtaining drift ratios and displacements of the facades, since most of researchers in the literature has proposed that structural damages can be directly associated with inter storey drifts. Therefore, this approach was adopted to identify the seismic vulnerability of the building.

After post-earthquake surveys, it has been observed that the facade walls are more brittle than interior walls. Besides, more stress concentration is expected to occur on facade regions due to discontinuities based on available openings. This makes facade walls more prone to be damaged, compared to interior walls.

5.2.1. Front facade

When the building was subjected to Earthquake force Ey, the displacement (Uy) contours occurred on the front facade, as indicated in Figure 5.4.

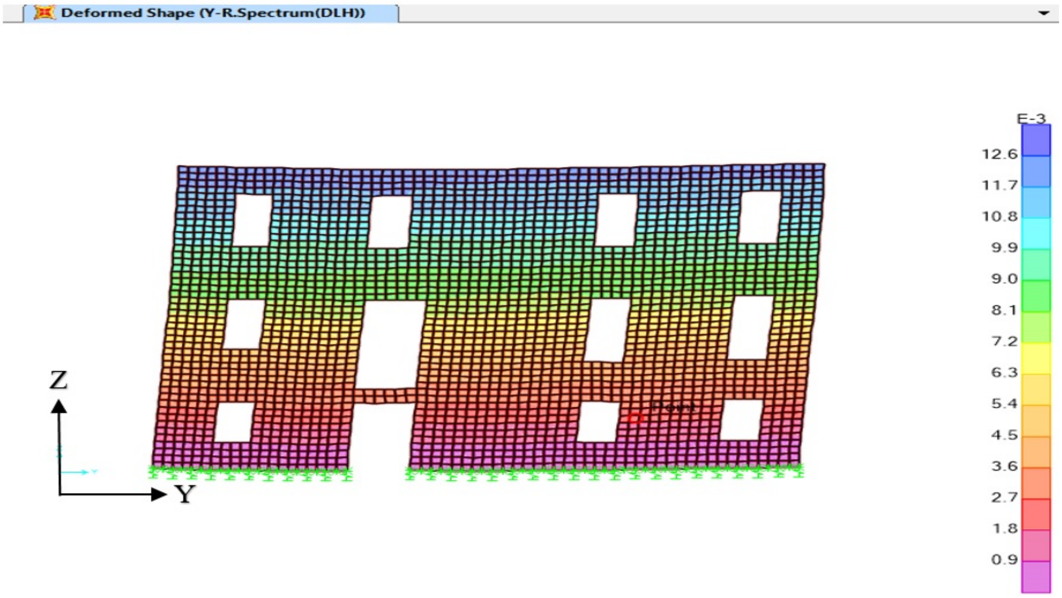

Figure 5.4. Displacement (Uy) contours on the front facade subjected to Earthquake force ”Ey”.

It can be interpreted from the displacement contours seen in Figure 5.4 that slabs at storey levels demonstrate almost rigid diaphragm behaviour, since the displacement values on the same vertical plane are very close to each other in the direction of earthquake force induced. Table 5.5 presents calculated drift ratios and inter-storey drifts.

Table 5.5. Displacements and drift ratios at storey levels due to Earthquake Force ”Ey”.

Storey Level	$\boldsymbol{\delta_x}$ **(m)**	$\boldsymbol{\delta_z}$ **(m)**	$\boldsymbol{\delta_y}$ **(m)**	$\boldsymbol{\Delta\delta_y}$ **(m)**	**Storey height (m)**	**Drift Ratio %**
Roof	0.0068	0.0052	0.012	0.0032	4.45	0.072
First Floor	0.0055	0.0051	0.0088	0.0054	4.85	0.111
Ground Floor	0.0019	0.0045	0.0034	0.0035	3.45	0.101

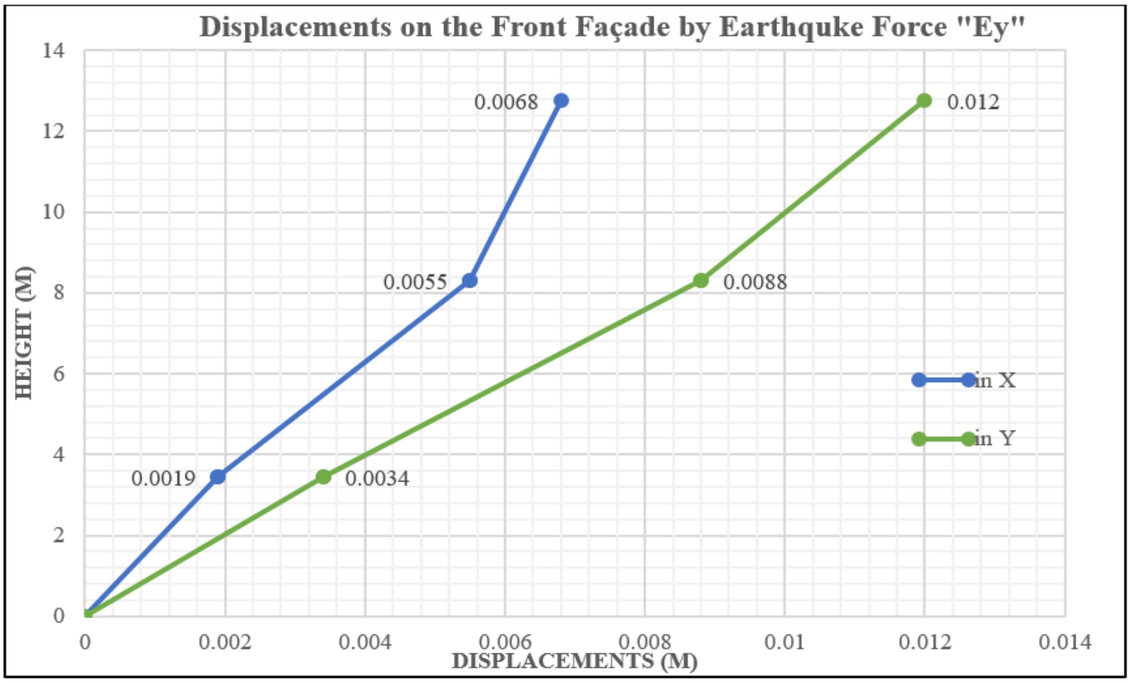

Figure 5.5. Displacements at the storey levels on the front facade.

5.2.2. Rear facade

When the building was subjected to Earthquake force Ey, the displacement (Uy) contours occurred on the rear facade, as indicated in Figure 5.6.

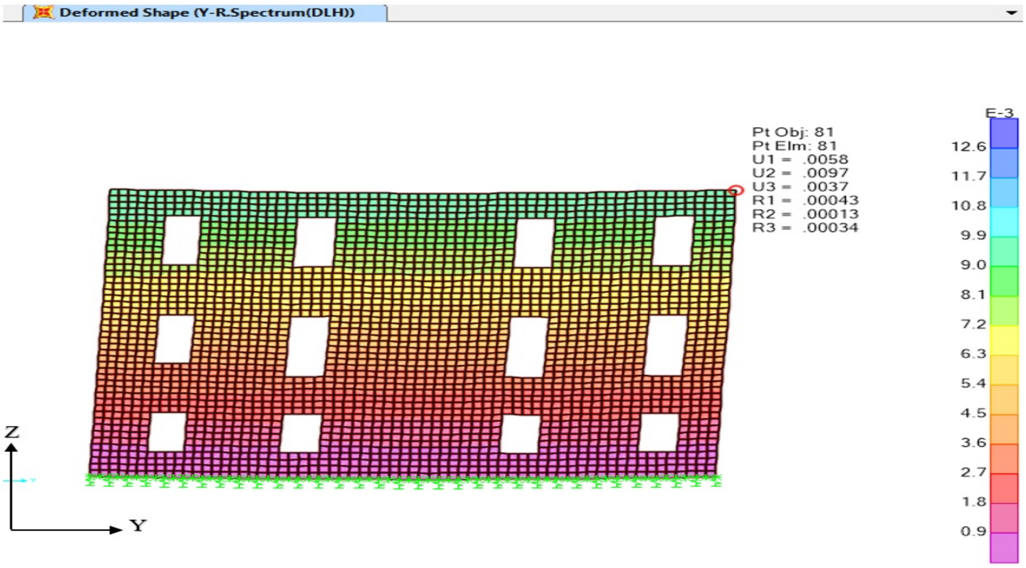

```
Pt Obj: 81
Pt Elm: 81
U1 =  .0058
U2 =  .0097
U3 =  .0037
R1 =  .00043
R2 =  .00013
R3 =  .00034
```

Figure 5.6. Displacement (Uy) contours on the rear facade subjected to Earthquake force ”Ey”.

It is seen that displacement values on the same horizontal plane are very close to each other in the direction of earthquake force induced, and a proper displacement distribution occurred throughout the wall. Despite the same geometric contour with the front facade, Uy and Ux displacement values on the rear facade are less compared to other. This is because the rear facade has more stiffness due to less total area of window and door openings.

Table 5.6. Displacements and drift ratios at storey levels due to Earthquake Force "Ey".

Storey Level	$\boldsymbol{\delta_x}$ **(m)**	$\boldsymbol{\delta_z}$ **(m)**	$\boldsymbol{\delta_y}$ **(m)**	$\boldsymbol{\Delta\delta_y}$ **(m)**	**Storey height (m)**	**Drift Ratio %**
Roof	0.0058	0.0037	0.0097	0.0029	4.45	0.065
First Floor	0.0047	0.0036	0.0068	0.0044	4.85	0.091
Ground Floor	0.0015	0.003	0.0024	0.0024	3.45	0.070

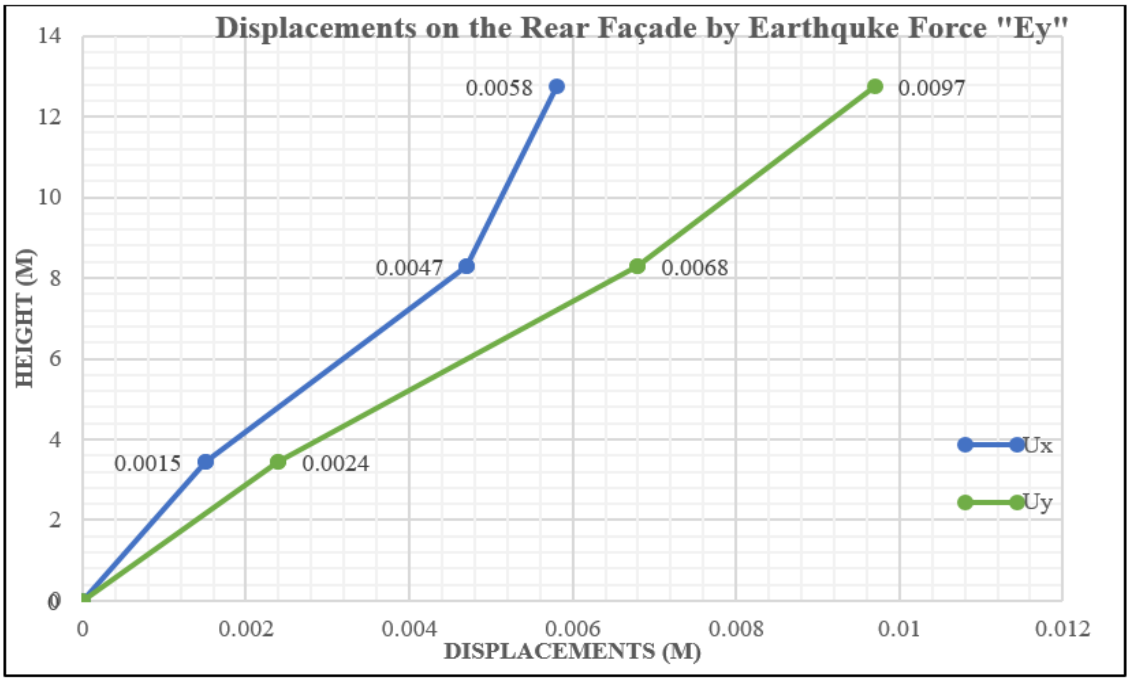

Figure 5.7. Displacements at the storey levels on the rear facade.

5.2.3. Left facade

When the building was subjected to Earthquake force Ex, the displacement (Ux) contours occurred on the left facade, as indicated in Figure 5.8.

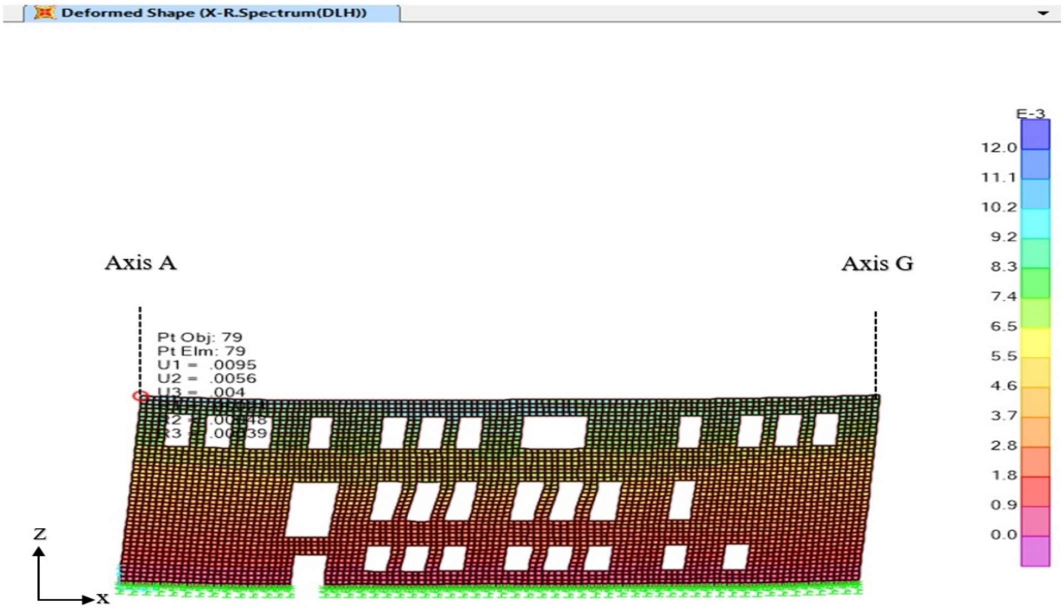

Figure 5.8. Displacement (Ux) contours on the left facade due to Earthquake force ”Ex”.

It is also observed that displacement values on the same horizontal plane are very close to each other in the direction of earthquake force induced, and a proper displacement distribution occurred throughout the wall.

Table 5.7. Displacements and drift ratios on Axis A at storey levels due to Earthquake Force “Ex”.

Storey Level	$\boldsymbol{\delta_y}$ **(m)**	$\boldsymbol{\delta_z}$ **(m)**	$\boldsymbol{\delta_x}$ **(m)**	$\boldsymbol{\Delta\delta_x}$ **(m)**	**Storey height (m)**	**Drift Ratio %**
Roof	0.0056	0.004	0.0095	0.003	4.45	0.066
First Floor	0.004	0.004	0.007	0.0046	4.85	0.094
Ground Floor	0.001	0.003	0.002	0.002	3.45	0.058

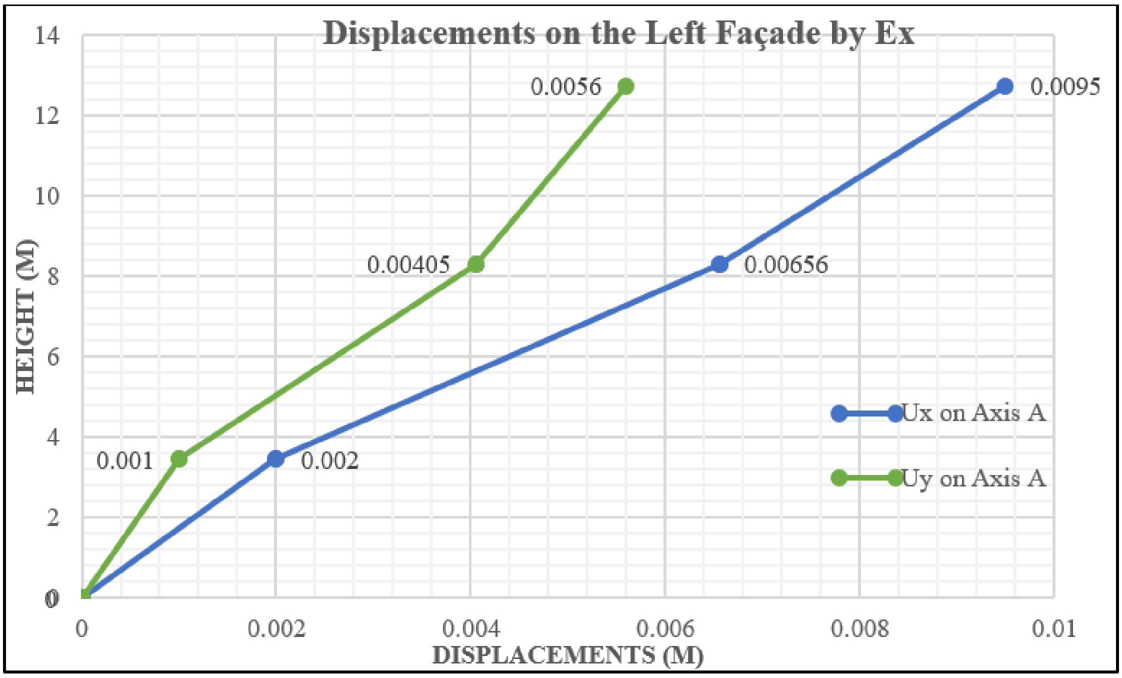

Figure 5.9. Displacements at the storey levels of the left facade on Axis A.

When Uy displacements are examined on the left facade, it is noticed that those values on the same vertical level increase as approaching to Axis G in Figure 5.10.

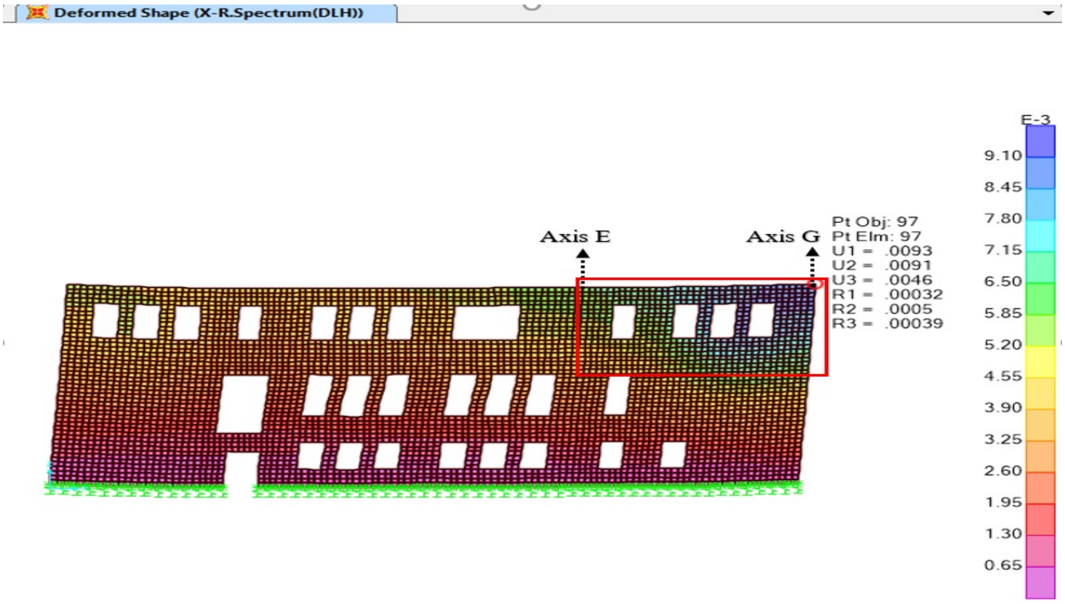

Pt Obj: 97
Pt Elm: 97
U1 = .0093
U2 = .0091
U3 = .0046
R1 = .00032
R2 = .0005
R3 = .00039

Figure 5.10. Displacement (Uy) contours on the left facade due to Earthquake force ”Ex”.

From the far-left edge of the facade up to Axis E, overall distribution of displacements occurred throughout the wall. Despite dominant earthquake force induced in x direction, displacement values in y direction represented by U2 coincided with displacement values in x direction represented by U1, as indicated between Axis E and Axis G on the top level in Figure 5.10.

Table 5.8. Displacements and drift ratios on Axis G at storey levels due to Earthquake Force "Ex".

Storey Level	$\boldsymbol{\delta_y}$ (m)	$\boldsymbol{\delta_z}$ (m)	$\boldsymbol{\delta_x}$ (m)	$\boldsymbol{\Delta\delta_x}$ (m)	**Storey height (m)**	**Drift Ratio %**
Roof	0.0091	0.0046	0.0093	0.0032	4.45	0.072
First Floor	0.0068	0.004	0.0061	0.0035	4.85	0.072
Ground Floor	0.0029	0.004	0.0026	0.0026	3.45	0.075

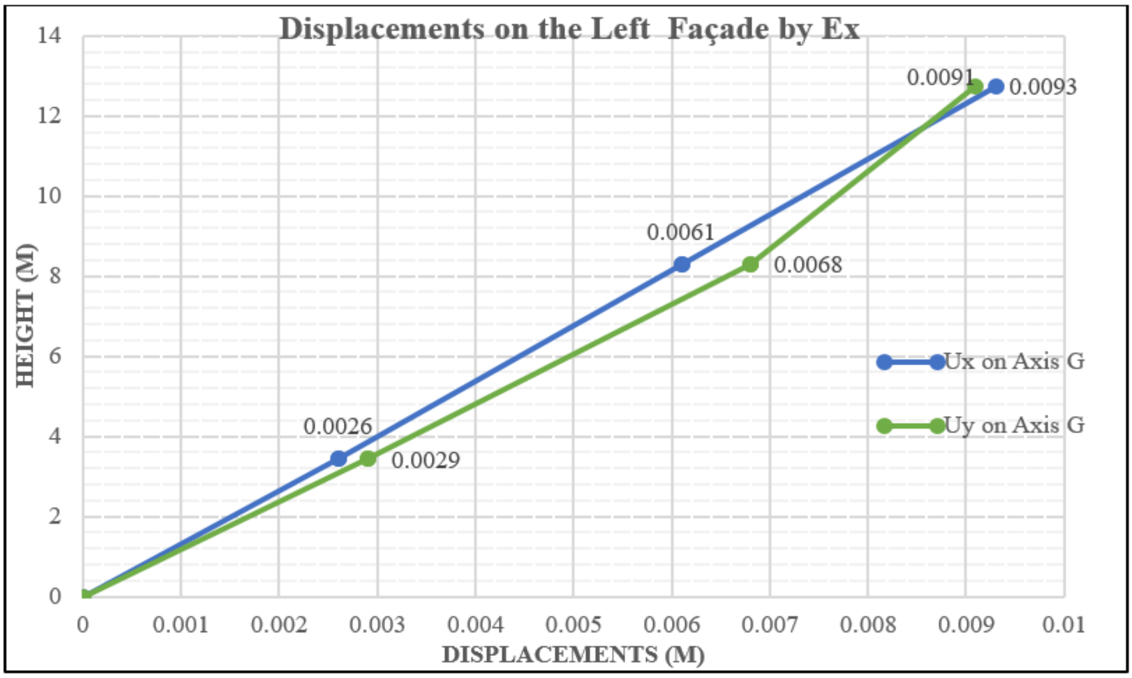

Figure 5.11. Displacements at the storey levels of the left facade on Axis G.

In contrast to displacements on Axis A of the left facade, Uy displacement values exceeded Ux displacements at ground and first storey levels with 0.0029 m and 0.0068 m, respectively. Slabs on ground and first floor extend along the left facade wall, except a division between Axis F and Axis G. This discontinuity of slabs may cause the building not to sufficiently withstand unfavourable impulse by a Ey component of the dynamic earthquake force induced. Since staircase void takes place behind the left facade wall between Axis F and Axis G, and this occasion accordingly yields loose in the stiffness, it could be a reason why Uy and Ux displacement values are close to each other under the dominant earthquake force Ex, as seen in Figure 5.11.

5.2.4. Right facade

When examining the displacement counters of the entire structure, it is observed that the largest displacements values up to 15.4 mm occurred at the top floor of right facade. Due to the geometry of u-shaped building, the slab discontinuity with an area of 79 square meters between Axis F and Axis B causes a remarkable degradation in stiffness. Therefore, the facade wall on longitudinal Axis 1 particularly tends to show more displacement in x direction.

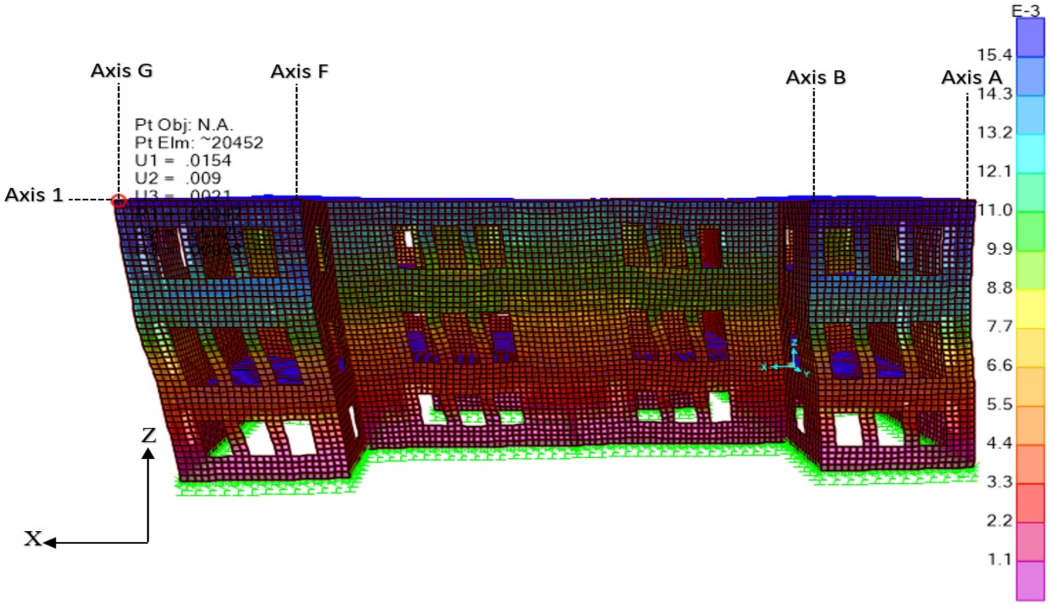

Figure 5.12. Displacement Ux contours on the right facade due to Earthquake force "Ex".

Table 5.9. Displacements and drift ratios on Axis G of the right facade at storey levels due to Earthquake Force “Ex”.

Storey Level	$\boldsymbol{\delta_y}$ (m)	$\boldsymbol{\delta_z}$ (m)	$\boldsymbol{\delta_x}$ (m)	$\boldsymbol{\Delta\delta_x}$ (m)	**Storey height (m)**	**Drift Ratio %**
Roof	0.009	0.0022	0.0154	0.0029	4.45	0.065
First Floor	0.0066	0.0022	0.0125	0.0083	4.85	0.171
Ground Floor	0.0025	0.0019	0.0042	0.0042	3.45	0.122

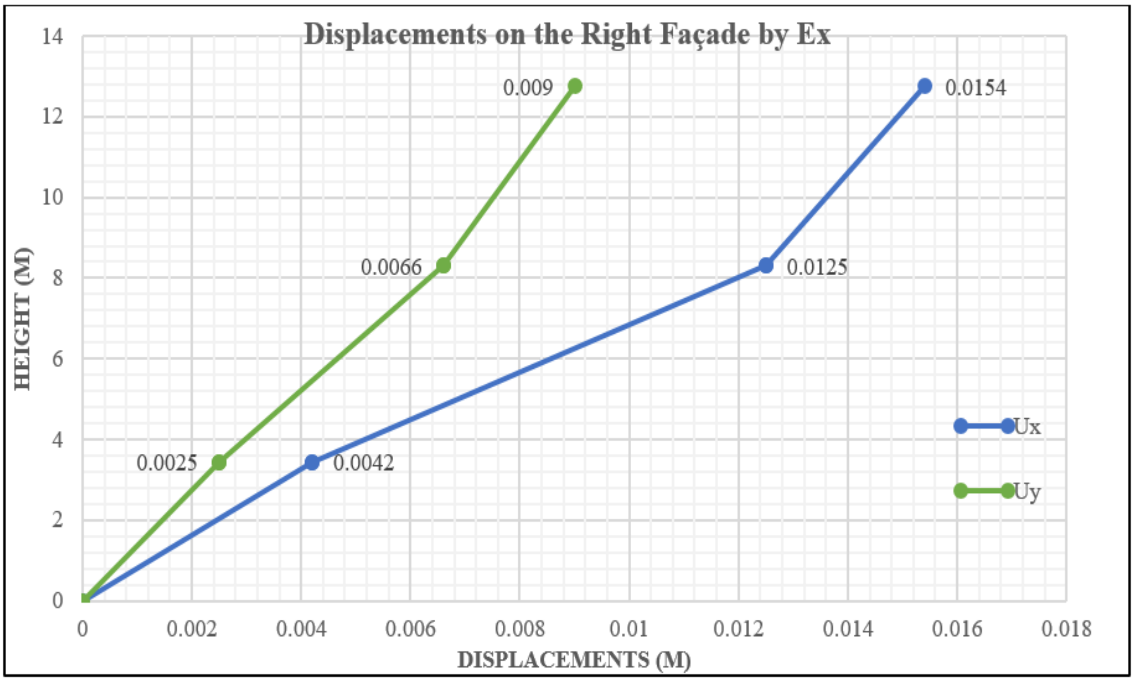

Figure 5.13. Displacements at the storey levels of the right facade.

Almost same displacement values in x direction occurred on the both ends of the right facade, since the building has a symmetric geometry. When compared to the left facade, any floor opening or staircase void behind the wall does not exist, thus continuity is provided and anticipated large difference between Ux and Uy displacements developed in dominant earthquake direction x, as seen in Figure 5.13.

5.3. Limit states of URM walls

Damage states of URM buildings should be predicted for performance assessment. The post-earthquake damage states of masonry structures may be categorized into three major structural performance levels named Immediate Occupancy (IO), Life Safety (LS) and Collapse Prevention (CP), explained as follows [25].

5.3.1. Immediate Occupancy (IO)

Structural Performance Level, Immediate Occupancy, is described as the post-earthquake damage state where only minor structural damage has occurred with no significant degradation in lateral resistance and strength. Therefore, force-resisting systems of the building maintain nearly all of their pre-earthquake strength and stiffness. In this damage state, some localized yielding and limited rupture of connections can be observed on the structures. The risk of life-threatening injury based on structural damage is very low and some minor structural maintenance can be needed.

5.3.2. Life Safety (LS)

Structural Performance, Life Safety, is described as the post-earthquake damage state where significant damage to the structure has occurred. However, the structure sustains stability and reserve capacity against either limited or total structural collapse. Some structural elements and components are severely damaged, but this has not resulted in large falling debris hazards, either within or outside the building [25]. Even though, injuries may occur during the earthquake, the total risk of life-threatening injury based on structural damage is anticipated to be low. If an immediate collapse risk is not expected for the damaged structure, it would be judicious to implement structural maintenances or assemble temporary bracing prior to reoccupancy.

5.3.3. Collapse Prevention (CP)

Structural Performance Level S-5, Collapse Prevention, is described as the post-earthquake damage state where the structure is on the threshold of experiencing either local or total collapse. Significant damage to the structure has occurred. Due to substantial degradation in strength and stiffness of lateral-resisting system, the structure does not maintain a residual capacity against collapse in accordance with criteria defined in this standard for Structural Performance Level. However, all significant components of the gravity load-resisting system must continue to carry their gravity load demands [25]. Falling hazards from structural debris may cause the significant risk of injury. Due to severely damage occurring, retrofitting or structural maintenance are not recommended. Since aftershock activity may lead the structure to collapse, the structure is not safe for reoccupancy.

5.4. Performance assessment in terms of drift ratios

In the researches, which aim at defining deformation capacity of URM walls, limit states simultaneously have been investigated, corresponding to the attainment of the global displacement capacity of the structures on the lateral force- drift curve. In order to define limit states of masonry structures, extensive tests programs have been performed, such as standard material tests, shaking table tests and quasi-static cycling tests on masonry walls subjected to horizontal and axial loads. In terms of inter-storey drifts, limit states are identified which refers to the first occurrence of local failure of portions of walls such as rocking in flexural, diagonal cracking and sliding in shear. According to some researches, proposed performance limit states corresponding to local failure modes in terms of inter-storey drift ratios are summarized in Table 5.10.

Table 5.10. Performance levels in terms of drift ratios based on local failure modes [32].

Author	**Failure Mode**	**Performance Level %**		
		IO	**LS**	**CP**
FEMA 356 (2000)	Rocking	0.1	0.3 h_{eff}/L	0.4 h_{eff}/L
Franklin *et al.* (2001)		0.1	0.9-1.5	1.2-1.9
Bosiljkov *et al.* (2008)		0.1	1.2-1.8	1.8-2.5
FEMA 356 (2000)	Sliding	0.1	0.3	0.4
Bosiljkov *et al.* (2008)		-	0.9	1.8
Alcocer *et al.* (2004)	Diagonal Tension	0.15	0.25	0.4
Bosiljkov *et al.* (2008		0.2-0.5	0.5-0.7	0.5-0.9

Additional studies were also performed to define limit states on the capacity curve obtained from lateral force vs drift ratio. Crack widths, the degradation of maximum resistance, and resulting drift values under loading were used in the definition of limit states, and proposed limit states in terms of drift ratios are summarized in Table 5.11.

Table 5.11. Performance levels in terms of drift ratios [32].

Author	**Performance Level %**		
	IO	**LS**	**CP**
FEMA 356 (2000)	0.3	0.6	1.0
Tomazevic (2007)	0.2-0.4	0.3-0.6	1.0-2.0
Calvi (1999)	0.1	0.3	0.5
Erbay (2007)	0.1	0.6	1

The drift ratios of the facade walls obtained from linear dynamic RSA were presented in Table 5.12 for comparison with the performance levels shown in both Table 5.10 and Table 5.11.

Table 5.12. Drift ratios of the facade walls obtained from the linear analysis.

Storey Level	**Front Facade Drift Ratio %**	**Rear Facade Drift Ratio %**	**Left Facade Drift Ratio %**	**Right Facade Drift Ratio %**
Roof	0.072	0.065	0.066	0.065
First Floor	0.111	0.091	0.094	0.171
Ground Floor	0.101	0.07	0.058	0.122

Generally, the measured drift ratios of the facade walls are in the rage of 0.09 % and 0.17 %. Since these drift ratio values do not exceed a limit value of 0.3 % representing Life Safety performance level, the building has attained the performance level of Immediate Occupancy.

Consequently, when compared to the drift ratio values of the facade walls to those limit values corresponding to the performance levels based on local failure nodes in Table 5.10, It can be interpreted that the performance level of the building under investigation meets Immediate Occupancy, since a maximum value of 0.171 % measured in the right facade wall is in the range of 0.15 % and 0.25 % corresponding to Diagonal tension failure, 0.1 % and 0.3 % corresponding to sliding failure, and 0.1 % and 0.9 % corresponding to rocking failure.

5.5. Performance assessment in terms of principal and shear stresses

It has been discussed that the types of stress are directly associated with possible local failure modes which control in-plane strength capacity of the URM walls. Therefore, the stress distribution can be evaluated to detect possible regions on the facade, which are prone to be damaged. As a result of linear dynamic RSA, the earthquake demand was obtained in terms of principal, compressive and shear stresses. The stress distributions obtained are presented in Figure 5.14.

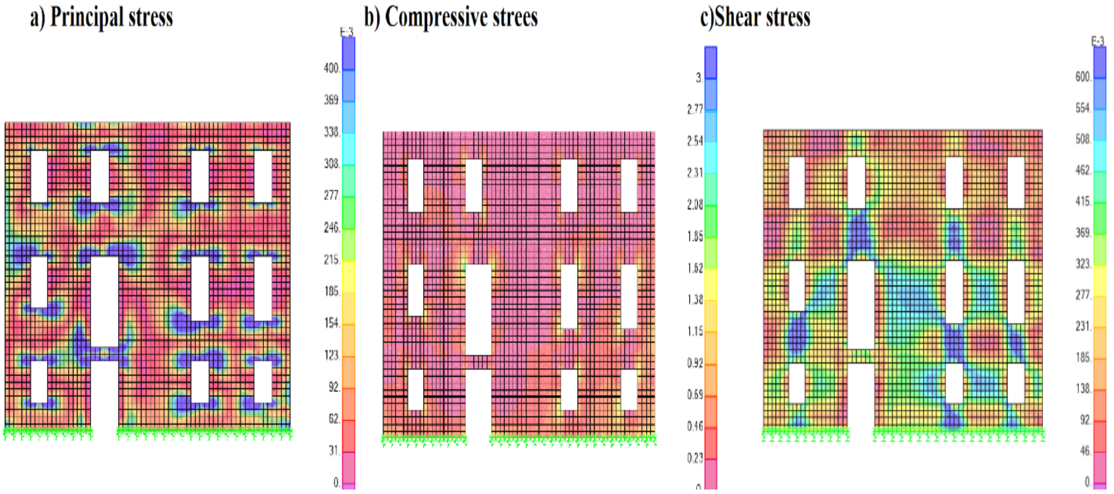

Figure 5.14. Principal, compressive and shear stress distributions on the front facade.

Principal stress concentration is mostly observed in the areas close to the openings. Due to discontinuities, these areas are more prone to bear massive cracking. It is seen that the average values of principal stresses around openings are 0.3 MPa that exceeds a threshold value of 0.15 MPa. If principal stresses emerging due to dynamic excitation exceed the tensile strength of walls or piers, diagonal cracks develop and diagonal tension failure mode occurs. Therefore, diagonal cracks around openings are anticipated. It is seen as one of the unwelcome failure modes.

When compressive stress distribution is examined, it is obvious that higher values of compressive stresses are observed at level of the vertical elements on the basement facade. However, the maximum stress corresponds to 30 % of the compressive strength value.

Shear strength with a value of 0.2 MPa were almost attained at the level of first floors but exceeded at the levels of ground and basement floors. The analysis of the shear stress distribution demonstrates that concentration spreads between adjacent openings in both vertical and horizontal plane. Exceedance of the threshold value can be detected in the areas more than half of the facade. The results obtained showed that the first damage by shear in the facade elements should occur at lower levels of seismic intensity.

6. EQUIVALENT FRAME MODELLING TECHNIQUE

EFM is a simplified method, which enables simulating in-plane behaviour of structural masonry walls and carrying out non-linear analysis for performance assessment of URM structures by means of their identification with a frame. Besides, the consideration of homogeneous and isotropic material idealization, and less necessity in amount of data and experimental study to determine mechanical material properties make EFM more practical. However, when taking FEM, one of the most used methods, into consideration, it was mentioned that FEM has been utilized as a very powerful analysis tool for the assessment of URM, but also suffered from high computational effort [33]. In Chapter 4, it was observed that results obtained by using FEM could be very dependent on the proper selection of mesh size, and an accurate calibration of the input parameters may be required by applying the procedure of finite elements model updating. Whereas, meshing or model updating has not been literally performed to build up a numerical model by means of EFM, since that is based on macro-elements discretization of URM walls (each macro-element represents an actual size of wall portions). In this method, each bearing wall is basically subdivided into a group of masonry panels where the deformation and non-linear response are concentrated, and rigid portions which connect these deformable panels [11]. Herein, a general concern is focused on the global response of masonry structures, in presence of proper connection between masonry panels that prevent the occurrence of local collapse mechanisms based on out-of-plane response of walls.

6.1. Validation of EFM accuracy

There have been numerous studies performed in literature. Particularly, experimental studies based on full-scale building prototypes can be accepted as the most useful ones in order to make available information related to EFM modelling performance. The detailed research including quasi-static cyclic tests conducted by Magenes and Calvi at University of Pavia on two-storey building prototype is a crucial reference to verify the modelling accuracy of EFM by providing comprehensive data used on the test setting for other interested researchers. Numerical results obtained from EFM simulations, in terms of seismic capacity and failure mechanisms, have confirmed a good agreement with the experimental results [5]. Another remarkable research regarding seismic performance of existing masonry buildings is Catania Project, which is accepted as an extensive nationwide research project in Italia. This project was investigated by a number of Italian universities, establishing numerical modelling of structural response with different approaches. The research team of Pavia University and Pasticier *et al.* (2008) carried out the seismic assessment based on EFM, using Sam Code and SAP 2000 (v.10) code, respectively. However, the research team of Genoa University conducted analyses based upon a finite elements model with layer failures while Basilicata research group utilized a macro model with crushing and shear failures [34]. The outcomes obtained from all research studies above were discussed by Pasticier *et al.* (2008), plotting base shear vs top displacement values. It was concluded that top displacement values obtained from EFM and FEM exhibited a good agreement, and also a remarkable correlation between the results obtained from Sam Code and SAP 2000 was provided for the location of storey mechanisms and local failure nodes occurred [9].

Consequently, a great number of studies carried out by applying EFM in the assessment and structural modelling of URM has verified its concordance with the analysis procedures recommended by the most advanced codes such as FEMA 440, Italian Building Code 2008, NZSEE 2015 and EN 1998-1. High computational efficiency and accuracy of EFM has made it one of the most popular tools for the analysis of structural masonry [4].

6.2. Discretization of Masonry Walls in Equivalent Frame

EFM in principle proposes the discretization of bearing masonry walls into finite structural macro-elements. The first step begins with the identification of main structural components consisting of piers and spandrels. Piers, which are vertical resisting elements bearing both gravitational and lateral loads, are identified by the extension of the vertical edges of the openings.

Spandrels, secondary horizontal elements, are located between two vertically aligned walls whose function is to connect adjacent piers to each other and transfer lateral and floor loads to piers. Finally, node panels are intended for the intersection of spandrels and piers, and modelled as fully rigid.

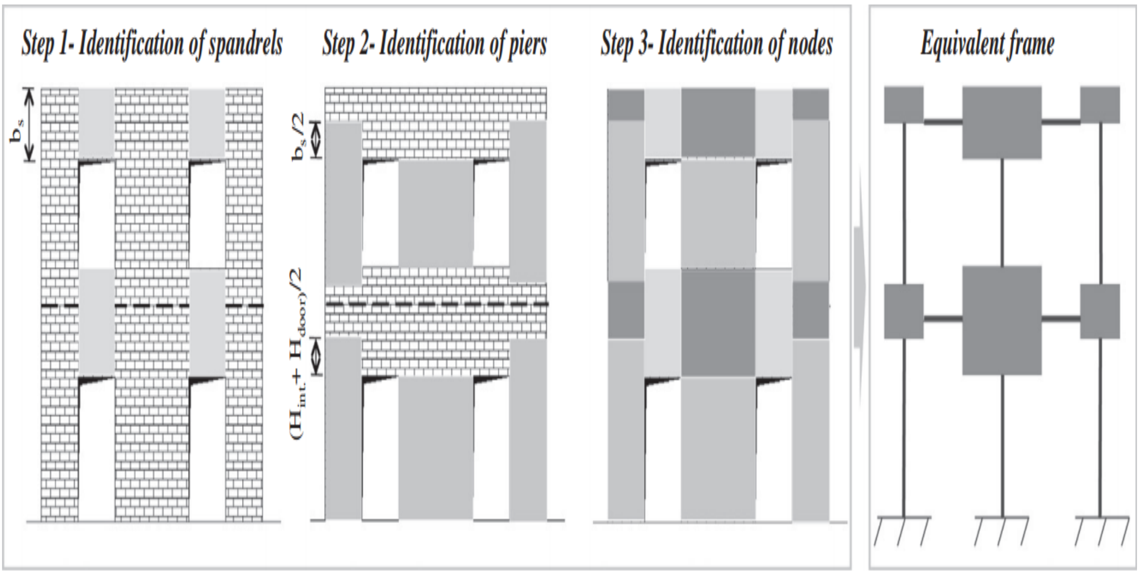

Figure 6.1. Schematization of equivalent frame idealization in case of regularly distributed openings [11].

Figure depicts how to identify panels composing an equivalent frame model step by step. The frame schematization of EFM proposed in literature takes inspiration from the damages observed after seismic events and experimental campaigns. Post-earthquake surveys have confirmed that the wall deformation concentrates in piers and spandrels. Therefore, these elements are recognised as deformable regions in equivalent frame modelling, whereas the node panels are only parts not affected by damages due to fully rigid assumption.

As previously mentioned, the definition of spandrel elements is based on vertical alignment and overlap of openings. In case of adjacent openings having same length in vertical arrangement, the length and height of spandrels are assumed to be equal to the span distance and the wall width between adjacent openings, respectively.

The criteria used in determining the height of masonry piers is associated with adjacent openings in general. According to a widely accepted criterion proposed by Dolce, M. (1991), It is assumed that cracks occur at the corner of openings with a 30^0 inclination, intersecting with the centre line of external piers represented by frame elements in modelling, as indicated in Figure 6.2. Consequently, this hypothesis provides an increased height for the external piers. This resulting height can be assumed to be equal to the height of adjacent opening or the average of the inter storey height and the opening height as shown in the step 2 of Figure 6.1 [11]. In case of perfectly aligned adjacent openings with a same height, internal piers located between them have an equal height. The geometry of the rigid nodes is defined on basis of where spandrels and piers overlap.

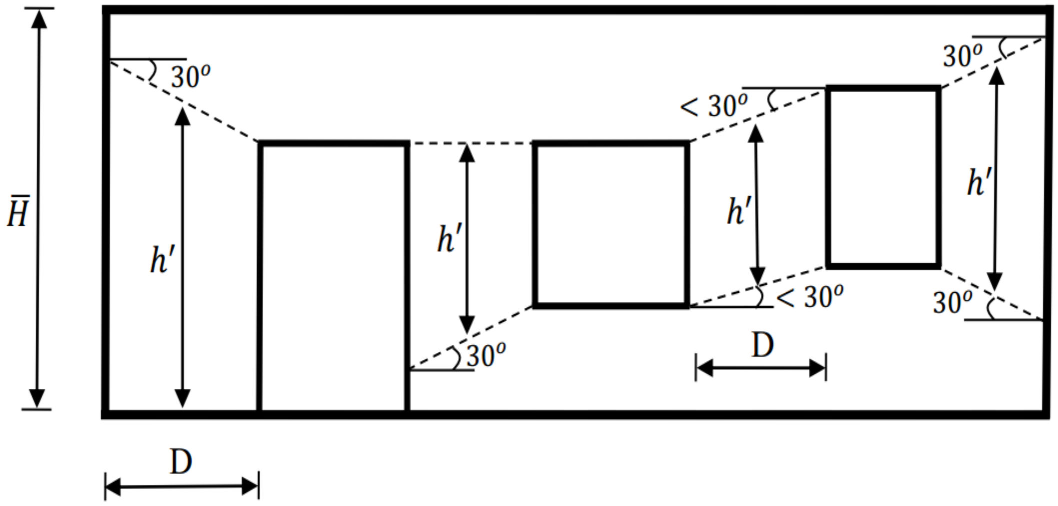

Figure 6.2. Effective height definition [3].

Dolce (1991) developed a criterion for the definition of effective heights. The criterion considers the equivalent stiffness of each pier, the mutual interaction with the surrounding spandrels and the coupling effect between spandrel and peers by assigning rigid end offsets. Equation 6.1 was proposed by Dolce (1991) to calculate the effective heights of piers.

$$h_{eff} = h' + \frac{D(H - h')}{3h'} \tag{6.1}$$

where D is the pier width, H is the pier height and h' is calculated, depending on the geometry and arrangement of openings as seen in Figure 6.2.

6.3. Equivalent Frame Model of the front facade

In order to generate the 2D EF model of the front facade, the criterion proposed by Dolce (1991) was adopted. Discretization of masonry walls was carried out in accordance with the schematization of equivalent frames depicted in Figure 6.1. Identified parameters obtained from model updating in Chapter 4 were used in modelling. Soil flexibility was also considered with the assignment of soil springs to the stone strip foundation of the building. With the assumption of the bearing walls properly connected to the floor, in-plane behaviour was only considered in analyses to accurately simulate the global response of the structure.

According to EN 1998.1, storey masses were obtained from the combination of total dead loads and 30% of live loads acting on the slabs, and calculated as 98.5 ton, 98.5 ton and 50.95 ton for ground, first and roof floors, respectively. The storey masses were lumped at their corresponding mass centers in lateral direction, and rigid diaphragm was assigned at each storey level.

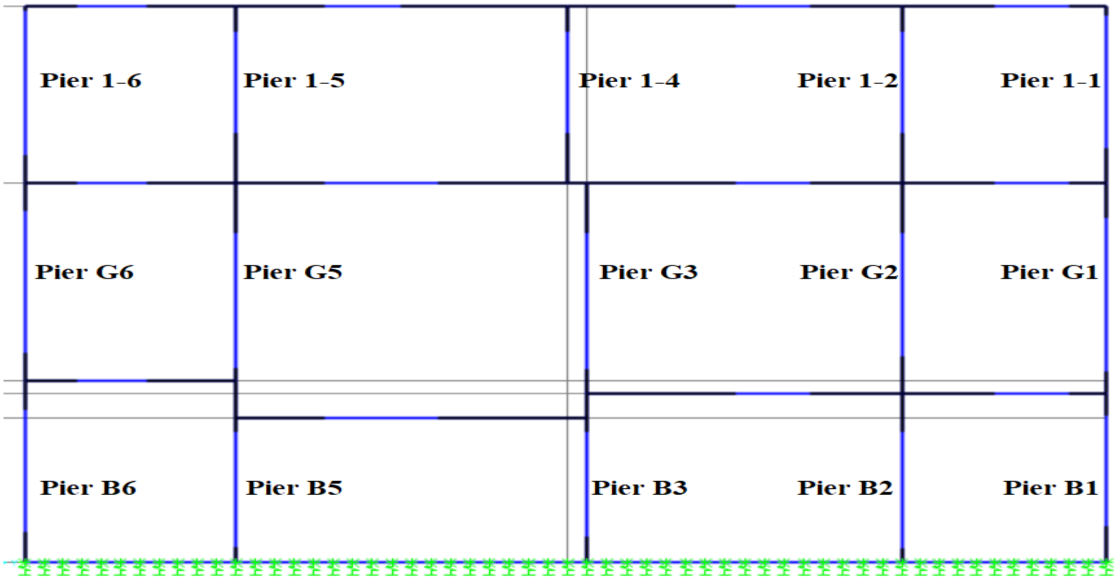

Figure 6.3. Labels of the piers and rigid offset lengths on the EFM.

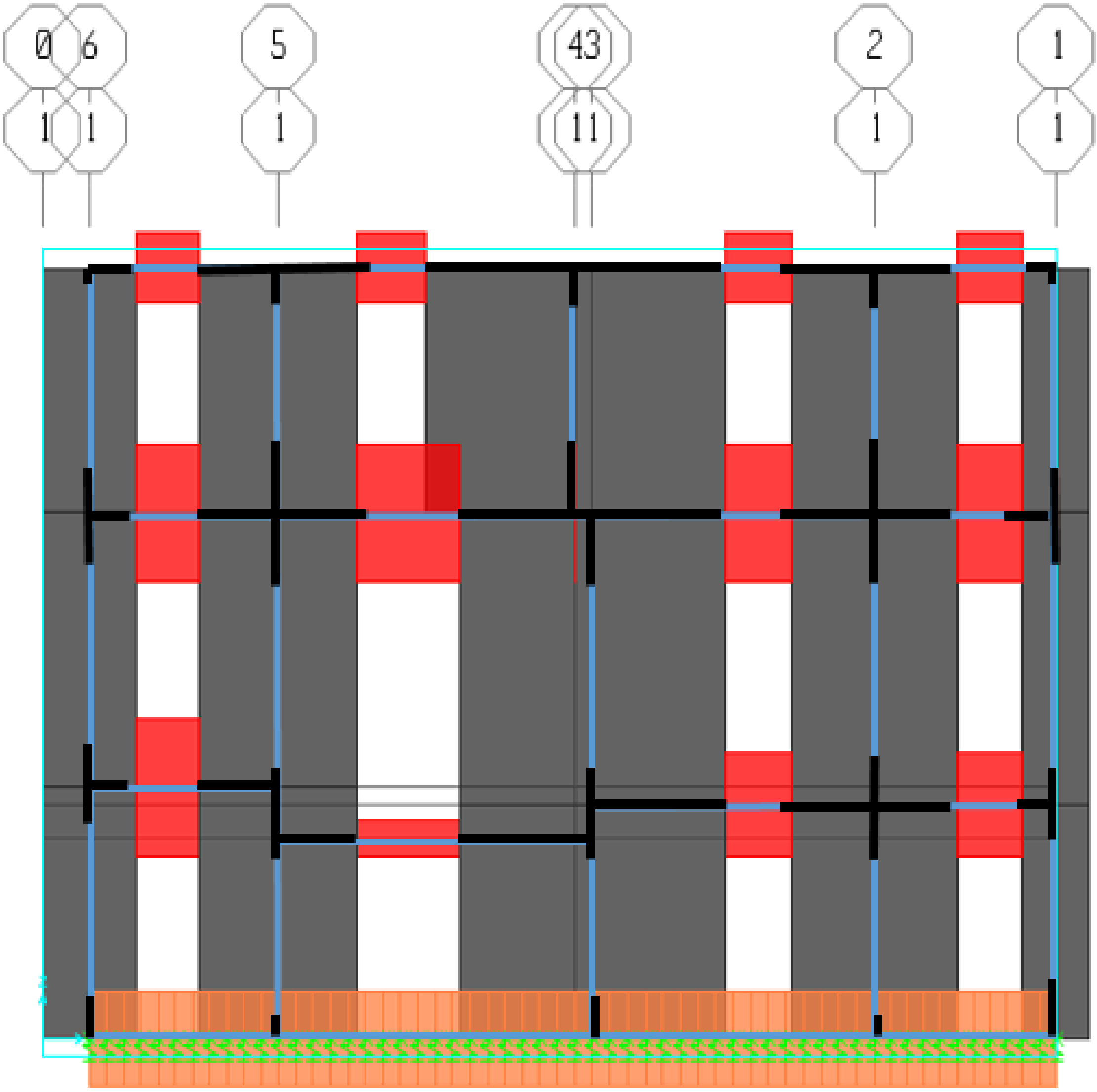

Figure 6.4. Illustration of the EFM with rigid offsets on the front facade.

Eventually, the EFM of the front facade was established, as shown in Figure 6.4 where the facade was discretized into piers in grey, spandrel in red and rigid nodes in black.

7. PERFORMANCE ASSESSMENT BY NON-LINEAR ANALYSES

This section includes the seismic performance assessment of the front facade which was modelled by using EFM technique. The non-linear behaviour of masonry was defined by means of lumped plastic hinges governed by in-plane failure mechanisms, and two nonlinear analysis methods were utilized for seismic evaluation. Pushover analysis was adopted as an incremental static nonlinear method where both mass proportional and mode proportional load cases were applied in analyses. As a non-linear dynamic method, a set of Non-Linear Time History (NLTH) analyses was used to perform series of simulations and incremental dynamic pushover curves were generated. Consequently, the seismic fragility curve was derived to achieve vulnerability assessment.

7.1. Determination of In-Plane capacities of the URM walls

The in-plane capacity of structural masonry determines the occurrence of non-linear behaviour and the attainment of limit states. It was mentioned that the major failure modes that govern the global seismic response of in-plane walls to the seismic excitation can be classified into 4 groups namely rocking, diagonal shear cracking, sliding shear and toe crushing in Chapter 2. The Equations (see Chapter 2) used to calculate in-plane capacities of URM walls were listed below.

- Equation (2.2) according to Italian code (2003) for diagonal tensile capacity.
- Equation (2.4) according to NZSEE (2015) for rocking capacity.
- Equation (2.9) according to Italian code (2003) for sliding shear capacity.
- Equation (2.11) according to Eurocode 8.3 for shear capacity.
- Equation (2.12) according to NZSEE (2015) for toe crushing capacity.

The modal analysis was conducted, and required variables in the equations were obtained from the results of modal analysis under gravity loads.

Table 7.1. Geometrical properties of the piers and main variables in the capacity equations.

PIER	**H (mm)**	**H_{eff} (mm)**	**D (mm)**	**t (mm)**	$\boldsymbol{\xi}$	$\boldsymbol{\sigma_0}$ (MPa)
Pier B6	3975	2685	1650	880	1.5	0.185
Pier B5	3975	2523	2800	880	1.42	0.225
Pier B3	3700	2300	4680	700	1	0.218
Pier B2	3700	2560	2920	700	1.27	0.245
Pier B1	3700	2400	1170	700	1.5	0.2
Pier G6	4355	3115	1650	690	1.5	0.1
Pier G5	4355	2955	2800	690	1.5	0.145
Pier G3	4630	2990	4680	690	1	0.142
Pier G2	4630	2700	2920	690	1.5	0.144
Pier G1	4630	3380	1170	690	1.5	0.13
Pier 1-6	3880	3160	1650	650	1.5	0.03
Pier 1-5	3880	2220	2800	650	1.39	0.05
Pier 1-4	3880	2220	5280	540	1	0.045
Pier 1-2	3880	2220	2920	540	1.33	0.05
Pier 1-1	3880	2900	1170	540	1.5	0.03

In Table 7.1, σ_0 is the mean vertical stress due to gravity loads and obtained from SAP 2000, and ξ is the coefficient dependent on pier aspect ratio (see Equation 2.2).

In plane capacities of URM walls were presented in Table 7.2. The lowest capacity values for all piers were obtained from Equation 2.9 which corresponds to sliding shear according to Italian code. Therefore, the non-linear behaviour of piers will be controlled by sliding shear failure mode.

Table 7.2. In-plane capacities of URM walls.

PIER	**Sliding Shear** V_u^s(kN)	**Rocking Capacity** V_r (kN)	**Toe Crushing** V_{tc} kN	**Diagonal Cracking** V_u^f(kN)	**Shear Capacity** V_f (kN)
Pier B6	77.95	147.08	166.54	369.24	381.48
Pier B5	249.81	623.34	689.92	688.81	718.05
Pier B3	478.46	1527.81	1690.47	1291.43	959.35
Pier B2	226.67	579.12	628.06	652.26	613.93
Pier B1	38.92	89.52	99.27	211.46	237.7
Pier G6	29.55	86.93	101.3	262.93	286.73
Pier G5	118.43	336.22	384.1	470.6	521.71
Pier G3	286.65	783.89	918.09	1175.89	830.55
Pier G2	136.51	338.43	402.08	490.22	520.7
Pier G1	18.36	44.45	51.07	193.3	207.82
Pier 1-6	8.33	39.58	47.65	171.26	181.27
Pier 1-5	52.57	176.37	231.02	326.7	319.3
Pier 1-4	128.19	478.67	636.51	702.75	492.3
Pier 1-2	47.25	159.02	208.36	295.18	276.52
Pier 1-1	3.82	18.85	23.26	100.89	108.35

It is important to recall that “flexural response tends to be dominated by rocking of piers rather than “beam” type behaviour, and failure is generally characterized by shear, either in diagonal tension mode or by sliding on the predefined planes of mortar”[7]. Besides, it was acknowledged that spandrels, vertical components without axial loads, are prone to early shear cracking but still the ultimate resistance is controlled by pier failure. As explained in Chapter 2.1, Pasticier *et al.* (2008) also employed both rocking and shear hinges to piers and only shear hinges at mid-heights of spandrels, and then performed pushover analysis for seismic assessment. After obtaining a result that the global response of the URM structure was characterized by the shear failure mode of the piers, only shear links were assigned to the mid-heights of the piers to reduce computational effort in NLTH analyses. Since the in-plane capacities of the facade under investigation were characterized by sliding shear, as seen in Table 7.2, and the researches explained above acknowledged that shear failure in terms of displacement demand was found as more brittle compared to other failure mechanisms, in this study only nonlinear shear hinge was assigned to the mid-heights of piers in an attempt to diminish dissipation of time and computational burden in incremental NLTH analyses.

The reason lying behind the assignment of shear hinges at mid-heights of the piers is that shear and principal stress concentrations occur through the deformable height of URM walls under dynamic excitations. When the stresses induced by Earthquake exceeds the threshold values, crack patterns emerge depending on the relative strengths of masonry components.

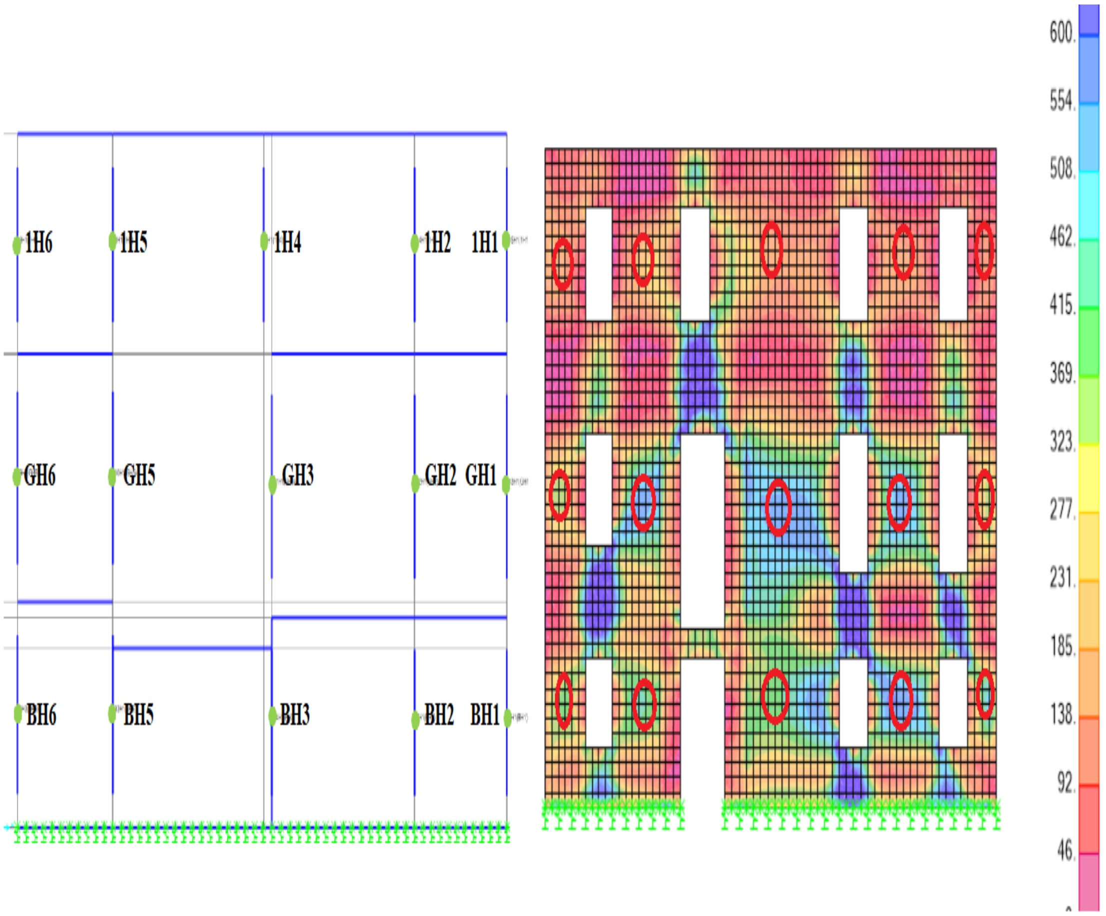

Figure 7.1. Verification of possible hinge locations described in the literature, based on comparison of EFM and FEM. (Red circles show the concentrated shear regions).

Shear strength with a value of 0.2 MPa were almost attained at the level of first floors but exceeded at the levels of ground and basement floors. In the locations of shear hinges assigned in the EFM, shear stress concentrations occurred after performing FEA. Spandrels, which were modelled as deformable elements between adjacent openings in vertical plane, were subjected to more shear stresses than their threshold values at the levels of basement and ground floors as well. Consequently, the distribution of stresses enabled verifying the possible shear hinge locations.

7.2. Determination of Limit States for global assessment

According to Eurocode 8.3, the limit states of URM walls were determined, which correspond to the attainment of the global displacement capacity on the pushover curve. The ultimate displacement capacity is described as the top displacement. In terms of top displacement, three limit states exist on the pushover curve.

- Limit state of Limited Damage (LD) is where the structure yields on the curve of idealized elasto-perfectly plastic force/displacement relationship.
- Limit state of Significant Damage (SD) is equal to $\frac{3}{4}$ of the top displacement capacity corresponding the total base shear.
- Limit state of Near Collapse (NC) is equal to below 80 percent of the peak resistance of the structure.

Structural collapse was assumed once the in-plane deformation capacity of piers was firstly reached due to the ultimate shear displacement controlled by shear hinges or the ultimate rotation controlled by rocking hinges [9]. According to Italian code (2008), the shear collapse corresponds to the achievement of the ultimate drift δ_u which is assumed to be 0.4% of the effective height of the pier [33-35].

Table 7.3. Ultimate displacements and shear capacities of piers.

PIER	**Italian Code**	
	Sliding shear V_u^s(kN)	**Near Collapse** δ_u(mm)
Pier B6	77.95	10.74
Pier B5	249.81	10.1
Pier B3	478.46	9.2
Pier B2	226.67	10.24
Pier B1	38.92	9.6
Pier G6	29.55	12.46
Pier G5	118.43	11.82
Pier G3	286.65	11.96
Pier G2	136.51	10.8
Pier G1	18.36	13.52
Pier 1-6	8.33	12.64
Pier 1-5	52.57	8.88
Pier 1-4	128.19	8.88
Pier 1-2	47.25	8.88
Pier 1-1	3.82	11.6

Shear hinge properties were defined using ultimate shear and strength capacities shown in Table 7.3.

7.3. Modelling of non-linear behaviour for pushover analysis

The masonry piers were modelled as elastoplastic with final brittle failure of the deformable parts and a rigid-perfectly plastic behaviour with final brittle failure was assumed for the plastic hinges.

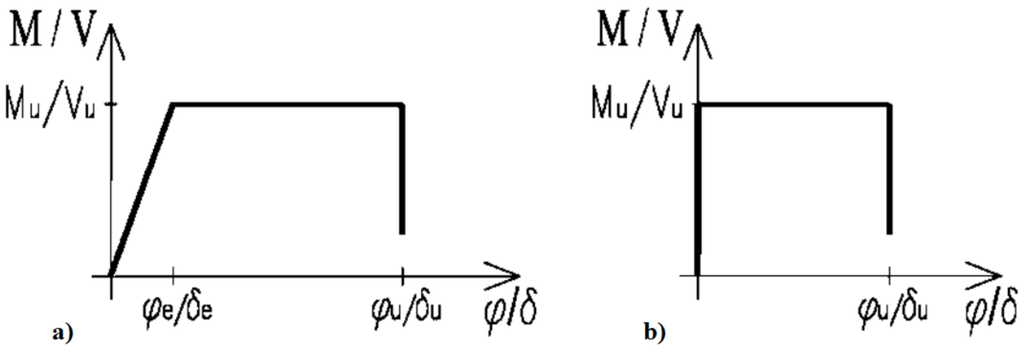

Figure 7.2. The pier and shear behaviours for PO a) the behaviour of pier, b) the behaviour of correspondent shear hinge [9].

In the pushover analysis, two different lateral load distributions were adopted. First load case (uniform distribution) was proportional to the floor masses. The latter case was proportional to the product of masses times first mode shapes.

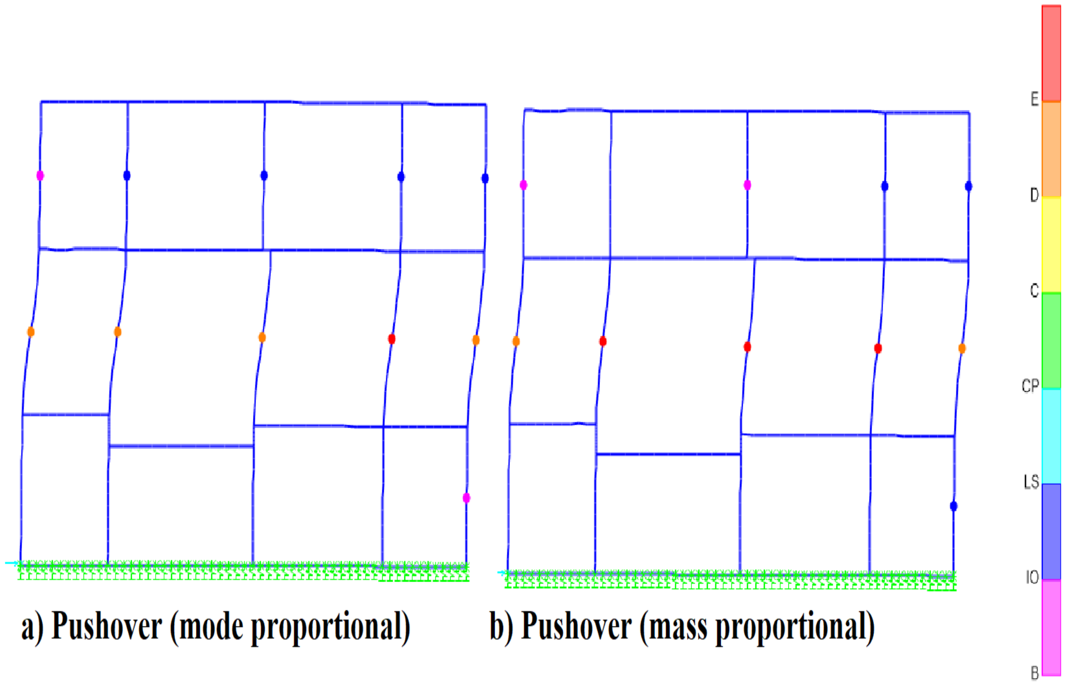
a) Pushover (mode proportional)

b) Pushover (mass proportional)

Figure 7.3. Comparison of hinges at δ_u =15.4 mm.

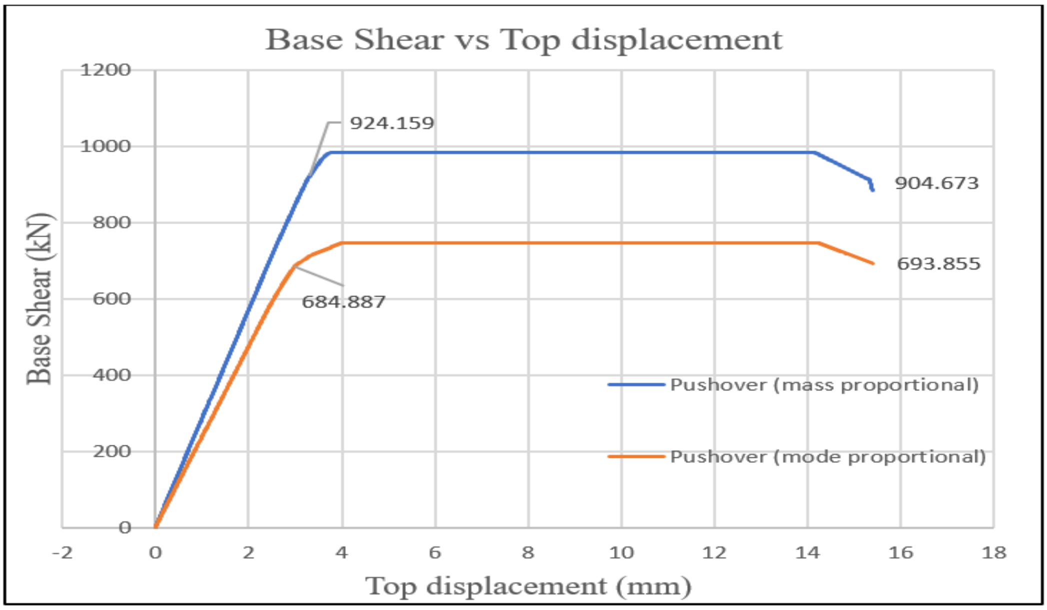

Figure 7.4. Pushover curves for both load cases.

After performing pushover analyses, the hinges occurred as shown in Figure 7.3 when the ultimate displacement capacity 15.4 mm was attained. The collapse of the facade was characterized by a storey mechanism emerging at the ground floor. More hinges reached limit state of limited damage represented by blue hinges under the mode proportional load case compared the other, due to the reverse triangular distribution of load, more static force was applied to the top floor. The striking point on the pushover curve is that there was a considerable difference about 24 % between the base shear capacities of both models.

Table 7.4. The results of Pushover analyses.

Non-linear Static Analysis	**Pushover (mode proportional)**		**Pushover (mass proportional)**	
Limit States	Limited Damage	Near Collapse	Limited Damage	Near Collapse
Base Shear (kN)	684	693	924	904
Top Displacement (mm)	2.98	15.4	3.41	15.4

7.4. Modelling of non-linear behaviour for Time History Analysis

In order to simulate the cyclic behaviour of piers by means of stiffness and strength degradation, hysteresis type pivot hinge was employed in NLTH analyses.

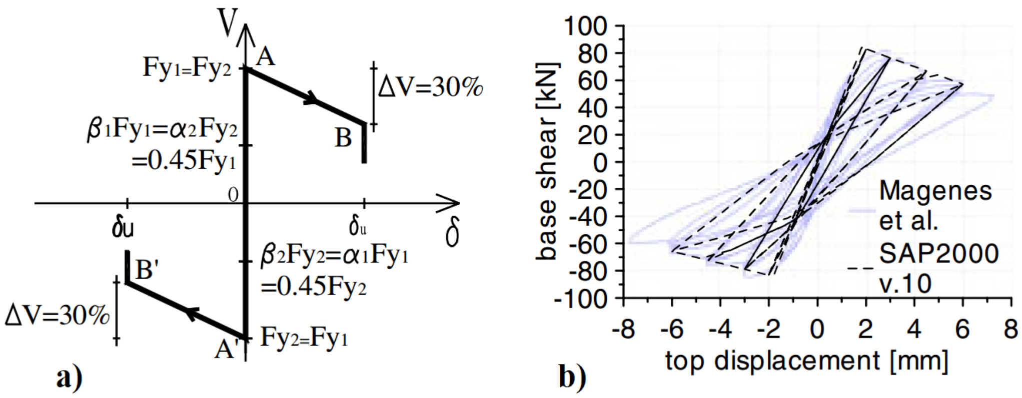

Figure 7.5. The pier and shear behaviours for NLTH a) the behaviour of pier, b) the behaviour of correspondent shear hinge [9].

The reference backbone curve was utilized to perform the non-linear hinge behaviour with the corresponding parameters controlling the degradation of stiffness and strength. The experimental curve was firstly generated by Anthoine *et al.* (1995) performing the quasi-static cyclic test. Afterwards, Magenes *et al.* proposed the parameters of the backbone curve that enables the pier to achieve the same behaviour with experimental curve, establishing the numerical model by SAP 2000.

The hinge parameters α_1, α_2, β_1, and β_2 which govern the stiffness degradation during the unloading procedure, were adopted for correlation with the experimental results. All parameters were taken as 0.45. Ultimate shear capacity of the pier was reduced to 70 % of the peak resistance.

7.5. Incremental Dynamic Analysis (IDA)

An incremental dynamic analysis can be performed by series of non-linear time history analyses. The main difference between IDA and NLTH is that the entire range of structural response is covered by IDA, whereas the results obtained from NLTH analysis only determines the response of the structure for that earthquake input selected. Each NLTH analysis uses the same seismic record with different Peek Ground Accelerations (PGA). By scaling the PGA values, it is aimed at leading the structure to reach all limit states from yield point to collapse. The selection of earthquake inputs is a significant phase to obtain reliable outcomes about vulnerability assessment, since a seismic event can vary from another one in terms of the frequency content, the energy content, the duration and such parameters, which give rise to different influences on the same structure.

Fifteen earthquake records were selected from PEER NGA West2 Data Base in accordance with the design response spectrum generated in Chapter 5 [36].

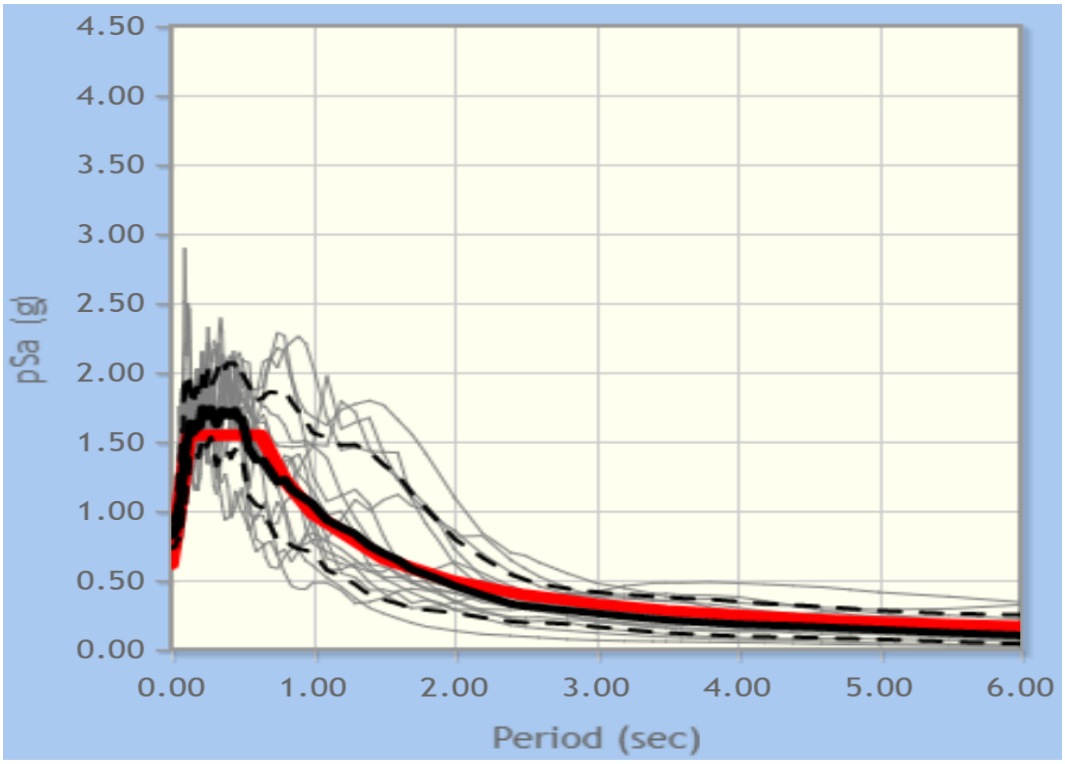

Figure 7.6. The spectra of selected ground motions.

The proper PGA scale factors at small intervals were utilized for 15 earthquake records so as to derive the entire incremental dynamic pushover curve with piecewise lines. As a result of this, the PGA values causing the structure to attain the limit states of limited damage, significant damage and near collapse were identified.

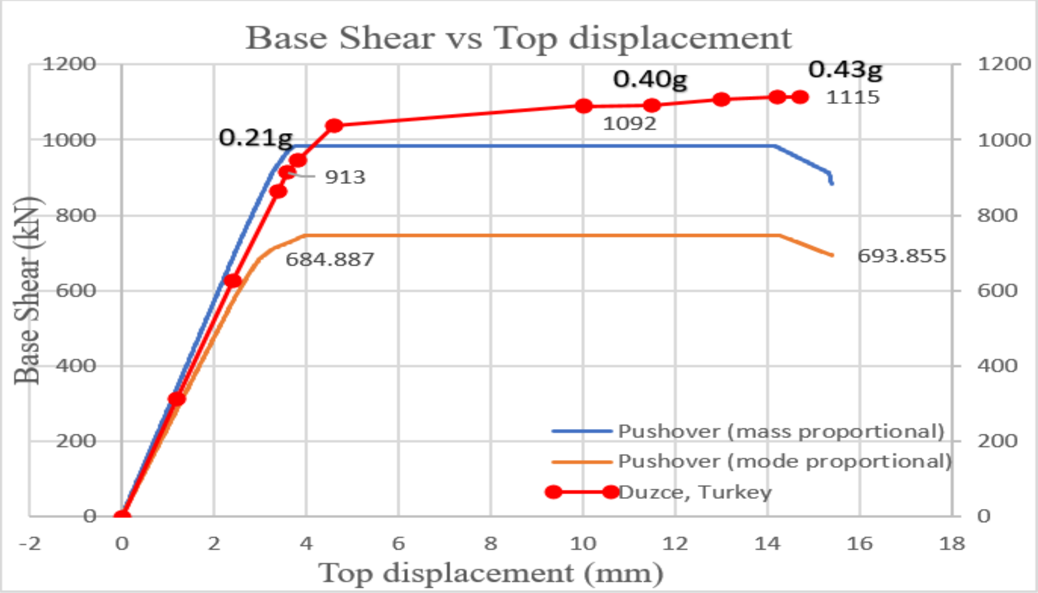

Figure 7.7. Comparison of IDA curve with Duzce EQ. record and Pushover curves.

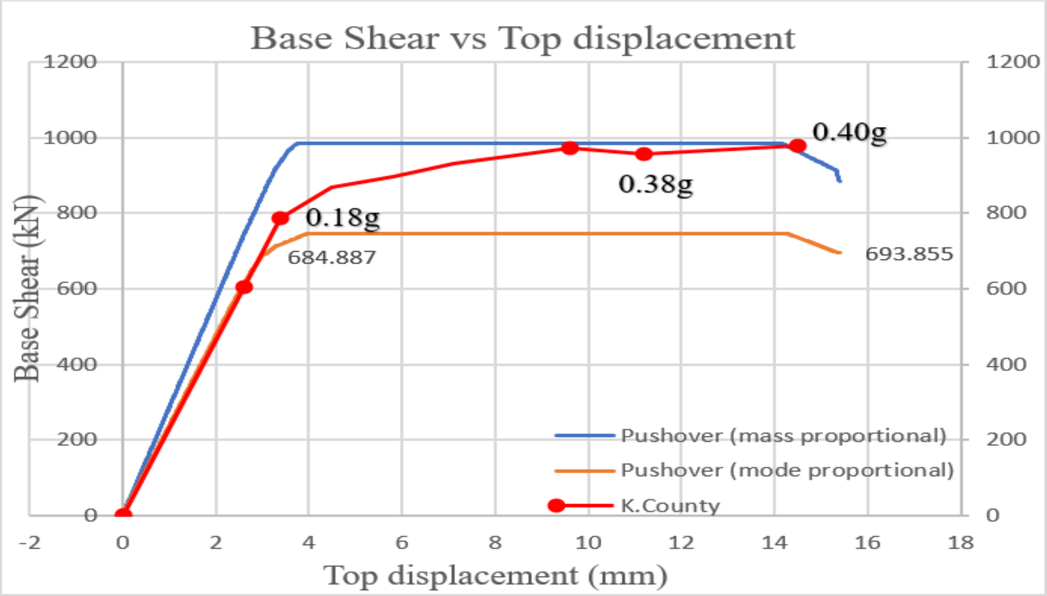

Figure 7.8. Comparison of IDA curve with K. County EQ. record and Pushover curves.

The results obtained from Figure 7.7 and Figure 7.8 showed a good agreement in terms of top displacement capacity of all models. Especially, the force/displacement response of the structure presented a similar behaviour when subjected to either K. County earthquake excitation or static force by pushover (mass proportional), except the yield point. By performing IDA with Duzce earthquake record, the PGA values leading the structure to reach limited damage, significant damage and near collapse limit states are 0.21 g, 0.40 g and 0.43 g, respectively, whereas those PGA values by using K. County earthquake record are 0.18 g, 0.38 g and 0.40 g for the same limit states, respectively. It can be observed that the same PGA of 0.40 g may result in different top displacement demand and different damage level for two earthquake ground motions.

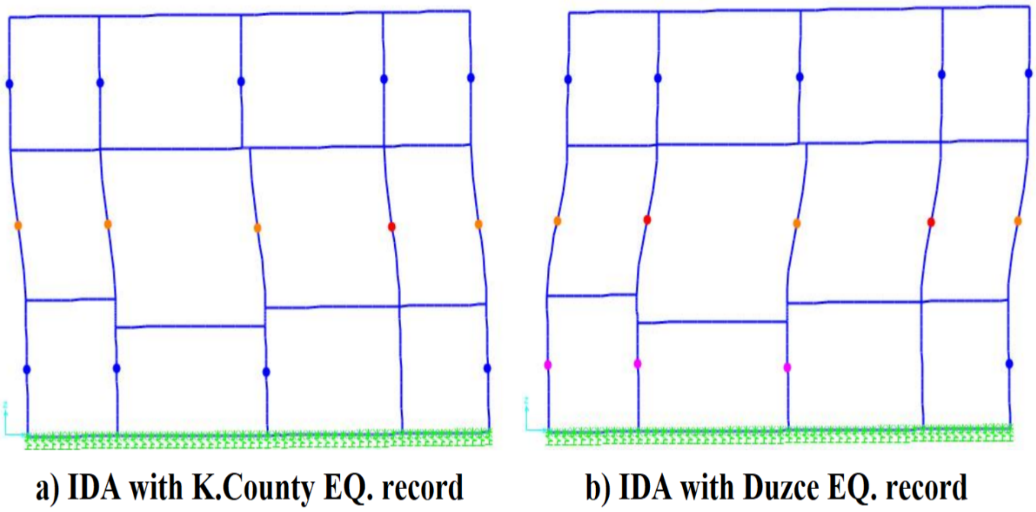

Figure 7.9. Illustration of hinges in Near Collapse State.

When the collapse mechanism occurred, only one pier reached its ultimate shear displacement capacity under K. County EQ. excitation, whereas both piers attained their displacement capacity simultaneously under Duzce EQ. excitation. Another considerable point is that a total of four piers in Figure 7.9.a showed limit state of limited damage until the system fails but only one pier has yielded in Figure 7.9.b. Primarily, these variations confirm how in-plane behaviour of URM walls may differ depending on the content of frequency and energy, and duration of earthquakes.

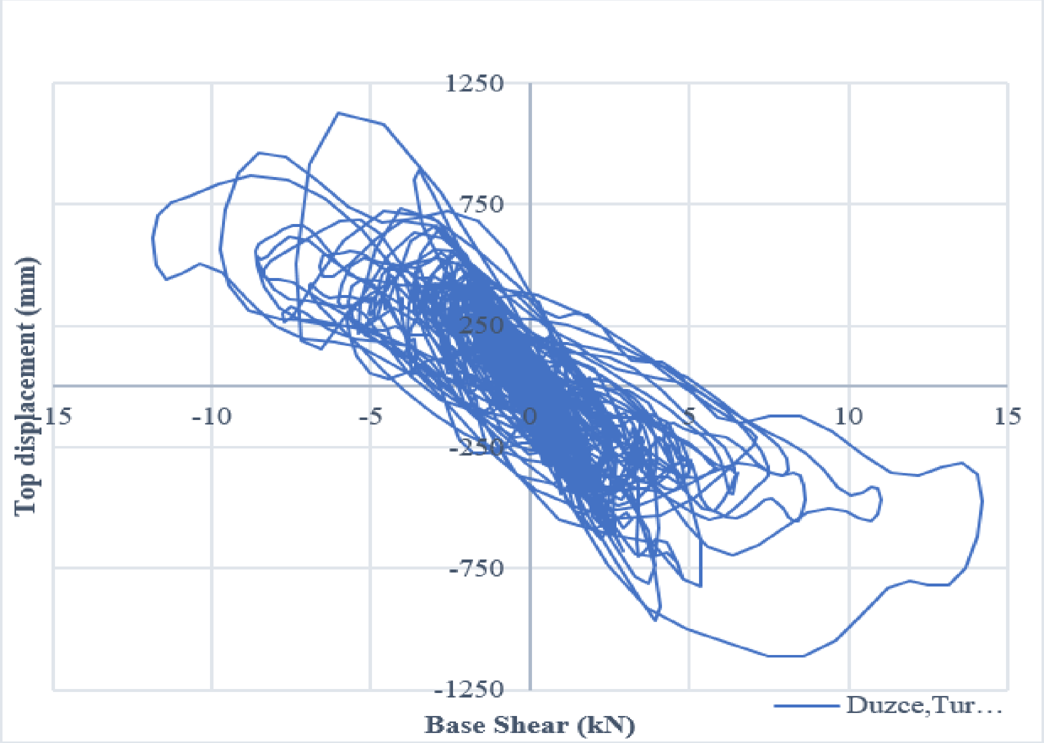

Figure 7.10. Base shear – top displacement relation by IDA with Duzce record.

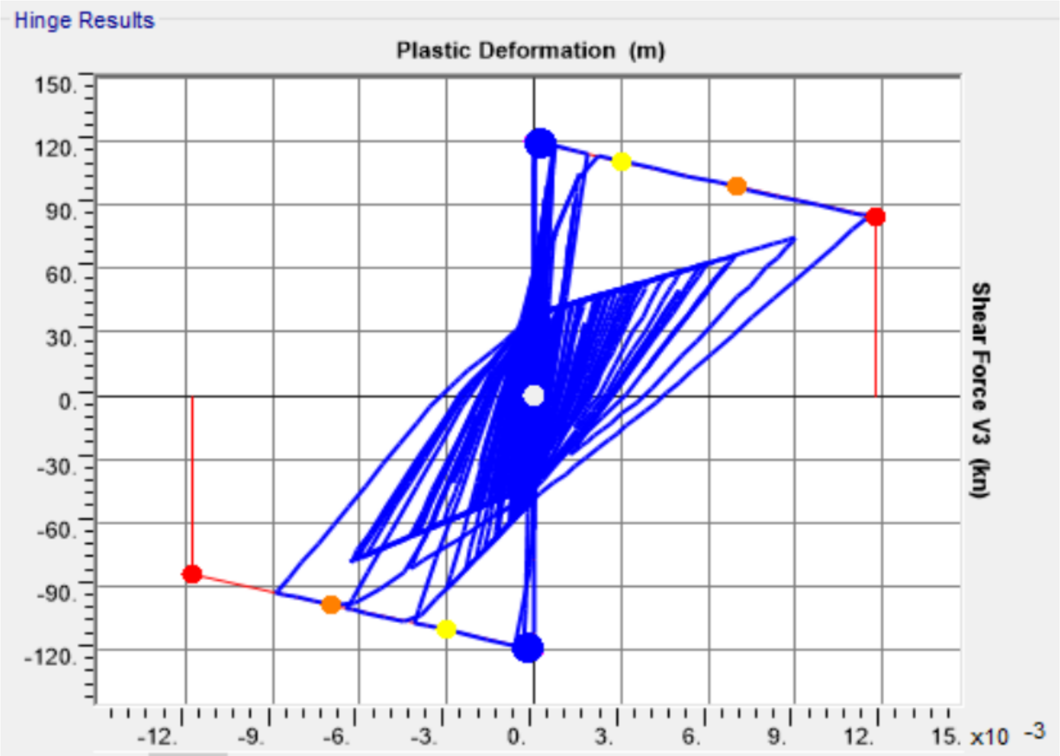

Figure 7.11. In-plane behaviour of GH5 hinge [37].

Figure 7.10 shows base shear and top displacement relation. In Figure 7.11, it is demonstrated that when the pier G5 firstly reached its ultimate capacity of 11.8 mm, the capacity reduced by 30 percent and reached 82.6 kN due to degradation in stiffness.

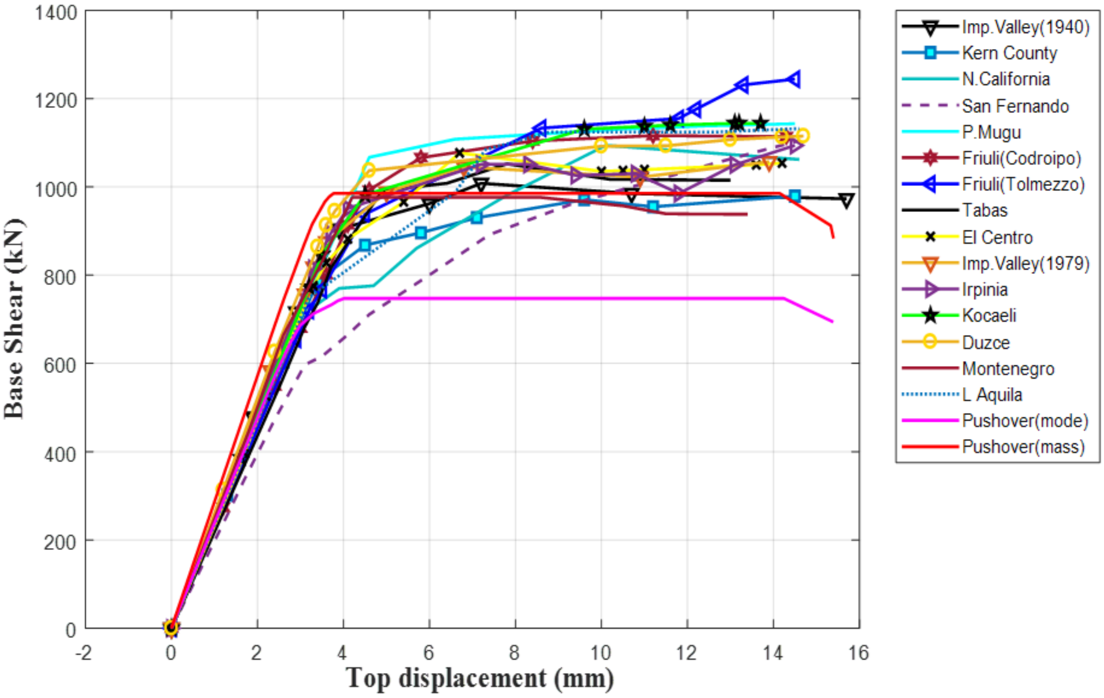

Figure 7.12. Incremental dynamic pushover curve.

After performing series of simulations by using a set of NLTH analyses, finally the incremental dynamic pushover curves were generated, as presented in Figure 7.12. According to the curves, it can be interpreted that the ultimate shear displacement capacity of the structure is about 15 mm. Despite differences in base shear values, a considerable agreement is provided at the yield point represented by limited damage state where the average shear force is 850 kN. The upper and lower bound in Figure 7.12 are represented by the curves obtained from Friuli (Tolmezzo) and Pushover(mode), respectively. It can be concluded that Pushover analysis, adopting the mass proportional load case, meets the mean of results obtained from IDA and thus it may be more applicable method for seismic performance assessment of URM walls, compared to pushover method adopting mode proportional load case.

Using 15 different earthquake ground motions, each PGA value that causes the structure to reach limit states were identified by IDA. These PGA values were marked depending on their corresponding limit states in Figure 7.12.

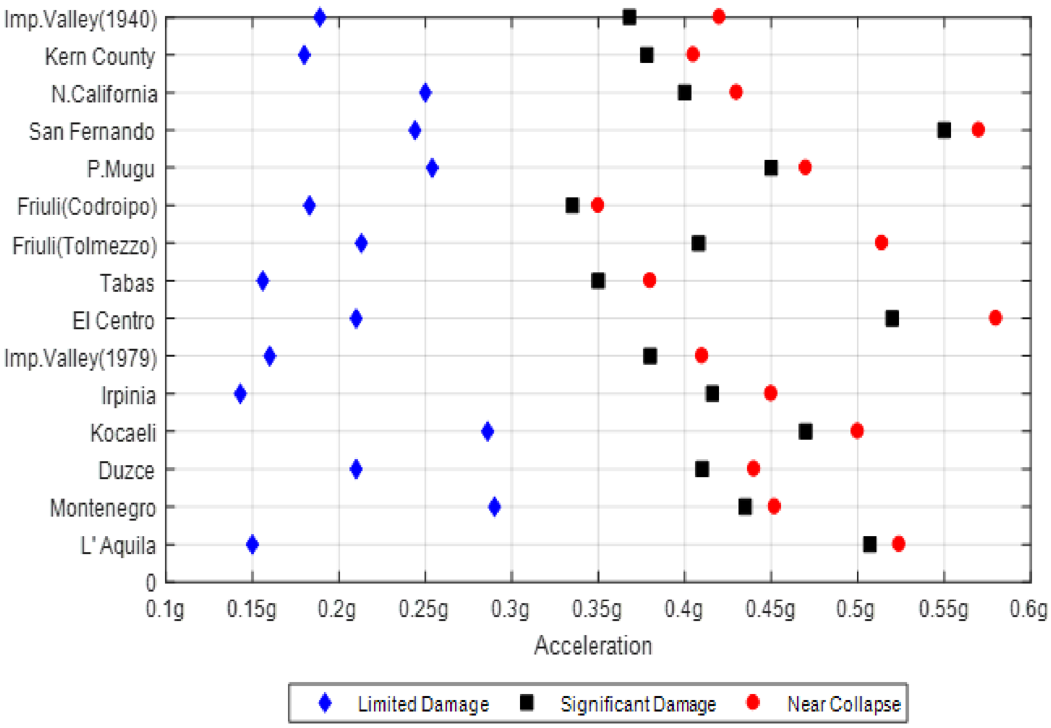

Figure 7.13. Summary of PGA values leading the structure to reach LD, SD and NC limit states.

7.6. Seismic fragility curve

Initially, the response of the structure was obtained by incremental dynamic analyses. Afterwards it was probabilistically defined in terms of PGA values. By carrying out the fragility assessment, it was aimed at predicting the PGA value for which the seismic response of a structure exceeds the capacity ending up failure. In order to perform a direct comparison with the PGA levels corresponding the four seismic zones described in the Italian seismic regulation, the PGA was considered as the seismic intensity parameter. The number of PGA was calculated as percentage at each interval of 0.05 g in Figure 7.13. The calculated percentages were summed up cumulatively. By making this calculation for the PGA values corresponding limit states separately, the seismic fragility curves were derived as seen in Figure 7.13.

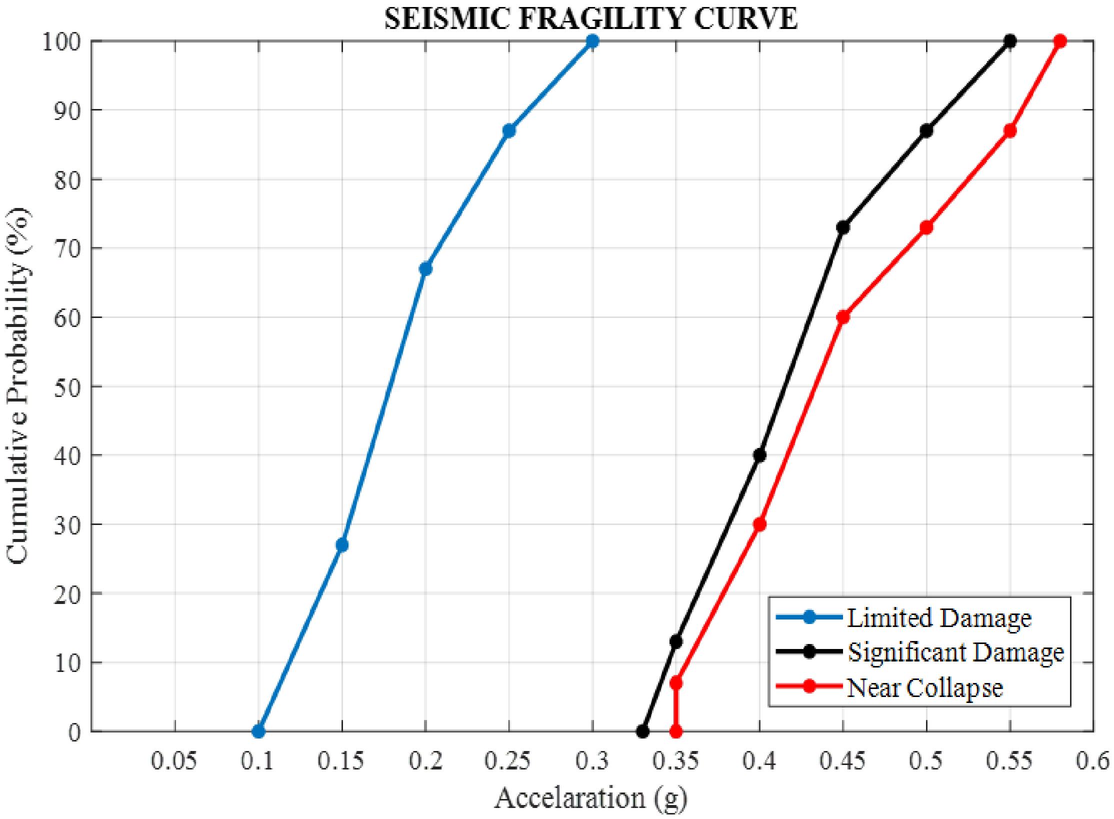

Figure 7.14. Seismic fragility curves corresponding the limit states.

The fragility curves provide an opportunity to assess the seismic vulnerability of the structures by direct comparison with the design PGA values proposed by the Italian seismic regulation code for a return period of 475 years. According to the code, a PGA of 0.35 g and above is defined as first category which represents the highest risk level buildings.

For the building under consideration, there was 30 % probability and 60 % probability to fail in seismic regions characterized by 0.4 g and 0.45 g, respectively. Moreover, significant damage probability of the building for the same level of PGA values constitutes 40 % and 75 % probability of collapse, respectively. Therefore, proper maintenance and retrofitting should be implemented so as to reduce the vulnerability.

7.7. Determination of strength reduction factor

In order to calculate Capacity Reduction Coefficient and Ductility Demand Coefficient as explained in Figure 7.15, the mean of IDAs results is obtained, and Linear Response Spectrum Analysis was performed on the 2D EFM of the front facade. Table 7.5 represents the displacements and base shear values obtained from IDAs using 15 earthquake records.The analysis results obtained from both the mean of IDAs and Linear RSA were plotted, as shown in Figure 7.16.

Table 7.5. Displacement and Forces obtained from IDAs.

Earthquakes	**Limited Damage**		**Significant Damage**		**Near Collapse**	
	δ_{top} (mm)	Force (kN)	δ_{top} (mm)	Force (kN)	δ_{top} (mm)	Force (kN)
Imp.Val(1940)	3.5	844	10.7	985	15.7	973
K. County	3.4	787	11.2	955	14.5	979
N. Calif	3.5	770	12.8	1094	14.6	1062
S. Fernando	3.3	616	11.4	1058	14.6	1105
P. Mugu	3.6	777	11.2	1134	14.5	1143
Friuli (Codroipo)	3.5	801	11.8	1116	14.3	1114
Friuli (Tolmezzo)	3.7	767	10.8	1155	14.5	1244
Tabas	3.7	815	10.2	1017	13	1015
El. Centro	3.3	776	11	1039	14.2	1054
Imp.Val (1979)	3.6	875	10.9	1022	13.9	1057
Irpinia	3.7	894	10.8	1030	14.5	1094
Kocaeli	3.5	847	11	1137	13.7	1144
Duzce	3.6	913	11.5	1093	14.7	1115
Montenegro	3.6	830	11.5	939	14.7	938
L'Aquila	3.2	750	11.6	1124	13.4	1132

The mean value of displacements in Limited Damage is calculated as 3.52 mm that represents Elastic displacement (δ_e) corresponding to yield point on the elasto-plastic curve. Ultimate displacement (δ_u) is obtained as 14.31 mm from the mean of displacements in Near Collapse. Eventually, the ultimate base shear is calculated as 1077.93 from the mean of forces in Near Collapse.

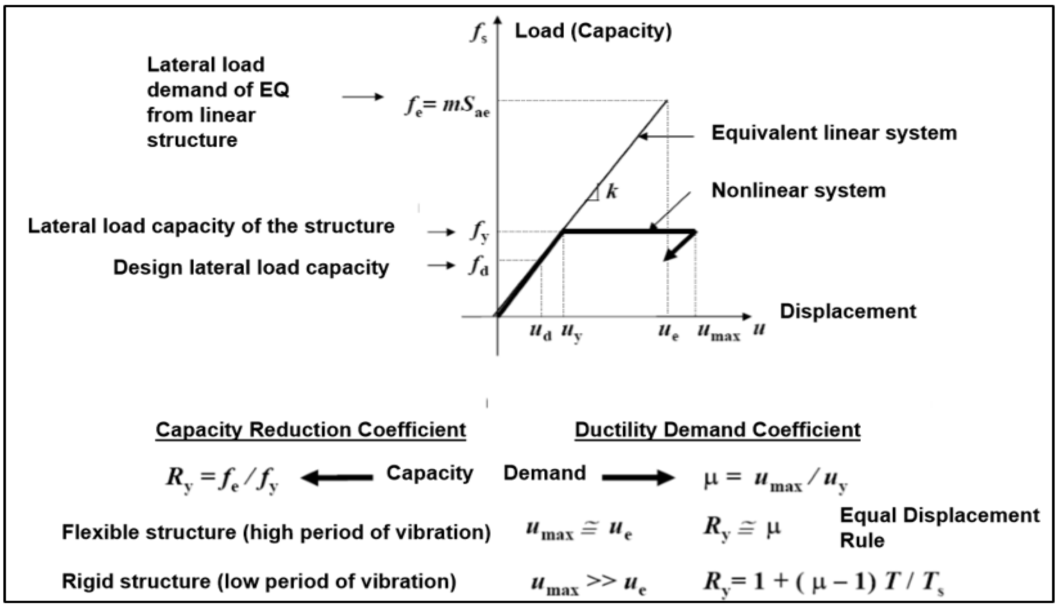

Figure 7.15. Capacity Reduction Coefficient and Ductility Demand Coefficient.

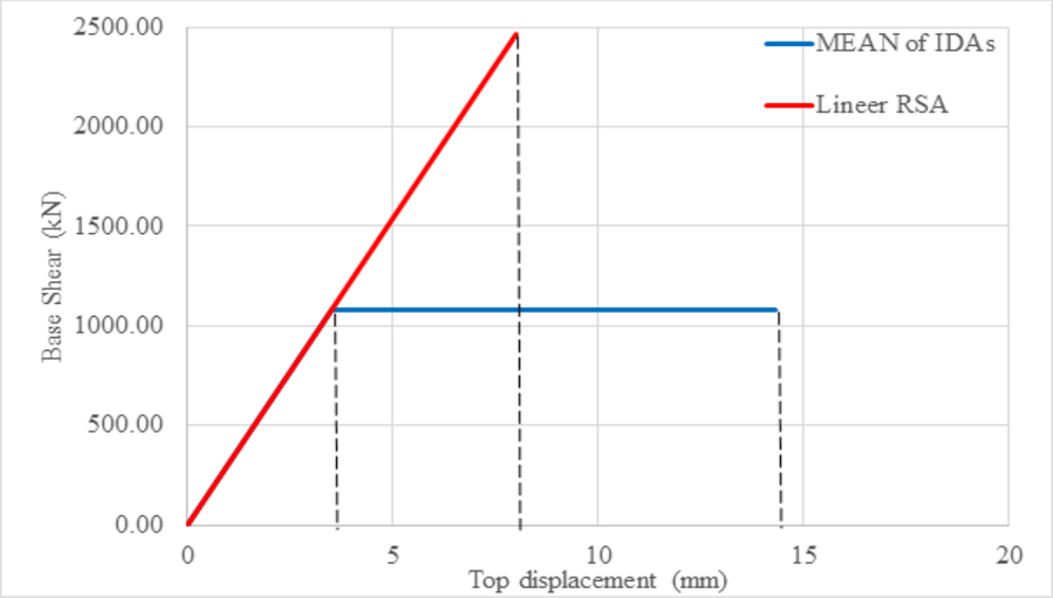

Figure 7.16. Base shear – top displacement obtained from Mean of IDAs and Linear Response Spectrum Analysis.

Table 7.6. Capacity Reduction Coefficient and Ductility Demand Coefficient.

Capacity Reduction Coefficient	**Ductility Demand Coefficient**
$R_y = f_e/f_y$	μ= U$_{max}$/ U$_y$
2.3	4.1

Capacity Reduction Coefficient and Ductility Demand Coefficient are calculated as 2.3 and 4.1, respectively. Ultimate displacement is larger than Elastic displacement, as expected for rigid structures (low period of vibration). The capacity reduction coefficient with a value of 2.3 meets the upper of the behaviour factor between 1.5 and 2.5 for unreinforced masonry proposed in EN 1998-1.

8. CONCLUSIONS AND FUTURE WORK.

8.1. Conclusions

The study presented in this thesis is primarily focused on both linear modelling by FEM and non-linear modelling by EFM in order to carry out seismic performance and vulnerability assessment of the historical building under investigation. So as to reduce the complexity and uncertainty of masonry, system identification technique is used and, OMA is performed. By use of model updating procedure, both the difference between theoretical and experimental modal behaviours has minimized, and the most appropriate material and soil properties have been provided for both linear and non-linear models. As a result, it has created a basis for carrying out the performance and vulnerability assessment of the building accurately. The main findings obtained from Linear RSA and both Non-linear IDAs and PO analyses are as follows:

(i) In comparison of each phase in FE modelling, it is observed that the reduction in mass due to removal of some areas for openings has a less influence than the reduction in stiffness on the modal period since the period has increased considerably upon removal of some areas.

(ii) As refining the mesh size from 60 x 60 to 15 x 15, it is observed that when a mesh size of 20 x 20 compared to a mesh size of 30 x 30, the major difference is that elapsed time for modal analysis becomes four times longer despite converged results.

(iii) In the region of 3D FEM where there is massive slab discontinuity between Axis B and Axis F on Right facade, the maximum displacement of 15.4 mm is attained due to a considerable reduction in the stiffness of lateral resisting elements.

(iv) As a result of linear analysis, the performance level of the building under investigation meets Immediate Occupancy, since a maximum value of 0.171 % measured in the right facade wall is in the range of 0.15 and 0.25 corresponding to Diagonal tension failure, 0.1 and 0.3 corresponding to sliding failure, and 0.1 and 0.9 corresponding to rocking failure.

(v) As a result of linear analysis, it is acknowledged that the average values of principal stresses around openings are 0.3 MPa that exceeds a threshold value of 0.15 MPa. Therefore, diagonal cracks around all openings are anticipated to develop.

(vi) The analysis of the shear stress distribution demonstrates that concentration spreads between adjacent openings in both vertical and horizontal planes. Exceedance of the threshold value can be detected in the areas more than half of the facade. Therefore, it is anticipated that the in-plane failure mode is characterized by shear.

(vii) The lowest capacity values for all piers are obtained from Equation 2.9 which corresponds to sliding shear according to Italian code.

(viii) It is observed that the distribution of shear stresses on FEM model verifies the possible shear hinge locations described in the literature.

(ix) The results of both Pushover analyses demonstrate when the ultimate displacement capacity 15.4 mm was attained, the collapse of the facade is characterized by a storey mechanism emerging at the ground floor.

(x) All simulations obtained from dynamic and static non-linear analyses detect the weak storey at the ground floor. A considerable agreement between the analyses is provided in terms of detecting the weak storey that governs the collapse state.

(xi) A 24 % difference between the base shear capacities of both pushover models is obtained.

(xii) It can be concluded that Pushover analysis, adopting the mass proportional load case, meets the mean of results obtained from IDAs and thus it may be more applicable method for seismic performance assessment for URM walls, compared to pushover method adopting mode proportional load case.

(xiii) The results of IDAs show the same PGA value can lead the URM structures to attaint different limit states depending on the content of frequency and energy, and duration of earthquakes.

(xiv) The upper and lower bound on Incremental Dynamic pushover curves are represented by the curves obtained from Friuli (Tolmezzo) and Pushover (mode proportional), respectively.

(xv) As a result of IDAs, the ultimate shear displacement capacity of the structure is about 15 mm. Despite differences in base shear values, a considerable agreement is provided at the yield point represented by limited damage state where the average shear force is 850 kN

(xvi) As a result of Seismic Fragility Curves, there are 30 % probability and 60 % probability to fail in seismic regions characterized by 0.4 g and 0.45 g, respectively. Since according to Italian code, a PGA of 0.35 g and above is defined as first category which represents the highest risk level buildings, maintenance and retrofitting must be implemented properly so as to reduce the vulnerability.

(xvii) Capacity Reduction Coefficient and Ductility Demand Coefficient are calculated as 2.3 and 4.1, respectively. Ultimate displacement is larger than Elastic displacement, as expected for rigid structures (low period of vibration).

8.2. Future work

(i) The objective of this future work is to establish mechanical models for deformation capacity of stone masonry, since there are no reliable and practical analytical models for the force-deformation relationship of stone masonry. The reason why stone masonry will be under investigation is that in the last few years only limited experimental studies have been carried out. Most of the research work were performed in an attempt to determine the in-plane cyclic behaviour of masonry structures consisting of clay solid or hollow bricks. When examining codes in literature such as FEMA 306 (based on solid clay masonry walls), NZSEE 2015 etc, it is seen that in terms of inter-storey drifts, limit states are identified which refers to the first occurrence of local failure of portions of walls such as rocking in flexural, diagonal cracking and sliding in shear. Particularly, limit states for stone masonry are required to be defined, corresponding to the attainment of the global displacement capacity of the structures on the lateral force - drift curve. In summary, this future work will encompass experimental tests (quasi-static cyclic and standard material tests) as well as the development of analytical and numerical models.

(ii) The objective of this future work is to quantify damage level of the structure using vibration based techniques, and to strengthen the damaged regions by using FRCM composites. The change in modal parameters and strength of reinforced structure compared to original condition will allow to identify the effectiveness of FRCM method. Accurate conditioning of the structure enables to detecting the level and region of strengthening. Retrofitting of the masonry structure by using FRCM materials will provide seismic upgrading, increase in load carrying capacity, and improvement of stiffness of the structure. Continuous monitoring of the reinforced structure subjected to environmental changes such as relative humidity, temperature, imposed strain etc. can be achieved by using Structural Health Monitoring (SHM) system.

REFERENCES

1. Salmanpour, A., N. Mojsilovic and J. Schwartz, “Deformation Capacity of Structural Masonry: A Review of Experimental Research”, *15th International Brick/Block Masonry Conference, Florianopolis*, Paper No. 4C2, 2012.

2. Gentile, C. and A. Saisi, “Ambient vibration testing of historic masonry towers for structural identification and damage assessment”, *Construction and Building Materials*, Vol. 21, No. 6, pp. 1311-1321, 2007.

3. Dolce, M., “Schematizzazione e modellazione degli edifici in muratura soggettiad azioni sismiche”, *L’Industria delle Costruzioni*, Vol. 25, No. 242, pp. 44-57, 1991.

4. Siano, R., V. Sepe, G. Camata, E. Spacone, P. Roca and L. Pela, “Analysis of the performance in the linear field of Equivalent Frame Models for regular and irregular masonry walls”, *Engineering Structures*, Vol. 145, pp. 190–210, 2017.

5. Magenes, G., R. G. Kingsley and G. M. Calvi, “Seismic testing of a full-Scale, two-storey masonry building: Test procedure and measured experimental response”, *the report: Experimental and Numerical Investigation on a brick Masonry Building Prototype - Numerical Prediction of the Experiment*, Report 3.0, 1995.

6. Lourenco, P.J.B.B., *Computational strategies for masonry structures*, Ph.D. Thesis, Delft University of Technology, Holland, 1996.

7. Magenes, G., and G. M. Calvi, “In-plane seismic response of brick masonry walls”, *Earthquake Engineering & Structural Dynamics*, Vol. 26, No. 11, pp. 1091-1112, 1997.

8. D’Ayala, D. and E. Speranza, “Definition of collapse mechanisms and seismic vulnerability of historic masonry buildings”, *Earthquake Spectra*, Vol. 19, No. 3, pp. 479–509, 2003.

9. Pasticier, L., C. Amadio and M. Fragiacomo, "Non-linear seismic analysis and vulnerability evaluation of a masonry building by means of the SAP2000 V.10 code", *Earthquake Engineering and Structural Dynamics*, Vol. 37, No. 3, pp. 467-485, 2008.

10. Salonikios, T., C. Karakostas, V. Lekidis and A. Anthoine, "Comparative inelastic pushover analysis of masonry frames", *Engineering Structures*, Vol. 25, pp. 1515-1523, 2003.

11. Lagomarsino, S., A. Penna, A. Galasco and S. Cattari, "Tremuri program: An equivalent frame model for the nonlinear seismic analysis of masonry buildings", *Engineering Structures*, Vol. 56, pp. 1787-1799, 2013.

12. Betti, M., L. Galano and A. Vignoli, "Time-history seismic analysis of masonry buildings: A comparison between two non-linear modelling approaches", *Buildings 2015*, Vol. 5, No. 2, pp. 597-621, 2015.

13. Simoes, A., R. Bento, A. Gago and M. Lopes, "Seismic vulnerability of old masonry 'Gaioleiro' Buildings in Lisbon", *Proceedings of the 15th world conference on earthquake engineering*, pp. 24-28, 2012.

14. Sonekar, K. and S. V. Bakre, "Pushover analysis of masonry buildings", *Journal of Civil Engineering and Environmental Technology*, Vol. 2, No. 11, pp. 18-22, 2015.

15. Petry, S., *Force-displacement response of unreinforced masonry walls for seismic design*, Ph.D. Thesis, Ecole Polytechnique Federale De Lausanne, No. 6462, 2015.

16. Magenes, G. and A. Penna, "Existing masonry buildings: General code issues and methods of analysis and assessment", *Eurocode 8 Perspectives from the Italian Standpoint Workshop*, Vol. 8, pp. 185-198, 2009.

17. New Zealand Society for Earthquake Engineering, *NZSEE 2015: Seismic assessment of Unreinforced Masonry Buildings*, Corrigendum n° 4, 2015.

18. Tomazevic, M., “Earthquake-resistant design of masonry buildings”, *Earthquake Spectra*, Vol. 1, 1999.

19. Federal Emergency Management Agency, *FEMA 274: Nehrp commentary on the guidelines for the seismic rehabilitation of buildings*, Washington D.C., 1997.

20. Federal Emergency Management Agency, *FEMA 306: Evaluation of earthquake damaged concrete and masonry wall buildings*, Washington D.C., 1998.

21. Turnsek, V. and P. Sheppard, “The shear and flexural resistance of masonry walls”, *Proceedings of the International Research Conference on Earthquake Engineering in Skopje*, pp. 517–573, 1980.

22. British Standards Institution, *Eurocode 6: Design of masonry structures Part 1-1: General rules for reinforced and unreinforced masonry structures*, 2005.

23. Italian Code, *Annex 2: Provisions for design, seismic evaluation and retrofit of buildings*, Italian Official Gazette, Vol. 105, 2003.

24. British Standards Institution, *Eurocode 8: Design of structures for earthquake resistance Part 3: Assessment and retrofitting of buildings*, 2005.

25. Federal Emergency Management Agency, *FEMA 356: Prestandard and commentary for the seismic rehabilitation of buildings*, Washington D.C., 2000.

26. Atamturktur, S., F. Hemez and C. Unal, “Calibration under uncertainty for finite element models of masonry monuments”, *Institution of Los Alamos National Laboratory (LANL) and Los Alamos, NM (United States)*, 2010.

27. Senkardesler, O., G. Erol and S. Soyoz, “Vibration-based FEM updating and seismic reliability estimation of a historical building in Istanbul”, *2^{nd} Conference on Earthquake Engineering and Seismology, Istanbul, Turkey*, 2014.

28. British Standards Institution, *Eurocode 1: Actions on structures Part 1-1: General*

actions-Densities, self-weight, imposed loads for buildings, 2002.

29. British Standards Institution, *Eurocode 8: Design of structures for earthquake resistance Part 1: General rules, seismic actions and rules for building*, 2004.

30. Bowles, J. E., *Foundation Analysis and Design*, The McGraw-Hill Companies, Inc., Singapore, 1997.

31. Deprem Teknik Esasları, *DLH 2008: Kıyı ve Liman Yapıları, Demir Yolları, Hava Meydanları İnşaatlarına İlişkin Deprem Teknik Yönetmeliği*, Resmi Gazete No. 27092, 2008.

32. Demirel, İ. O., *A nonlinear equivalent frame model for displacement based analysis of unreinforced brick masonry buildings*, Master's Thesis, Middle East Technical University Civil Engineering Department, Ankara, Turkey, 2010.

33. Rizzano, G. and R. Sabatino, "Non-linear static analysis of masonry structures by means of Equivalent Frames simplified approach", 8th *International Masonry Conference Dresden*, 2010.

34. Gambarotta, L. and S. Lagomarsino, "Damage models for the seismic response of brick masonry shear walls. Part II: The continuum model and its applications", *Earthquake Engineering and Structural Dynamics*, Vol. 26, pp. 441-462, 1997.

35. Italian Code, *NTC 2008: Technical standards for Buildings in Italian*, D.M. Suppl. ord. n° 30 alla G.U. No. 29, 2008.

36. Pacific Earthquake Engineering Research, *PEER NGA West2 Data Base*, University of California, Berkeley, USA.

37. CSI (Computers and Structures Inc.), *Integrated Finite Element Analysis and Design of Structures SAP2000 v19*, Berkeley, USA, 2017.